Chapter 4

Effect of Internal and External Concentration Polarizations on the Performance of Forward Osmosis Process

Amrit Bhinder, Simin Shabani and Mohtada Sadrzadeh

Additional information is available at the end of the chapter

http://dx.doi.org/10.5772/intechopen.71343

Abstract

Forward osmosis (FO) as an osmotically driven membrane process is severely affected by the concentration polarization phenomenon on both sides of the membrane as well as inside the support layer. Though the effect of internal concentration polarization (ICP) in the porous support on the draw solution side is far more pronounced than that of the external concentration polarization (ECP), still the importance of ECP cannot be neglected. The ECP becomes particularly important when the feed flow rate is enhanced to increase the permeation flux by increasing the agitation and turbulence on the membrane surface. To capture the effect of ECP a suitable value of mass transfer coefficient must be determined. In this chapter, an FO mass transport model that accounts for the presence of both ICP and ECP phenomena is first presented on the basis of solution-diffusion model coupled with diffusion-convection. Then, three methods for the estimation of mass transfer coefficient based on empirical Sherwood (Sh) number correlations, pressure-driven reverse osmosis (RO), and osmosis-driven pressure retarded osmosis (PRO) are proposed. Finally, a methodology for the prediction of water flux through FO membranes using the theoretical model and calculated/measured parameters (hydraulic permeability, salt resistivity of the support layer, and mass transfer coefficient) is presented.

Keywords: forward osmosis, concentration polarization, mass transfer coefficient, reverse osmosis, pressure retarded osmosis

1. Introduction

With the increasing application of membrane-based separation processes in desalination and wastewater treatment, vast efforts have been devoted to making them more energy efficient.

In the hunt of more economical and efficient method, forward osmosis (FO) has been developed as an alternative to the conventional pressure-driven separation processes like reverse osmosis (RO) and nanofiltration (NF) [1–3]. FO is an osmotically driven membrane separation process, where water molecules are transferred from a dilute feed solution to a more concentrated draw solution through a semi-permeable membrane which selectively rejects a broad range of dissolved contaminants in the wastewater [3]. The driving force for water transport is the chemical potential difference between the draw and feed solutions, thus eliminating the use of hydraulic pressure and consequently enhances energy efficiency [4–6].

Besides being energy efficient, FO process is less prone to fouling as compared to pressure-driven NF and RO processes. However, FO suffers from an enhanced concentration polarization effect inside the support layer known as internal concentration polarization (ICP), where the solvent (commonly water) permeates through the support and dilutes the draw concentration at the inner side of the active layer. The ICP reduces the real driving force for mass transfer, thereby reducing the performance of the FO process, significantly [7, 8]. In addition to ICP, FO suffers from an external concentration polarization (ECP). In fact, in a typical pressure driven process, ECP occurs on one side of the membrane (feed side), whereas in the FO, this phenomenon happens on both sides (feed and draw). The polarization that occurs on the feed side is concentrative and is different in nature from the dilutive polarization on the draw side due to incoming permeate flux. The first polarization is called concentrative ECP and the second one that takes places in the draw side is termed as dilutive ECP. The ICP is not affected by the hydrodynamics of the flow and is more severe than the ECP which makes the theoretical study of transport phenomena in an FO process very challenging.

Early attempts to model the mass transfer through an FO membrane was conducted by Lee et al. [9]. They considered the ICP inside the porous support and developed a model to predict the performance of a pressure retarded osmosis (PRO) process. In the PRO process, which is used for energy generation from an osmotic pressure difference, the membranes are oriented in the exact opposite configuration of FO with the active layer facing the draw solution. Later, Loeb et al. [10] followed the same approach and developed a model for the FO process. McCutcheon et al. [11] coupled the boundary layer film theory to capture the effect of ECP on the active layer as well as the ICP in the porous support for both FO and PRO processes. Suh and Lee [12] fine-tuned this model by considering the dilutive ECP phenomenon on the draw side which was neglected by previous researchers. They suggested that the effect of diluted draw solution on the ECP must be taken into account, particularly for low cross-flow velocities and high water flux. Even though the above models provide a comprehensive framework of relationships for the ICP and ECP on both sides of FO membranes and can predict the flux satisfactorily at a particular flow rate, they are not sufficiently sensitive to a change in the feed flow rate.

The change in water flux with a change in the flow rate is captured by the mass transfer coefficient (k) on either side of the membrane. The mass transfer coefficient is commonly calculated using Sherwood (Sh) number relations which are empirical correlations as a function of Reynolds Schmidt numbers [13]. The Sh number relationships available in the literature were either adapted from the analogy between heat and mass transfer or were derived for flow in

non-porous smooth [13–15]. These relations were later modified for the ultrafiltration (UF) experiments [13, 14]. UF is a pressure-driven process with a different flow hydrodynamics from FO process which is driven by the osmotic pressure gradient. Also, the topology of a typical UF membrane is rougher (on a microscopic scale) and porous than an FO membrane that might affect the Sh number which is a linear function of a frictional factor. Hence, the correlations of Sh number derived from UF experiments may not be valid for the FO process.

Although extensive research has been carried out on the derivation of empirical and semi-empirical Sh number correlations for pressure driven membrane processes (at various operating conditions and spacer geometries) [14, 16, 17], no such efforts have been made to better understand the boundary layer phenomena in an FO process. It is worth mentioning that, based on the film theory the severity of the ECP depends upon the value of mass transfer coefficient. Since the concentration profile in the boundary layer is exponential in nature, a small error in the value of mass transfer coefficient may magnify error to a large extent. Hence, to develop a robust model for the FO process, there is crucial need to find an appropriate correlation of mass transfer coefficient for each specific membrane process with certain hydrodynamic properties of channel and membrane characteristics.

In this chapter an attempt has been made to provide (i) the theoretical background of internal and external concentration polarization phenomena, and (ii) different methods that can be used for the estimation of mass transfer coefficient in the FO process. Since the support layer of a thin film composite FO membrane is made from a porous material (e.g., polysulfone, PSf), having a similar structure and porosity as that of a UF membrane, the literature Sh number correlations might be valid on this side of the membrane. But for the selective layer of the membrane, which is smooth and non-porous, these relationships are not necessarily usable. Hence, more practical methods to get an estimate of the value of mass transfer coefficient on the active side of the membrane in an FO process by (i) RO and (ii) PRO experiments are proposed. These mass transfer coefficients can then be used in the theoretical model to predict the water flux with a change in the feed flow velocity.

2. Theory

2.1. Water flux in FO

Water flux in a pressure-driven membrane separation process is directly proportional to the applied pressure (Δp) and the osmotic pressure difference between the two solutions ($\Delta\pi$) [11].

$$J_w = A(\Delta p - \sigma\Delta\pi) \tag{1}$$

where A is the pure water permeability, and σ is the reflection coefficient which describes the fraction of the solutes reflected or rejected by the membrane. For ideal membranes with no solute transport, its value is unity. In an FO process, no pressure is applied ($\Delta p = 0$) and the

water flux through the membrane is just due to the difference in the osmotic pressures of the draw and feed solutions, given by:

$$J_w = A(\pi_{D,b} - \pi_{F,b}) \tag{2}$$

where $\pi_{D,b}$ and $\pi_{F,b}$ are the osmotic pressures of the draw and feed solutions, respectively.

2.2. Concentration polarization

In an FO operation, the actual flux is far less than the theoretical flux obtained from Eq. (2) which shows a decline in driving force. On the feed side, where the solvent permeates through the membrane, the solutes are retained by the membrane increasing their concentration on the membrane surface that is referred to as concentrative ECP. The permeate entering the draw side dilutes the draw solution at the membrane surface that is known as diluted ECP. **Figure 1(a)** and **(b)** depict concentrative and dilutive ECP, as well as ICP, occurring in FO and PRO processes. Both these phenomena contribute to a decrease in the net osmotic driving force across the membrane and hence lowering the flux.

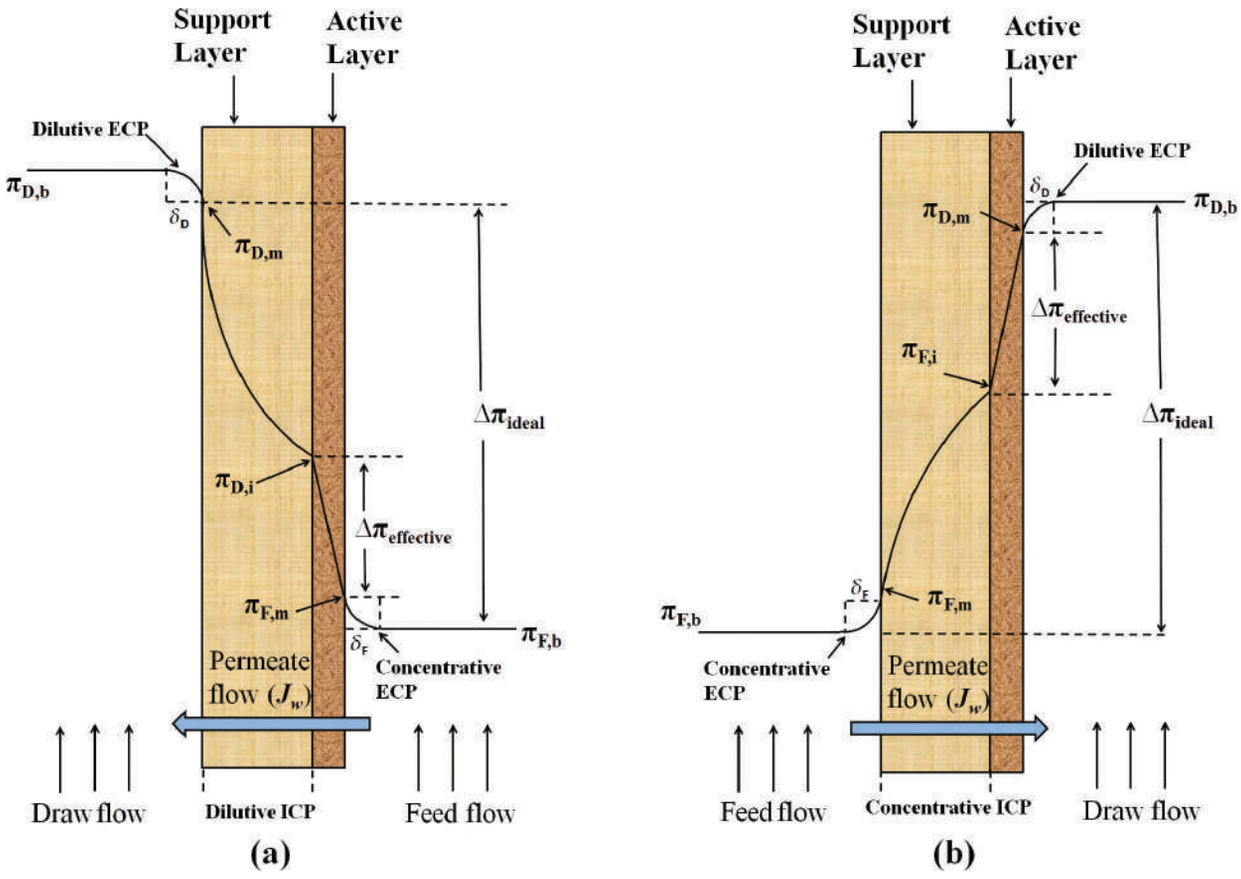

Figure 1. Direction of water flux and the concentration profile developed across the membrane in (a) FO mode and (b) PRO mode.

The ECP can be mitigated by inducing turbulence which enhances the mixing and consequently levels the concentration difference between the bulk and adjacent solution to the membrane surface. However, the concentration polarization in FO is not just limited to ECP. The structure of FO membranes is typically asymmetric, i.e. a thin active layer which governs the molecular transport rate is coated on a porous support that provides mechanical strength. In the FO mode (when active layer and support are facing the feed and draw solutions, respectively), a more severe concentration polarization takes places inside the porous support layer of the membrane, known as ICP. The enhanced dilution of the draw solution inside the porous support contributes to a massive decline in the osmotic pressure difference, thereby decreasing the flux more severely.

2.2.1. Internal concentration polarization

At steady state, the salt leakage (J_s) from the active layer (if the membrane is not perfect) originates from the convective flow of solute ($J_w c$) away from the active layer and diffusive flow of solute $D^{"}dc/dx$ toward the active layer due to concentration gradient inside the porous support [18]:

$$J_s = J_w c - D^{"} \frac{dc}{dx} \tag{3}$$

where c is the concentration of solute at any point inside support layer, $D^{"}$ is the salt diffusion coefficient in the porous support and is given by:

$$D^{"} = \frac{D\varepsilon}{\tau} \tag{4}$$

where D is the diffusivity of solute in water, and ε and τ are the porosity and tortuosity of the support, respectively. Appropriate boundary conditions (as shown in **Figure 2**) are represented as:

$$c = c_{D,i} \text{ at } x = 0$$

$$c = c_{D,m} \text{ at } x = t$$

Applying these boundary conditions a relation for the concentration of solution inside the porous support near the active layer ($c_{D,i}$) is derived as follows:

$$c_{D,i} = \frac{c_{D,m} + J_s/J_w}{\exp(J_w K)} - \frac{J_s}{J_w} \tag{5}$$

where $c_{D,m}$ is the concentration of solution on the support layer adjacent to the bulk solution. Here $K = \tau t/(D\varepsilon)$ is defined as the solute resistivity inside the porous support.

Considering a perfect membrane with 100% salt rejection, the value of J_s can be neglected, and Eq. (5) simplifies to:

$$c_{D,i} = \frac{c_{D,m}}{\exp(J_w K)} \tag{6}$$

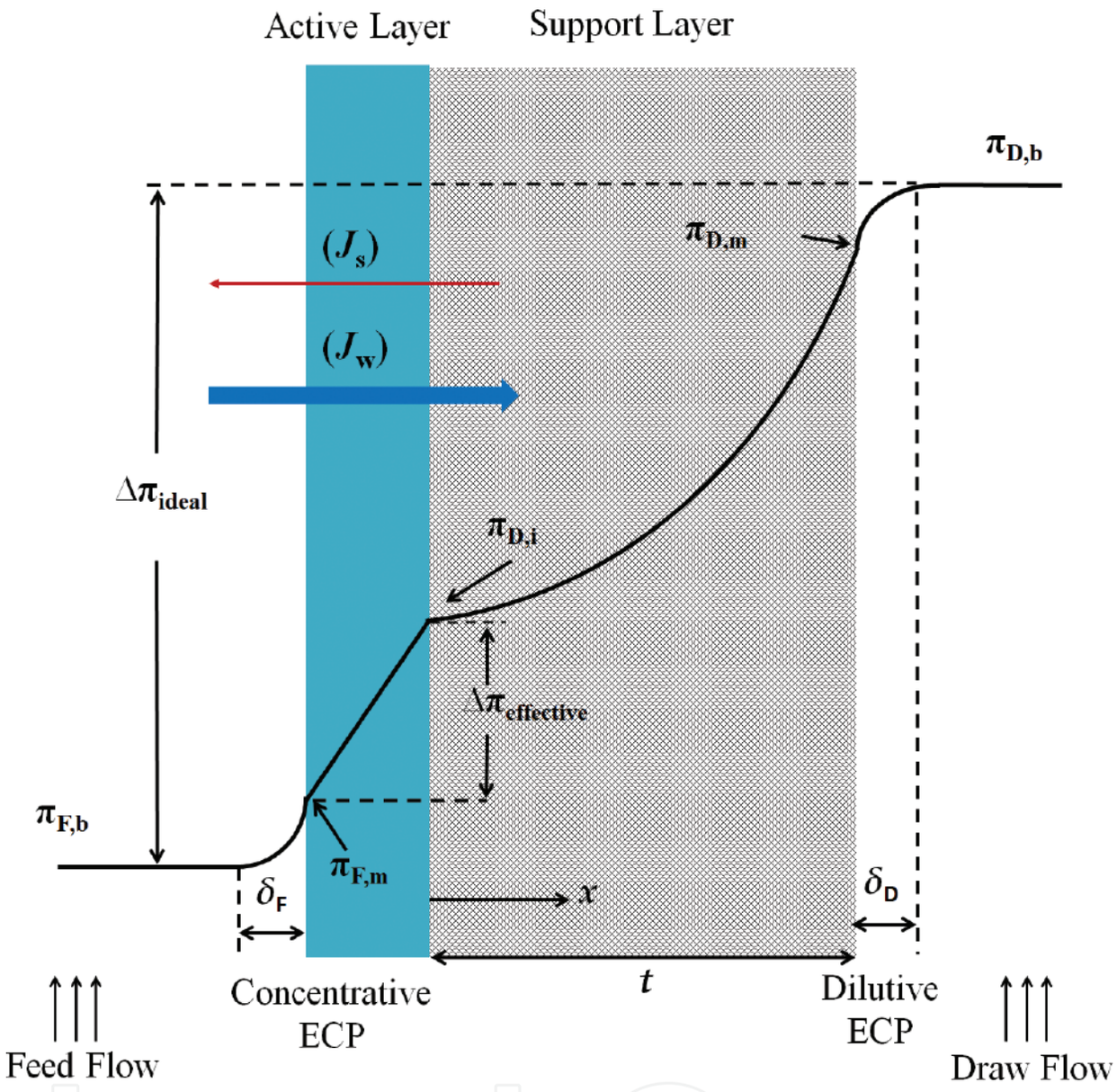

Figure 2. Concentration profiles (considering dilutive ECP) and the concentration boundary thickness developed on both sides of the membrane during an FO osmosis process.

The salt concentration ratio is approximately proportional to the osmotic pressure ratio of the solution, which gives:

$$\pi_{D,i} = \frac{\pi_{D,m}}{\exp(J_w K)} \tag{7}$$

The actual flux is generated by the concentration difference across the active layer of the membrane and is given by [1, 11]:

$$J_w = A(\pi_{D,i} - \pi_{F,m}) \tag{8}$$

Substituting Eq. (7) in Eq. (8), the following equation is obtained for the actual flux through the membrane:

$$J_w = A\left[\pi_{D,m}\exp(-J_w K) - \pi_{F,m}\right] \tag{9}$$

2.2.2. External concentration polarization

The concentrative ECP occurring on the feed side of the membrane can be captured by using the same differential equation and applying appropriate boundary conditions between the membrane surface and bulk solution on the feed side [1, 7]:

$$c = c_{F,b} \text{ at } x = 0$$

$$c = c_{F,m} \text{ at } x = \delta_F$$

where $c_{F,m}$ and $c_{F,b}$ are the concentrations of solute on the membrane surface and in the bulk feed solution, respectively. δ_F is the thickness of concentration boundary layer on the active layer of the membrane. Solving the differential equation and applying the above boundary conditions the following relation is derived for the electrolyte concentration on the membrane surface:

$$c_{F,m} = \left(c_{F,b} + \frac{J_s}{J_w}\right)\exp\left(\frac{J_w \delta_F}{D}\right) - \frac{J_s}{J_w} \tag{10}$$

Again for a high solute rejecting membrane $J_s \approx 0$, hence

$$c_{F,m} = c_{F,b}\exp\left(\frac{J_w \delta_F}{D}\right) \tag{11}$$

D/δ_F in this equation is mass transfer coefficient on the feed side of the membrane (k_F). By replacing the concentrations in Eq. (11) with the corresponding osmotic pressures and substituting this equation into Eq. (9), the following equation for flux is obtained:

$$J_w = A\left[\pi_{D,m}\exp(-J_w K) - \pi_{F,b}\exp\left(\frac{J_w}{k_F}\right)\right] \tag{12}$$

The effect of ICP in the support layer and ECP on the feed side are accounted in Eq. (12). By considering the effect of dilutive ECP on the draw side, a concentration boundary layer forms on the support layer of the membrane and $\pi_{D,m}$ will not be equal to $\pi_{D,b}$. Using appropriate boundary conditions:

$$c = c_{D,m} \text{ at } x = 0$$

$$c = c_{D,b} \text{ at } x = \delta_D$$

The following equation is derived for the concentration of solution on the support layer ($c_{D,m}$).

$$c_{D,m} = \left(c_{D,b} + \frac{J_s}{J_w}\right)\exp\left(-\frac{J_w \delta_D}{D}\right) - \frac{J_s}{J_w} \tag{13}$$

where $c_{D,b}$ is the bulk draw solution concentration and δ_D is the thickness of concentration boundary layer on the porous support. Applying similar assumption of $J_s \approx 0$ and inserting the mass transfer coefficient on the draw side of the membrane as $k_D = D/\delta_D$ we get:

$$c_{D,m} = c_{D,b} \exp\left(-\frac{J_w}{k_D}\right) \tag{14}$$

Finally, the modified flux equation by incorporating the ICP in the support layer and ECP on both sides of the membrane is acquired as follows:

$$J_w = A\left[\pi_{D,b} \exp(-J_w K) \exp\left(-\frac{J_w}{k_D}\right) - \pi_{F,b} \exp\left(\frac{J_w}{k_F}\right)\right] \tag{15}$$

A summary of the main mass transfer equations, boundary conditions, and concentration relations is presented in **Table 1**.

A similar analogy can be applied when the process is operated in the PRO mode. In this mode, the feed and draw solutions face the support and active layers, respectively. Hence, the ECP occurs on the draw side and is dilutive in nature, i.e. the draw solution becomes diluted near the membrane surface by the incoming permeate that leads to a decrease in osmotic driving force. The dilutive ECP phenomenon provides the following relation for the ratio of draw solution concentration on the membrane surface ($c_{D,m}$) and in the bulk solution ($c_{D,b}$) [7]:

$$\frac{c_{D,m}}{c_{D,b}} = \exp\left(-\frac{J_w}{k}\right) \tag{16}$$

where k is the mass transfer coefficient on the draw side of the membrane.

On the feed side of the membrane, the ICP occurs that increases the concentration of salt inside the porous support and makes it concentrative in nature, thus decreasing the driving force. The modulus for concentrative ICP is given by the following relation:

$$\frac{c_{F,i}}{c_{F,b}} = \exp(J_w K) \tag{17}$$

Assumption	Mass transfer equation	Boundary condition	Concentration relations
ICP in the support layer	$J_s = J_w c - D'' \frac{dc}{dx}$	$\begin{cases} x = t, & c = c_{D,m} \\ x = 0, & c = c_{D,i} \end{cases}$	$c_{D,i} = \frac{c_{D,m} + J_s/J_w}{\exp(J_w K)} - \frac{J_s}{J_w}$
ECP on the draw side	$J_s = J_w c - D'' \frac{dc}{dx}$	$\begin{cases} x = 0, & c = c_{D,m} \\ x = \delta_D, & c = c_{D,b} \end{cases}$	$c_{D,m} = \left(c_{D,b} + \frac{J_s}{J_w}\right) \exp\left(-\frac{J_w \delta_D}{D}\right) - \frac{J_s}{J_w}$
ECP on the feed side	$J_s = J_w c - D'' \frac{dc}{dx}$	$\begin{cases} x = 0, & c = c_{F,b} \\ x = \delta_F, & c = c_{F,m} \end{cases}$	$c_{F,m} = \left(c_{F,b} + \frac{J_s}{J_w}\right) \exp\left(\frac{J_w \delta_F}{D}\right) - \frac{J_s}{J_w}$

Table 1. A summary of governing equations and conditions considering both ECP and ICP [12].

where $c_{F,i}$ and $c_{F,b}$ are the concentrations of the feed solution inside the porous support close to the active layer and in the bulk solution, respectively. By incorporating the dilutive ECP and concentrative ICP phenomena in the PRO process, an analytical model, analogous to FO, is obtained as follows:

$$J_w = A\left[\pi_{D,b}\exp\left(-\frac{J_w}{k}\right) - \pi_{F,b}\exp\left(J_w K\right)\right] \tag{18}$$

3. Standard experiments to use the data analysis model

Draw solutions with various concentrations of a particular salt in deionized water are first prepared. Then, the properties of both feed and draw solutions like viscosity, density, diffusion coefficient, and osmotic pressure are measured or taken from literature [19]. The Osmotic pressure of unknown feed and draw solutions can be found experimentally by using automatic osmometers. This instrument estimates the osmotic pressure by measuring the depression in the freezing point of the solution. The osmotic pressure of at least three solutions is measured, and a linear relationship is obtained between the osmotic pressure and the concentration.

The FO experiments are conducted by a cross-flow filtration setup. The schematic diagram of a typical setup is shown in **Figure 3**. The membrane cell has channels on both sides of the membrane for the flow of feed and draw solutions. The length, width, and depth of the channels should be measured precisely for the calculation of mass transfer coefficient. The effective filtration area of the membrane is measured to calculate the water flux. Feed and permeate spacers are typically used on both draw and feed channels in the cell to provide mechanical

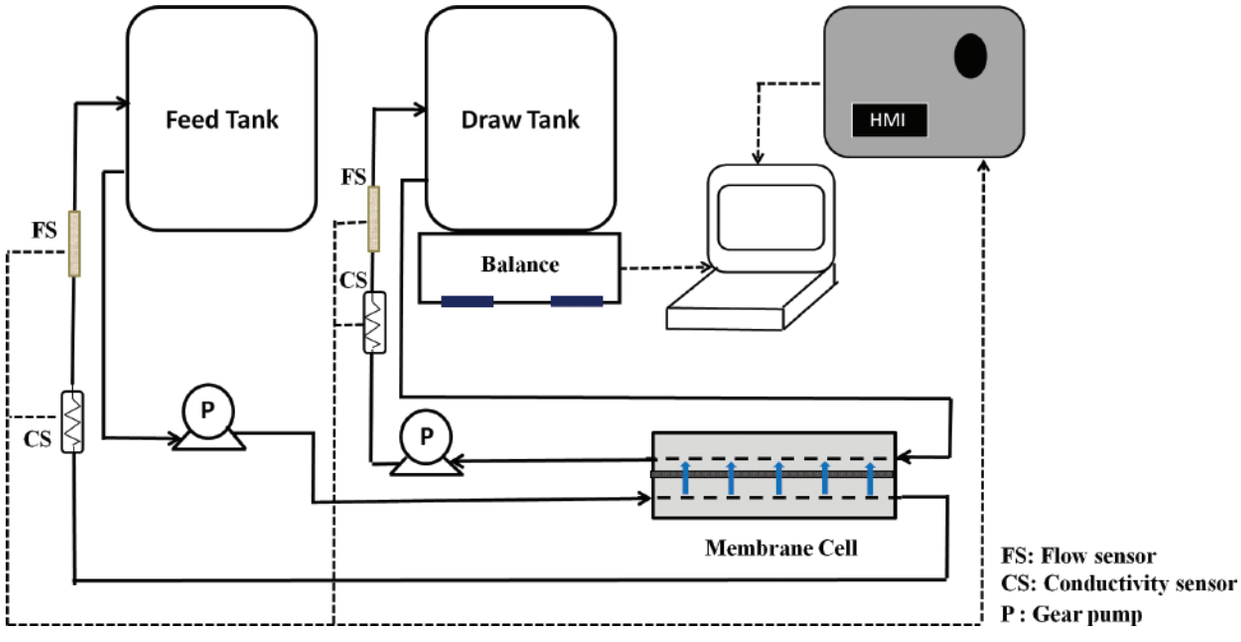

Figure 3. Schematic of a bench scale cross-flow FO setup.

support to the membrane. The feed and draw solution flow rates and the temperature of the experiment are maintained at certain values and are used for the calculation of mass transfer coefficients and osmotic pressure, respectively. The water flux through the membrane can be calculated by recording the change in the weight of the draw solution with time using a weighing scale. During the experiment, the conductivity and temperature of both feed and draw solutions must be monitored.

The same setup but opposite configuration is utilized for the PRO experiments. For both FO and PRO experiments, membranes are needed to be kept in the DI water for about 24 hours before experiments. After mounting the membranes in the module, the flow rates of the feed and the draw solutions are adjusted to desired values. The system is allowed to stabilize, and then the change in weight of the draw solution is recorded over time. Due to the change of draw solution concentration, a certain amount of concentrated draw solution needs to be gradually added to the solution. The conductivity of the draw solution is monitored online, and the addition of concentrated solution stopped when the conductivity of the draw solution reaches to the desired concentration of the solution. A similar procedure needs to be followed to increase the concentration the feed solution.

The pure water permeability of the membrane should be acquired using an RO setup with DI water as feed solution. The water flux is measured at different transmembrane pressures, and the slope is obtained as pure water permeability (A).

4. Estimation of mass transfer coefficient

The value of mass transfer coefficient depends on the hydrodynamics of the flow, applied driving force, water flux through the membrane, characteristics of the membrane (roughness and porosity) and the type of *solute* [14]. In this section, we provide three different methodologies to find the mass transfer coefficient: (i) empirical equations based on Sh number, (ii) pressure-driven method using RO, and (ii) osmotic pressure-driven method using PRO.

4.1. Empirical equations based on Sh number

Mass transfer coefficient is a parameter which describes the ratio between the actual mass (molar) flows of species into or out of a flowing fluid and the driving force that creates that flux. Mass transfer coefficient depends on module configuration, solute diffusion coefficient, viscosity, density, and velocity of feed solution [20]. It is related to the Sh number which shows the ratio of the convective mass transfer to diffusive rate and can be defined as follows [21]:

$$k = \frac{\mathrm{Sh} \cdot D}{d_h} = a\,\mathrm{Re}^b\,\mathrm{Sc}^c \left(\frac{d_h}{L}\right)^d \tag{19}$$

where a, b, c, and d are constants, D is the diffusion coefficient of solute in draw or feed solution, L is the length of the tube or channel, d_h is the hydraulic diameter of channel calculated

by ($2wh/(w + h)$) in which w and h are the width and the height of the channel. *Re* and *Sc* in Eq. (19) are Reynolds and Schmidt numbers, respectively.

$$\mathrm{Re} = \frac{\mathrm{d}_h \cdot v}{\nu} \tag{20}$$

$$\mathrm{Sc} = \frac{\nu}{D} = \frac{\mu}{\rho D} \tag{21}$$

In these equations, ν is the kinematic viscosity, μ is the dynamic viscosity, v is the flow velocity, and ρ is the flow density [20]. The mass transfer coefficient correlations are classified based on the channel flow geometry and various flow regimes in **Table 2**.

Eqs. (22)(a) and (b) are widely used to calculate the mass transfer coefficient in both feed and draw side of FO membrane. However, the implementation of these empirical equations in forward osmosis process has brought some controversial debates. These equations were derived based on ultrafiltration (UF) process which suffers more severely from concentration polarization phenomenon as compared to FO process. Hence, they are not necessarily valid for the evaluation of dilutive and concentrative ECP in FO [20]. Moreover, UF membranes differ from FO ones structurally as the former is porous while the latter is mainly dense composite membranes. Besides, the Sh number is correlated to the frictional factor which might be different for FO and UF processes [14, 19].

It is worth mentioning that Eq. (22)a is only valid where the length of the entry region is equal to $0.029 d_h Re$ while in most lab-scale FO cells the length of the channel is shorter than the entry

Flow geometry	Laminar regime (Re < 2000)-(a)	Turbulent regime (Re > 2000)-(b)	Equation
Rectangular channels w/o spacers	$Sh = 1.85\left(\mathrm{ReSc}\frac{d_h}{L}\right)^{0.33}$	$Sh = 0.04\mathrm{Re}^{0.75}\mathrm{Sc}^{0.33}$	(22)
Rectangular channels w/ spacers	$Sh = 0.46(\mathrm{ReSc})^{0.36}$	$Sh = 0.0096\mathrm{Re}^{0.5}\mathrm{Sc}^{0.6}$	(23)
Tube	$Sh = 1.62\left(\mathrm{ReSc}\frac{d_h}{L}\right)^{0.33}$	$Sh = 0.023\mathrm{Re}^{0.83}\mathrm{Sc}^{0.33}$	(24)
Radial cross flow system	$Sh = 1.05\left(\mathrm{ReSc}\frac{h}{R_c}\right)^{0.38}$	$Sh = 0.275\left(\mathrm{Re}^{1.75}\,\mathrm{Sc}\frac{2h}{L}\right)^{0.33}$	(25)*
Stirred cell	$Sh = 0.23\mathrm{Re}^{0.567}\mathrm{Sc}^{0.33}$	$Sh = 0.03\,\mathrm{Re}^{0.66}\,\mathrm{Sc}^{0.33}\,\mathrm{Pe}_{\mathrm{test}}^{0.16}$	(26)**

*R_c is the radius of the flow channel and h is the half channel height.
**$\mathrm{Pe}_{\mathrm{test}}$ is the test Peclet number which is equal to ($J_w h/D$).

Table 2. Mass transfer coefficient for different flow regimes and geometry [22].

length. Therefore, this equation does not seem to be suitable for investigating the transport phenomena in the lab-scale. Regarding Eq. (22)b, it was derived based on the pressure drop during turbulent flow in RO and UF experiments, whereas in FO process, the pressure drop is insignificant due to the absence of hydraulic pressure [13, 19]. Hence, a significant amount of research is underway to modify the common Sh number equations in the literature. For example, Tan and Ng [19] proposed an exact solution to evaluate the local mass transfer coefficient for the hydrodynamic boundary layer in FO process. The local Sh number was derived from the Navier-Stokes equations for the fluid flow parallel to a flat and non-porous surface as follows:

Laminar boundary layer

$$Sh = 0.332\,\mathrm{Re}_y^{1/2}\,\mathrm{Sc}^{1/3} \quad \mathrm{Re} \le 2\times10^5 \tag{27}$$

Turbulent boundary layer

$$Sh = 0.0292\,\mathrm{Re}_y^{0.8}\,\mathrm{Sc}^{0.33} \quad \mathrm{Re} > 2\times10^5 \tag{28}$$

Hence, mean mass transfer coefficient, k_c, can be obtained as follows:

$$k_c = \frac{\int_0^L k\,\mathrm{d}y}{\int_0^L \mathrm{d}y} = \frac{0.664D\,\mathrm{Re}_t^{1/2}\,\mathrm{Sc}^{1/3} + 0.0365D\,\mathrm{Sc}^{1/3}\left[\mathrm{Re}_L^{4/5} - \mathrm{Re}_t^{4/5}\right]}{L} \tag{29}$$

where, Re_t and Re_L are the transition Reynolds number and Reynolds number at L, respectively, and L is the length of the channel. Experimental investigation showed that the mass transfer coefficient developed from boundary layer concept (k_c) provided more accurate results as compared to that obtained from UF experiments in Eq. (22).

4.2. Evaluating mass transfer coefficient by RO experiment

The film theory is generally applied to capture the effect of the ECP on a membrane surface. Using this theory, the concentration profile near the membrane surface is obtained as a function of permeation flux and mass transfer coefficient:

$$J_w = k\ln\left(\frac{c_m}{c_b}\right) \tag{30}$$

where c_m and c_b are the concentration at the membrane surface and in bulk, respectively. By estimating the concentration at the membrane surface the value of mass transfer coefficient is calculated using Eq. (30). The concentration at the membrane surface can be calculated from the osmotic pressure difference across the membrane. By measuring the water flux and salt rejection in an RO experiment and coupling these with the pure water flux, an estimate of the osmotic pressure difference across the membrane can be made, and consequently, the mass transfer coefficient is calculated by the following equation:

$$k = \frac{1}{J_w}\ln\left(\frac{\Delta\pi}{2R_g T c_b R_j}\right) \tag{31}$$

where R_j is the salt rejection by the membrane, R_g is the universal gas constant, and T is absolute temperature. The detailed procedure to derive Eq. (31) is described elsewhere [23].

4.3. Evaluating mass transfer coefficient in the PRO mode

Using DI water as the feed solution in the PRO mode, the water flux through the membrane can be calculated by a reduced form of Eq. (18) as follows:

$$J_w = A\left[\pi_{D,b}\exp\left(-\frac{J_w}{k}\right)\right] \tag{32}$$

The mass transfer coefficient can be calculated by rearranging this equation.

5. Flux prediction

The current models developed are mainly focused on finding an accurate value of solute resistivity (K), and very less attention has been paid to find a proper value of mass transfer coefficient for FO [7, 11, 12]. There are no direct techniques to determine the value of the structural parameters of a membrane, primarily porosity and tortuosity, so its value is typically evaluated by fitting the experimental data to the transport model [24]. In this technique, the value of K directly depends upon the mass transfer coefficient. Hence, there is a crucial need for finding an accurate value of mass transfer coefficient.

Investigating the current models developed for FO, it was also observed that they are insensitive to a change in the feed flow rate, while our earlier investigations demonstrated that the flux changes moderately with the flow rate [25]. In the previous sections, it was shown that the mass transfer coefficients could be obtained by three methods. Hence, it is suggested that the researchers critically compare the results obtained from the three sets of mass transfer coefficient and utilize the one that increases the sensitivity of the flux results to the feed flow rate.

To start with the modeling of the FO, the hydraulic permeability (A) and salt resistivity of the support layer (K) needs to be determined. The hydraulic permeability of the membrane is determined by the RO setup as discussed earlier. Salt resistivity coefficient depends upon the structural parameters of the membrane, such as porosity, tortuosity, and thickness and on the diffusion coefficient of salt (D). Since the structural parameter is an intrinsic property of the membrane, it is assumed to be constant for a particular membrane [7, 11]. The salt diffusion coefficient is also constant at a specific temperature and is not changing significantly in a narrow range of molarities [26, 27]. Hence, the value of K at a particular temperature is constant and can be evaluated by rearranging Eq. (15). As an example, **Table 3** presents the experimental FO data that is used to determine the value of K for a thin film composite FO membrane. In this experimental research, DI water and NaCl are used as feed and draw solutions, respectively. The detailed properties of the membrane are presented elsewhere [28]. All experiments were conducted at 23°C and the values of mass transfer coefficients obtained

Draw concentration (M)	Osmotic pressure (draw side) (bar)	Feed concentration (M)	Osmotic pressure (feed side) (bar)	Flux (LMH)	K (s/m) × 10^5
1.5	75.4	0.05	2.05	10.2	6.99
1.5	75.4	0.1	4.13	9.0	6.70
1.5	75.4	0.25	10.57	6.4	6.8
1.5	75.4	0.5	21.7	4.2	6.73
1.5	75.4	1.0	47.9	1.5	7.14
Average	—	—	—	—	6.9

Table 3. FO experiments for calculation of K. Tests were conducted at 23°C.

from RO test were used for the calculation of K. As expected, the K values were almost constant for different feed concentrations. Hence, the average K value of 6.9 can be reasonably used for prediction of water flux.

Obtaining hydraulic permeability (A), salt resistivity of the support layer (K), and mass transfer coefficients of both feed and permeate side (k_D and k_F) the model water flux is calculated by Eq. (15). A typical representation of matching between theoretical and experimental results is to plot the model predicted values of water flux along with the experimental values as a function of the driving force (osmotic pressure of the draw solution), as shown in **Figure 4**.

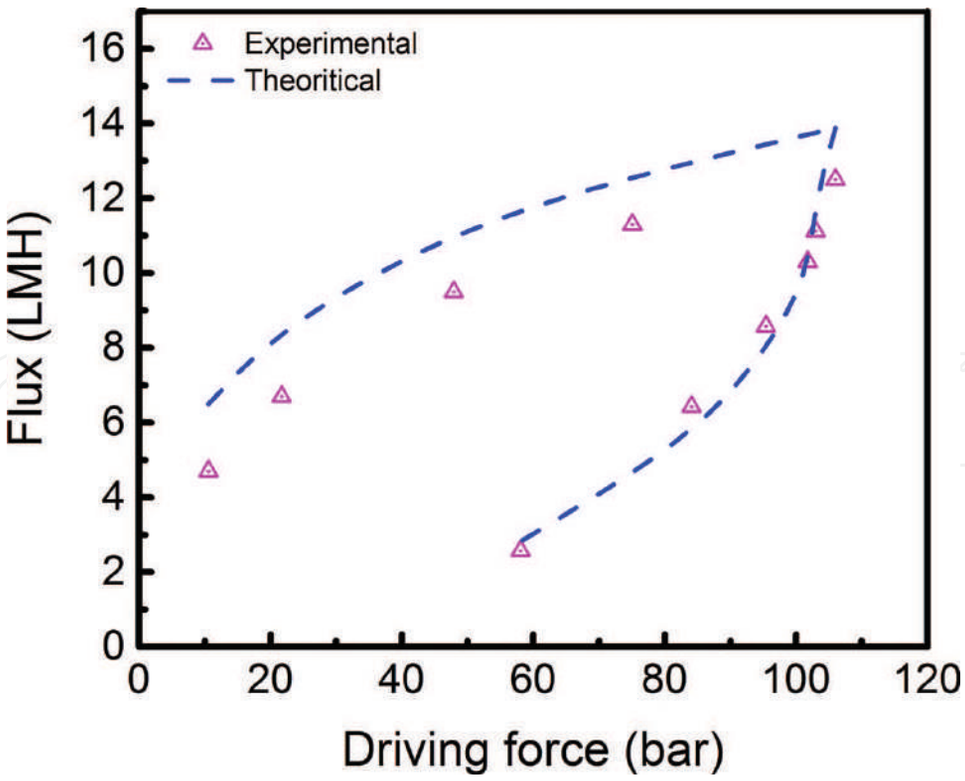

Figure 4. Typical comparison of experimental FO data and predicted fluxes by the model as a function of osmotic driving forces.

Draw concentration	Feed concentration	Experimental flux (LMH)		Theoretical flux (LMH) (*k* from RO experiment)		Theoretical flux (LMH)* (*k* from Sh number in Eq. (22))	
		Feed flow 1 LPM	Feed Flow 3 LPM	Feed flow 1 LPM	Feed flow 3 LPM	Feed flow 1 LPM	Feed flow 3 LPM
0.25 M	0.05 M	3.9	4.5	3.8	4.2	4.1	4.1
0.5 M	0.05 M	5.6	7.7	5.8	6.4	6.1	6.1
1 M	0.05 M	8.7	10.1	8.2	9.0	8.5	8.5
1.5 M	0.05 M	9.9	11.6	9.6	10.6	9.9	9.9

*The value of *K* for this case was found using Eq. (15).

Table 4. The sensitivity of the model to predict change in flux with the change in the values of ***k*** with the experimental results.

It is well known that increasing the feed flow rate increases the water flux through the membrane by enhancing the mixing near the membrane surface, thereby reducing the effect of ECP (concentrative ECP in the case of FO). The change in the flow rate is reflected through the change in the mass transfer coefficient. Hence it is recommended to test the sensitivity of the FO developed model to the variation of feed flow rate. As a case study, the experimental results and the model predictions obtained using two mass transfer coefficients, one from Eq. (22) and the other one from RO tests, are presented in **Table 4**. As can be observed, mass transfer coefficients yield results that match well with experimental data. However, using the values of *k* obtained from Eq. (22), the fluxes were found to be insensitive to flow rates, whereas *k* values evaluated by RO experiment resulted in more reasonable predictions at higher feed flow rate as well.

6. Conclusion

In this chapter, the governing equations of transport through an FO membrane were presented based on the mass balance in the concentration boundary layers on both sides of the membrane (ECP) and inside the support layer (ICP). Although ICP is reported in the literature to play a significant role in the reduction of the effective osmotic driving force, the impact of ECP is usually underestimated. The ECP primarily depends upon the value of mass transfer coefficient (*k*), and the exponential nature of concentration profile in the boundary layer makes ECP very sensitive to the value of *k*. Hence, another theme of this chapter was to provide appropriate methods for the estimation of mass transfer coefficient. Previous studies were all based on using the Sh number correlation developed from the UF experiments to predict the flux in the FO process. The main shortcoming of these studies was the insensitivity of the model predictions to a change in the feed flow rate. Hence other experimental methods based on RO and PRO were proposed to provide a better estimation of mass transfer coefficient. In summary, the results obtained in this study suggest that both

ECP and ICP play a key role in the performance of FO membrane and thus the mass transfer coefficient (*k*) which mainly affects the ECP is as important as solute resistivity (*K)* which is reflected in the ICP effect.

Acknowledgements

The authors gratefully acknowledge the financial support provided by the Natural Sciences and Engineering Research Council of Canada (NSERC) and Canada's Oil Sands Innovation Alliance (COSIA).

Nomenclature

A	pure water permeability ($Lm^{-2}\ h^{-1}\ bar^{-1}$)
B	solute permeability ($Lm^{-2}\ h^{-1}$)
c	concentration of solute ($mol\ L^{-1}$)
d_h	hydraulic diameter (m)
D	diffusion coefficient ($m^2\ s^{-1}$)
n	van't Hoff factor
J	flux ($Lm^{-2}\ h^{-1}$)
k	mass transfer coefficient (ms^{-1})
K	solute resistivity (m)
L	length of channel (m)
p	hydraulic pressure (bar)
R_g	universal gas constant ($Jmol^{-1}\ K^{-1}$)
R_j	salt rejection
Re	Reynolds number
Re_L	Reynolds number at the end of membrane channel
Re_t	transition Reynolds number
Sc	Schmidt number
Sh	Sherwood number
T	absolute temperature (K)

Greek symbols

δ	thickness of ECP boundary layer (m)
ε	porosity of membrane support
μ	dynamic viscosity (Pa.s)
ν	kinematic viscosity ($m^2\ s^{-1}$)
ρ	density of water ($kg\ m^{-3}$)
τ	tortuosity of membrane support
π	osmotic pressure (bar)
σ	reflection coefficient
v	velocity (ms^{-1})

Subscripts

b	bulk solution
D	draw solution
F	feed solution
i	interface between support layer and active layer of membrane
m	membrane surface
s	solute
v	pure water
w	water

Author details

Amrit Bhinder, Simin Shabani and Mohtada Sadrzadeh*

*Address all correspondence to: sadrzade@ualberta.ca

Department of Mechanical Engineering, Donadeo Innovation Center for Engineering, Advanced Water Research Lab (AWRL), University of Alberta, Edmonton, AB, Canada

References

[1] Klaysom C, Cath TY, Depuydt T, Vankelecom IFJ. Forward and pressure retarded osmosis: Potential solutions for global challenges in energy and water supply. Chemical Society Reviews. 2013;**42**:6959-6989. DOI: 10.1039/c3cs60051c

[2] Chung T-S, Li X, Ong RC, Ge Q, Wang H, Han G. Emerging forward osmosis (FO) technologies and challenges ahead for clean water and clean energy applications. Current Opinion in Chemical Engineering. 2012;**1**:246-257. DOI: 10.1016/j.coche.2012.07.004

[3] Cath T, Childress A, Elimelech M. Forward osmosis: Principles, applications, and recent developments. Journal of Membrane Science. 2006;**281**:70-87. DOI: 10.1016/j.memsci.2006.05.048

[4] Hickenbottom KL, Hancock NT, Hutchings NR, Appleton EW, Beaudry EG, Xu P, et al. Forward osmosis treatment of drilling mud and fracturing wastewater from oil and gas operations. Desalination. 2013;**312**:60-66. DOI: 10.1016/j.desal.2012.05.037

[5] Lutchmiah K, Verliefde a RD, Roest K, Rietveld LC, Cornelissen ER. Forward osmosis for application in wastewater treatment: A review. Water Research. 2014;**58**:179-197. DOI: 10.1016/j.watres.2014.03.045

[6] McCutcheon JR, McGinnis RL, Elimelech M. A novel ammonia—Carbon dioxide forward (direct) osmosis desalination process. Desalination. 2005;**174**:1-11. DOI: 10.1016/j.desal.2004.11.002

[7] Mccutcheon JR, Elimelech M. Modeling water flux in forward osmosis: Implications for improved membrane design. AICHE Journal. 2007;**53**:1736-1744. DOI: 10.1002/aic

[8] Mehta GD, Loeb S. Internal polarization in the porous substructure of a semipermeable membrane under pressure retarded osmosis. Journal of Membrane Science. 1978;**4**:261-265. DOI: 10.1016/S0376-7388(00)83301-3

[9] Lee KL, Baker RW, Lonsdale HK. Membranes for power generation by pressure-retarded osmosis. Journal of Membrane Science. 1981;**8**:141-171. DOI: 10.1016/S0376-7388(00)82088-8

[10] Loeb S, Titelman L, Korngold E, Freiman J. Effect of porous support fabric on osmosis through a Loeb-Sourirajan type asymmetric membrane. Journal of Membrane Science. 1997;**129**:243-249. DOI: 10.1016/S0376-7388(96)00354-7

[11] McCutcheon JR, Elimelech M. Influence of concentrative and dilutive internal concentration polarization on flux behavior in forward osmosis. Journal of Membrane Science. 2006;**284**:237-247. DOI: 10.1016/j.memsci.2006.07.049

[12] Suh C, Lee S. Modeling reverse draw solute flux in forward osmosis with external concentration polarization in both sides of the draw and feed solution. Journal of Membrane Science. 2013;**427**:365-374. DOI: 10.1016/j.memsci.2012.08.033

[13] van den Berg GB, Racz IG, Smolders CA. Mass transfer coefficients in cross-flow ultrafiltration. Journal of Membrane Science 1989;**47**:25-51. doi:10.1016/S0376-7388(00)80858-3

[14] Gekas V, Hallstrom B. Mass transfer in the membrane concentration polarization layer under turbulent cross flow. Journal of Membrane Science. 1987;**30**:153-170. DOI: 10.1016/S0376-7388(00)81349-6

[15] Belfort G, Nagata N. Fluid mechanics and cross-flow filtration: Some thoughts. Desalination. 1985;**53**:57-79. DOI: 10.1016/0011-9164(85)85052-9

[16] Koutsou CP, Yiantsios SG, Karabelas AJ. A numerical and experimental study of mass transfer in spacer-filled channels: Effects of spacer geometrical characteristics and Schmidt number. Journal of Membrane Science. 2009;**326**:234-251. DOI: 10.1016/j.memsci.2008.10.007

[17] Rodrigues C, Rodrigues M, Semiao V, Geraldes V. Enhancement of mass transfer in spacer-filled channels under laminar regime by pulsatile flow. Chemical Engineering Science. 2015;**123**:536-541. DOI: 10.1016/j.ces.2014.11.047

[18] Phillip WA, Yong JS, Elimelech M. Reverse draw solute permeation in forward osmosis: Modeling and experiments. Environmental Science and Technology. 2010;**44**:5170-5176. DOI: 10.1021/es100901n

[19] Tan CH, Ng HY. Modified models to predict flux behavior in forward osmosis in consideration of external and internal concentration polarizations. Journal of Membrane Science. 2008;**324**:209-219. DOI: 10.1016/j.memsci.2008.07.020

[20] Mulder M. Basic Principles of Membrane Technology. 2nd ed. Dordrecht: Kluwer Academic; 1996. DOI: 10.1007/978-94-009-1766-8

[21] Heldman DR, Moraru CI. Encyclopedia of Agricultural, Food, and Biological Engineering. 2nd ed. New York: Taylor & Francis; 2010. DOI: 10.1081/E-EAFE2

[22] Wang J, Dlamini DS, Mishra AK, Pendergast MTM, Wong MCY, Mamba BB, et al. A critical review of transport through osmotic membranes. Journal of Membrane Science. 2014;**454**:516-537. DOI: 10.1016/j.memsci.2013.12.034

[23] Al Mamun MA, Sadrzadeh M, Chatterjee R, Bhattacharjee S, De S. Colloidal fouling of nanofiltration membranes: A novel transient electrokinetic model and experimental study. Chemical Engineering Science. 2015;**138**:153-163. DOI: 10.1016/j.ces.2015.08.022

[24] Manickam SS, Mccutcheon JR. Model thin film composite membranes for forward osmosis: Demonstrating the inaccuracy of existing structural parameter models. Journal of Membrane Science. 2015;**483**:70-74. DOI: 10.1016/j.memsci.2015.01.017

[25] Bhinder A, Fleck BA, Pernitsky D, Sadrzadeh M. Forward osmosis for treatment of oil sands produced water: Systematic study of influential parameters. Desalination and Water Treatment. 2016;**57**:22980-22993. DOI: 10.1080/19443994.2015.1108427

[26] Lobo V. Mutual diffusion coefficients in aqueous electrolyte solutions. Pure and Applied Chemistry. 1993;**65**:2613-2640. DOI: 10.1351/pac199365122613

[27] Vitagliano V, Lyons PA. Diffusion coefficients for aqueous solutions of sodium chloride and barium chloride. Journal of the American Chemical Society. 1956;**76**:1549-1552. DOI: 10.1021/ja01589a011

[28] Khorshidi B, Bhinder A, Thundat T, Pernitsky DJ, Sadrzadeh M. Developing high throughput thin film composite polyamide membranes for forward osmosis treatment of SAGD produced water. Journal of the American Chemical Society. 2016;**511**:29-39. DOI: 10.1016/j.memsci.2016.03.052

IntechOpen

Chapter 5

Temperature Effect on Forward Osmosis

Sangwoo Shin and Albert S. Kim

Additional information is available at the end of the chapter

http://dx.doi.org/10.5772/intechopen.72044

Abstract

Forward osmosis, or simply, osmosis, refers to a process by which a solvent moves across a semipermeable membrane due to the difference in the solute concentration established across the membrane. Because of its spontaneous nature, forward osmosis has received immense attention during the last few decades, particularly for its diverse applications, which include municipal wastewater treatment, seawater desalination, membrane bioreactor, potable water purification, food processing, drug delivery, energy generation, and so forth. Of many parameters that determine the performance of the forward osmosis process, the most fundamental factor that impacts performance is temperature. Considering the importance of the temperature on the forward osmosis process, there have been only a limited number of studies about the effect of temperature on the osmosis-driven process. In this chapter, we discuss the temperature effect on the forward osmosis process from two main aspects. First, we provide an extensive and in-depth survey on the currently available studies related to the anisothermal osmosis phenomena. Second, we then discuss a state-of-the-art theoretical framework that describes the anisothermal forward osmosis process that may shed light on achieving an enhanced performance via temperature control.

Keywords: forward osmosis, temperature, thermal effect, concentration polarization, water flux, solute flux, membrane scaling

1. Introduction

Osmosis, one of the most fundamental transport processes responsible for homeostasis in living organisms, has a rich history of applications—ranging from food preservation to water treatment and drug delivery. Osmosis occurs when a solute concentration difference is established across a semipermeable membrane. Due to the chemical potential imbalance, the water molecules will spontaneously migrate across the membrane toward the higher solute concentration side. Such a process has been regarded as one of the most central mechanisms that dictates the

membrane-based water treatment technologies. The most widely utilized process, in our opinion, is reverse osmosis (RO) for solute removal, which requires an external hydraulic pressure to overcome the osmotic pressure difference across the membrane. In contrast to RO, the process that exploits the spontaneous transport of solvent molecules driven by the osmotic phenomenon is referred to as forward osmosis (FO) or direct osmosis (DO), which is, in principle, the same as the original osmosis.

FO was first conceptualized by Batchelder as a means for water treatment since the 1960s [1]. Since then, there has been a growing interest in applying FO to wastewater treatment technologies either as a stand-alone or in combination with other technologies such as membrane distillation, thermal distillation, or reverses osmosis [2]. Particularly, FO has been utilized in space stations for wastewater reclamation due to its excellent long-term stability and low energy consumption [3, 4]. Not limited to wastewater treatment, FO has also been explored extensively for many useful applications such as seawater desalination [5–7], portable hydration bags [8], food processing [9–11], pharmaceutical systems [12–14], and energy conversion [15, 16].

Unlike RO, FO is purely an osmosis-driven process, which is thermodynamically spontaneous. The osmotic pressure difference $\Delta\pi$, which is a driving force for the FO process, may be expressed using van't Hoff's law as

$$\Delta\pi = RT\Delta C \tag{1}$$

for weakly interacting molecules, where ΔC is the solute concentration difference, R is the gas constant, and T is the temperature. From the equation, it can be noted that the temperature is one of the most critical factors determining the rate of osmosis. In addition, temperature further changes viscosity, diffusivity, and density, which are important parameters in momentum and energy transfer phenomena. Despite the importance of temperature on FO process and despite the fact that there exist a number of papers that address the temperature effect, the reported data are widely scattered and does not show an agreeable consensus. In this chapter, we aim to provide a holistic understanding of the temperature effect on an osmotic phenomenon. Our intention is not to give an exhaustive review of the FO process in detail but to focus on the temperature effect and hopefully to provide insight for better control over the osmotic phenomenon. Readers who wish to learn about the FO process more in detail may refer to the following review papers [2, 8, 17].

2. Operating principle

2.1. Mechanism

In the FO process, the solvent (water) transport is driven solely by osmotic pressure difference without the need of any external hydrostatic pressure, allowing for lower energy consumption compared to RO. To extract water from the feed solution, the osmotic pressure at the opposite side of the membrane must be higher, which requires a highly concentrated solution; this concentrated solution is typically referred to as the draw solution. Draw solutes need to be

inert and easily removable. A semipermeable membrane separates the feed solution and the concentrated draw solution where the chemical potential difference allows the water to flow through the membrane while leaving behind the solutes in the feed stream. Regions of high and low solute concentrations refer to those of low and high solvent chemical potentials, respectively. As the semipermeable membrane restricts the solute transport and maintains chemical potential differences of both solute and solvent, water migrates from its high solvent chemical-potential region (i.e., of low solute concentration) to low solvent chemical-potential region (i.e., of high solute concentration). Such a water transport leads to dilution of the draw solution where the diluted draw solution can be further recycled such that the initial solute concentration is recovered. Particularly for desalination applications, the solutes in the draw solution (osmotic agent or draw solutes) are chosen to be inert, nontoxic, and easily removed to obtain the desalinated water with ease. One example includes NH_4CO_2, which can be easily removed by decomposing at a moderately elevated temperature (~60°C) followed by low-temperature distillation [18, 19]. Extra energy is, however, necessary to re-dissolve NH_4CO_2 into the draw solution for a continuous FO operation.

2.2. Concentration polarization

The water flux across the membrane results in concentration of the feed solution and dilution of the draw solution since the membrane mainly allows passage of water molecules. This phenomenon, referred to as concentration polarization (CP), has an adverse impact on the efficacy of the FO process since such an effect reduces the effective osmotic pressure difference across the membrane, thus hindering water transport.

CP is highly influenced by the morphology of the membranes. The membranes used in the FO process consist of a thin, dense layer that rejects the solutes (active layer) followed by a coarse, thick porous layer (support layer or porous substrate) to reinforce the mechanical stability against fluid pressure and shear. This configuration makes the membrane asymmetric in which the orientation of the membrane with respect to the direction of the water flux (i.e., from low to high osmotic pressure) leads to significantly different transport dynamics [20].

Typically in the FO process, the active layer is placed against the feed stream in order to minimize fouling since the support layer is more susceptible to colloidal fouling due to the large pores. This configuration is called FO mode, as shown in **Figure 1(a)**. However, the downside of placing it in this way is that there is a significant dilutive internal concentration polarization (ICP) in the thick porous substrate. This is because the support layer is in contact with the concentrated draw solution hindering the solute diffusion, which significantly reduces the water flux (**Figure 1(a)**).

In contrast, when the active layer is placed against the draw stream, one can expect a higher water flux since this configuration can avoid the dilutive ICP at the expense of accelerated membrane fouling. This configuration is called the pressure-retarded osmosis (PRO) mode, as shown in **Figure 1(b)**, typically realized in standard PRO systems. To avoid any confusion, we will refer to the membrane configuration in which the active layer is placed against the feed solution as the *FO mode*, whereas the opposite case is the *PRO mode* during FO processes.

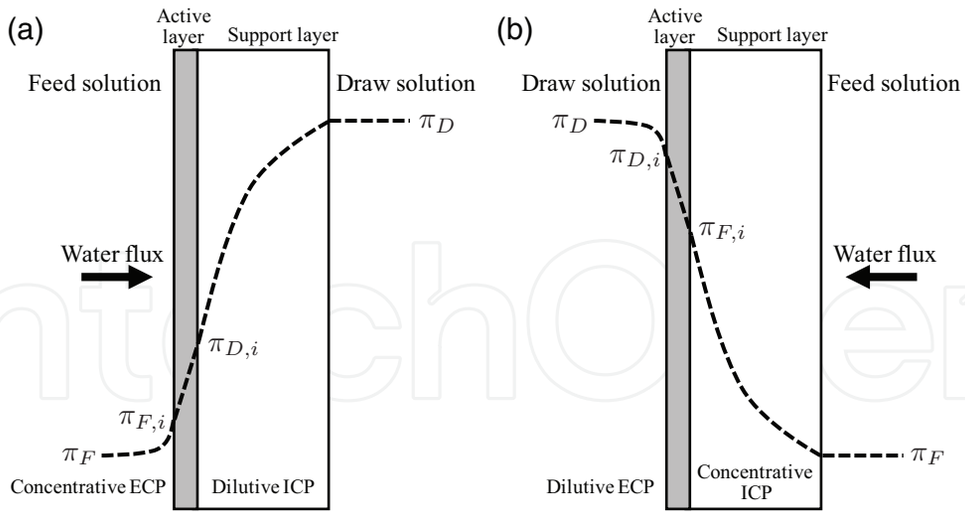

Figure 1. Influence of CP on the osmotic pressure distribution in the FO process. The membrane is configured in (a) FO mode and (b) PRO mode.

3. System temperature effect on FO

The first quantitative experiments on temperature-dependent osmosis go back almost a century ago [21]. Traxler demonstrated the osmosis of pyridine by using a thin rubber sheet as a semipermeable membrane within a uniform system temperature, ranging from 5 to 85°C (**Figure 2(a)**). He showed that as the temperature is increased, the transport of pyridine across the membrane is also increased (**Figure 2(b)**). In this chapter, such a uniform temperature will be refered to as 'system temperature' indicating the absence of local or transmembrane temperature gradient.

From the van't Hoff equation, the osmotic pressure is directly proportional to the system temperature, which is an indispensable factor for the FO process. However, temperature not only influences the osmotic pressure but also impacts many other key properties that are important to the transport process such as viscosity, diffusivity, solubility, density, and so forth. Such a change in the properties not only influences the water flux but also alters the solute rejection/diffusion and membrane fouling. In this section, we provide a summary of how the system temperature influences the water transport, solute rejection, and membrane fouling. We note that the experimental studies that will be covered in the following sections employ a circulating crossflow type setup (in contrast to a dead-end type as seen in Traxler's experiments in **Figure 2**).

3.1. Water flux

The most direct consequence of raising the system temperature is the increased water flux across the membrane due to lowered water viscosity and increased water diffusivity, which effectively increases the water permeability across the membrane. Since the transport of water through the active layer of the membrane follows the solution-diffusion mechanism [22], it is

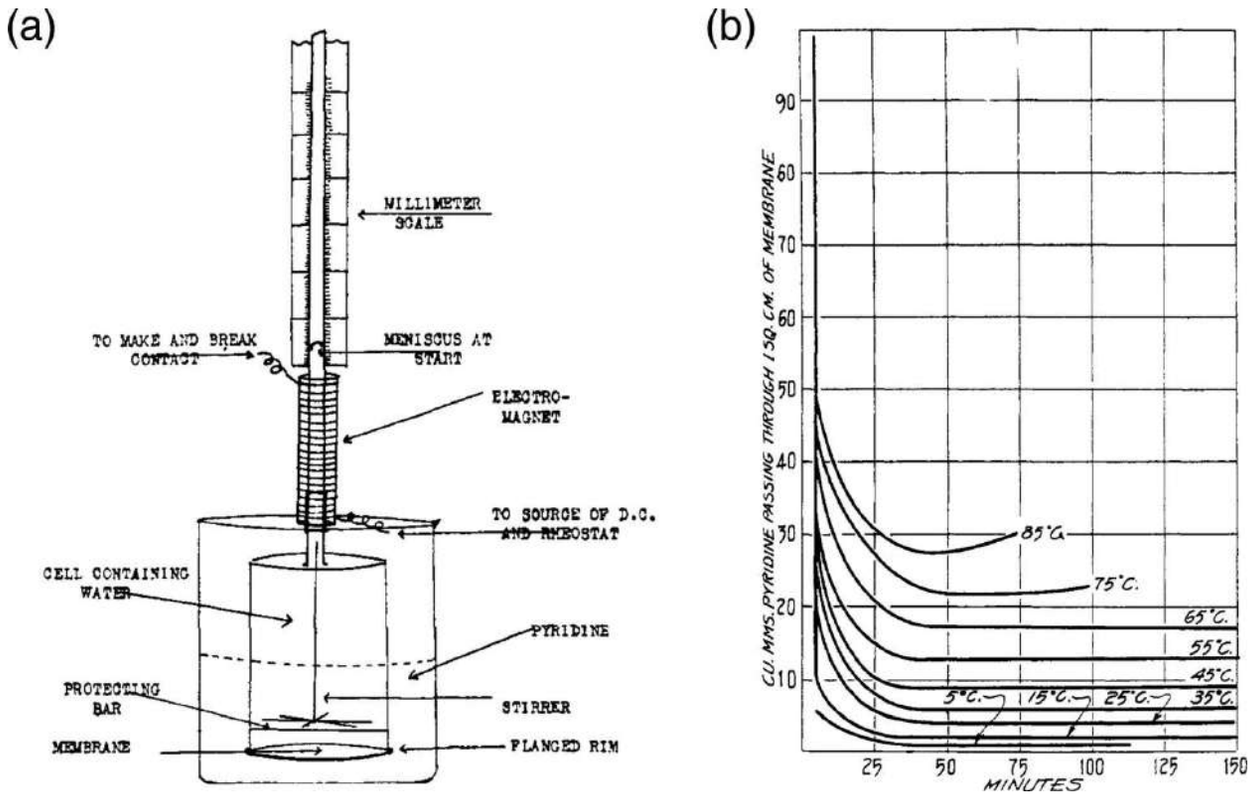

Figure 2. The first quantitative experiments reported on the effect of temperature on the osmosis phenomenon. (a) A schematic of the experimental setup that allows temperature control via a thermostat. (b) Transport of pyridine across a rubber membrane under various temperature conditions. Reprinted with permission from Ref. [21]. © 1928 American Chemical Society.

commonly believed (and also observed) that the diffusivity D exhibits an Arrhenius relation, that is, $D \sim \exp(-s/T)$, where s is an empirical constant related to the activation energy [23, 24]. However, we also note a counterexample where Petrotos et al. failed to show such a behavior [25].

On the basis of our survey, the available literature related to the temperature-dependent FO reported increased water flux with temperature. **Table 1** provides a summary of experimental conditions and resulting water flux from the available literature [23–31]. Here, we define a new quantity to indicate how much solvent flux increases with respect to the system temperature, as indicated in the last column of **Table 1**:

$$j_M = \frac{J_{w,M} - J_{w,0}}{T_M - T_0}, \tag{2}$$

where $J_{w,M}$ and $J_{w,0}$ are the water fluxes at a given maximum system temperature T_M and at base temperature T_0, respectively. The survey shows that raising the temperature does increase the water flux, but the extent of such an increase varies across the literature, especially depending on the membrane orientation. This observation implies that the CP phenomena are uniquely influenced by the temperature, leading to variations in the water flux.

Reference	Feed solution (concentration)	Draw solution (concentration)	Membrane[1]	Mode[2]	Temperature (°C)	$J_{w,0}$ (LMH)	j_M[3] (LMH/°C)
[25]	Tomato juice (0.13 M)	NaCl (3.9 M)	PA		26–58	1.5	0.030
[26]	NaCl (0–86 mM)	KCl (0.5–3 M)	CT	FO	25–45	19	0.43
[27]	Deionized water	NaCl (0.5 M)	CT		20–40	5.5	0.14
			PA			17	0.49
[23]	Sucrose (0–1.65 M)	NaCl (2–4 M)	CT		20–30	24	0.91
	Sucrose (0–0.7 M)	NaCl (4 M)	PA			2.5	0.15
[28]	NaCl (0.1 M)	NaCl (1 M)	CT	PRO	20–40	11	0.89
				FO		9.4	0.59
[29]	NaCl (0–1 M)	NaCl (1.5 M)	CT	PRO	20–40	43	1.4
				FO		18	0.63
[24]	NaCl (60 mM)	Na_2SO_4 (1.5 M)	CT		25–45	15	0.35
[30]	NaCl (0.2–0.5 M)	NH_4HCO_3 (3 M)	CE	PRO	30–50	5.4	0.10
[31]	Deionized water	NaCl (1.2 M)	CT	FO	20–30	14	0.61

[1]PA: polyamide; CT: cellulose triacetate; CE: cellulose ester
[2]FO mode: active layer placed against feed solution; PRO mode: active layer placed against draw solution
[3]$j_M = J_{w,M} - J_{w,0} / T_M - T_0$; $J_{w,M}$: water flux at maximum temperature T_M; $J_{w,0}$: water flux at base temperature T_0

Table 1. A summary of influence of temperature on the water flux.

McCutcheon and Elimelech were the first to study the influence of temperature on the CP phenomena [29]. Raising the temperature increases the water flux because of the decreased water viscosity in solutions (and/or solubility) and increased water solubility and diffusivity within the membrane. At the same time, however, the higher flux also increases both the ICP and ECP, which essentially limit the water flux as a feedback hindrance. Therefore, such a self-limiting behavior driven by two counteracting effects leads to the fact that the temperature has a "modest" effect on the water flux at high water flux conditions [29]. This self-hindering effect of the solvent flux is unavoidable in most membrane separation processes. It is similar to the fact that, in RO, applying high pressure initiates increasing permeate flux, which will eventually bring more solutes from the bulk phase to the membrane surface, enhancing the CP. Therefore, additional gain of the RO permeate flux is not as much as anticipated when the pressure is increased.

The change in the temperature influences the CP phenomena in different ways depending on the orientation of the membrane. This is because the formation of the ICP, which is the most critical factor that limits the driving force, is dependent on the membrane configurations. In the PRO mode, the concentrative ICP is developed in the feed side (see **Figure 1(b)**). By reducing the ICP using deionized water as the feed, the water flux was shown to be highly dependent on the temperature, confirming the impact of ICP on the FO process [29].

In the presence of solutes in the feed side so that the ICP is present, however, the water flux was shown to be almost insensitive to the temperature, at least in the operating temperature range (20–40°C). This behavior is attributed to the coupled interaction between ICP and ECP.

Although the increased solute diffusion at higher temperature mitigates the concentrative ICP in the support layer so that the water flux can be increased, such an increased water flux carries more solutes from the feed bulk phase to the vicinity of the support layer surface and enhances the dilutive ECP, thereby reducing the osmotic driving force. Therefore, the two opposing effects on the water transport effectively limit the enhancement of the water flux such that the temperature has a marginal effect on the overall water flux. If both water and solute diffusivities increase in a similar behavior, the net diffusive transport must be more or less the same.

In the FO mode, however, the water flux was shown to be significantly influenced by the temperature. Overall, the water flux was observed to be lower than the PRO mode due to the presence of the dilutive ICP. This was proven mathematically using the method of proof by contradiction [32]. Such a low water flux effectively suppresses the extent of concentrative ECP in the feed side. Also, the influence of concentrative ECP on the water flux is less important than the dilutive ECP in the draw solution side because the initial solute concentration in the bulk phase is much lower at the feed solution than the draw solution. This implies that the ECP has a minor effect on the driving force in the FO mode. Therefore, when the membrane is placed in the FO mode, the water flux is significantly influenced by the temperature since the ICP is the only major factor that determines the driving force.

One assumption McCutcheon and Elimelech had made while analyzing their data were the insignificant solute diffusion across the membrane [29], which otherwise leads to further ICP. Obviously, commercially available membranes are known to permit diffusion of the solutes, which can impact the formation of the CP effect. Since the solute diffusion is also sensitive to the temperature, the transmembrane solute flux should also lead to a change in the water flux. We discuss the effect of temperature on the solute diffusion and rejection in the following section.

3.2. Diffusion and rejection of solutes

It is of general consensus that the transmembrane solute diffusion increases with temperature. A number of groups have recently investigated experimentally the temperature effect on the transmembrane solute diffusion and the solute rejection [26–28].

Xie et al. recognized that the effective size of the solute molecules was the most important parameter for the transmembrane solute diffusion [27], which was predicted theoretically using the integral equation theory [33]. Hydration of charged organic solutes results in an increase in the effective solute size, which directly influences the solute diffusion and rejection rate, as it was well understood that the rejection of the charged organic solutes would be much higher than the neutral organic solutes. In this regard, neutral solutes were more likely to diffuse across the pores than the charged solutes in both the cellulose triacetate membranes and polyamide membranes. This implies that increasing the temperature leads to higher solute diffusion due to the increased solute diffusivity. Moreover, increasing the temperature leads to faster dissolution of the solutes into the membrane such that even hydrophobic neutral solutes absorb into the membrane at an order of magnitude higher rate at elevated temperatures.

Notably, the ratio between the water flux J_w and the solute flux J_s was shown to be more or less constant regardless of the system temperature [27]. Such a constant ratio implies that the

structural properties may not change, at least in the operating temperature range (20–40°C). In fact, although it is documented in the literature that the RO membrane properties such as pore sizes may change when the temperature is above 40°C [34], it was reported in various FO studies that the membrane structural properties do not change significantly below 45°C [26, 27]. However, it is more reasonable to say that the structural properties of FO membranes change with temperature in a way that the ratio between solvent and solute fluxes remain almost constant. In a solution-diffusion model, permeabilities of solvent and solutes, A and B, respectively, are believed to increase with membrane temperature. The permeate concentration is controlled by only their ratio, A/B. If A and B increase with T while A/B remains less sensitive to T, then the solute diffusion can be seen phenomenologically insensitive to temperature. This is because although higher T increases both the solute and solvent fluxes, it is only the ratio that influences the concentration of solutes passing through the membrane. This topic is discussed theoretically in detail in Section 5.

Meanwhile, You et al. showed that the transmembrane solute diffusion was also shown to be dependent on the membrane orientation regardless of the temperature in which the PRO mode was shown to exhibit higher solute flux across the membrane than the FO mode, which is similar to the behavior of the water flux [28].

3.3. Membrane scaling

Membrane scaling occurs when the solute concentration is high enough to initiate precipitation. This is directly related to solute rejection and the CP phenomena, implying that membrane scaling should also be temperature-dependent.

Zhao and Zou studied how the temperature influences the membrane scaling over time, which is important in long-term operations [24]. Due to the fast water flux at elevated temperature,

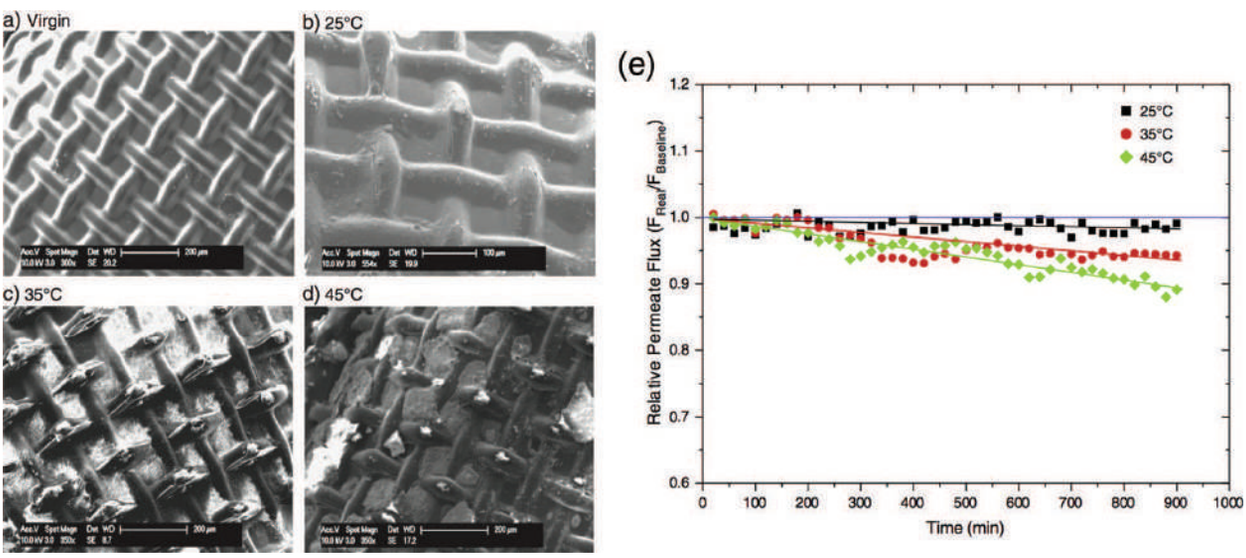

Figure 3. Temperature-dependent membrane fouling and associated water flux decline. (a–d) Scanning electron microscope images of the (a) virgin and (b–d) fouled membranes at various temperatures; (b) 25°C; (c) 35°C; (d) 45°C; and (e) water flux ratio over time at each temperatures. Reprinted with permission from Ref. [24]. © 2011 Elsevier.

increase in the final concentration of the feed solution (i.e., concentration after 28 hours of running) was accelerated by more than 100% when the temperature was raised from 25 to 45°C, which led to faster membrane scaling. Concentrative polarization is also enhanced when the water flux is increased, which results in an accelerated membrane scaling. This was confirmed by directly visualizing the fouled membrane by using a scanning electron microscope (**Figure 3(a)–(d)**) and also by measuring the decrease in flow rate over time (**Figure 3(e)**), showing faster decline of water flux over time at elevated temperatures due to the scaling. In addition to higher solute concentration near the membrane surface driven by the temperature-enhanced solvent flux, the changes in solubility limits for inorganic species may contribute to the accelerated fouling behavior.

4. Transmembrane temperature gradient in FO

One step further, we can also consider a case where the temperature is unevenly distributed across the membrane. In such a case, the temperature gradient may allow independent control of transport on either side of the membrane. In practice, temperature gradients can occur frequently; temperature of the feed solution can increase due to the heat released from the hydraulic pumping or when the solution is pretreated. Likewise, the temperature of the draw solution may change due to the post-treatment process for recovery and recycling of draw solutes such as thermal and membrane distillation. Since heating only on one side of the solution requires lower energy than heating up the entire system, imposing a temperature gradient across the membrane may offer an energy-efficient control over the osmotic phenomena.

In the presence of a temperature gradient, van't Hoff's law (of Eq. (1)) cannot be used directly to calculate the osmotic pressure difference since it relies on the assumption of the constant system temperature. A full theory accounting for the temperature gradient in osmosis may result in highly nonlinear effects on the FO performance. Furthermore, the temperature gradient may provide an additional complexity to the coupled mass and heat transfer phenomena within the membrane. In this section, we provide a summary of how the temperature difference between the feed and the draw solution influences the FO performance, including the water transport and solute diffusion/rejection.

4.1. Water flux

Although the temperature dependence on the water flux shows an agreeable consensus as shown in **Table 1**, the anisotropic temperature effect is shown to differ largely across various studies. When the temperature on either side of the solutions is increased, the water flux becomes higher than that at the base temperature, but lower than when the temperatures of both sides of the solutions are increased. It is, however, left unclear which side of the solution has more influence on the FO process when heated as this does not have an agreeable consensus. **Table 2** provides a summary of the effect of temperature difference on the FO process under various experimental parameters. For simplicity, we define

$$j_F = \frac{J_{w,MF} - J_{w,0}}{T_{MF} - T_0} \tag{3}$$

and

$$j_D = \frac{J_{w,MD} - J_{w,0}}{T_{MD} - T_0} \tag{4}$$

as included on the right-hand side of **Table 2**. Eqs. (3) and (4) refer to the water flux increase per temperature change when the *feed side* or the *draw side* is heated only, respectively. Phuntsho et al. calculated using a commercial software (OLI Stream Analyzer) where the osmotic pressure difference across the membrane can be higher when the draw side is heated in contrast to heating the feed side [26]. However, the temperature difference not only changes the osmotic pressure difference but also gives spatial nonlinearity to other important transport properties such as the solution viscosity as well as solvent/solute diffusivity in bulk phases and their solubilities in the membrane phase, which may impact the CP phenomena in various ways depending on the membrane orientation.

In general, regardless of either the feed or draw, raising the temperature on either side leads to increase in both the water flux and the solute flux. Xie et al. stated that raising the feed solution temperature leads to enhanced diffusivity of the water molecules, whereas raising the draw solution temperature leads to decreased draw solution viscosity and increased draw solute diffusivity, both of which lead to increased water flux and reverse solute flux [27]. However, the degree to which the water flux and solute flux are increased varies across the literature [10, 26–28, 31, 35, 36] (see **Table 2**).

Reference	Feed solution	Draw solution	Membrane	Mode	Temperature (°C)	$J_{w,0}$ (LMH)	j_F [1] (LMH/°C)	j_D [2] (LMH/°C)
[10]	Pineapple juice (0.37 M)	Sucrose (40 wt%)+NaCl (12 wt%)	CT		25–45	1.2	0.045	
[26]	NaCl (0–86 mM)	KCl (0.5–3 M)	CT	FO	25–45	19	0.048	0.12
[27]	Deionized water	NaCl (0.5 M)	CT		20–40	5.5	0.045	0.065
			PA			17	0.125	0.175
[35]	NaCl (0–0.5 M)	NH_4HCO_3 (1–4 M)	CT	PRO	25–45	2.5		0.028
				FO		1.9		0.018
[28]	NaCl (0.1 M)	NaCl (1 M)	CT	PRO	20–40	11	0.54	0.19
				FO		9.4	0.41	0.18
[36]	Anthocyanin (24 μM)	NaCl (6 M)	CT	PRO	25–40	4.9	0.013	
				FO		13	0.53	
[31]	Deionized water	NaCl (1.2 M)	CT	FO	20–30	14	0.22	0.54

[1] $j_F = J_{w,MF} - J_{w,0} / T_{MF} - T_0$; Feed side heated. $J_{w,MF}$: water flux at the maximum feed temperature T_{MF}.
[2] $j_D = J_{w,MD} - J_{w,0} / T_{MD} - T_0$; Draw side heated. $J_{w,MD}$: water flux at the maximum draw temperature T_{MD}.

Table 2. A summary of influence of temperature difference on the water flux.

Phuntsho et al. showed that increasing the *draw solution* temperature resulted in more water flux compared to increasing the temperature of the feed solution [26]. Their membrane was oriented in the PRO mode where the active layer was facing the draw solution. They argued that increasing the draw temperature led to reduced solution viscosity and increased draw solute diffusivity. This change resulted in the reduction of dilutive ICP on the draw side, thereby increasing the water flux. Again, such a behavior is attributed to the fact that the dilutive ICP plays a more significant role than the concentrative ECP in determining the water flux [26]. Such a preferential water flux increase due to the increased draw temperature was also observed by Xie et al. [27] and Cath et al. [31].

You et al. showed, however, that regardless of the membrane orientation, the water flux increased more when the *feed solution* temperature is increased rather than the draw solution [28], which is in a disagreement with the observations made by Phuntsho et al. [26], Xie et al. [27], and Cath et al. [31]. You et al. argued that the water diffusion kinetics is more important than the thermodynamic driving force (i.e., osmotic pressure difference) of the solution in determining the water flux, thus the feed temperature governs the water flux rather than the draw solution temperature [28].

Interestingly, in Nayak and Rastogi's study [36], the water flux in the FO mode was shown to be higher than the water flux in the PRO mode particularly when the molecular size of the feed solute is large enough such that the external concentration polarization cannot be ignored. They also showed that this is indeed true for concentrating anthocyanin, which is a large sugar molecule. In their work, the water flux in the FO mode was measured to be 260% higher than that in the PRO mode.

4.2. Solute diffusion/rejection

As mentioned in the preceding section, Xie et al. showed that the neutral solutes are more likely to diffuse through the membrane than the charged ones due to their smaller hydrodynamic size [27]. In this sense, transmembrane temperature differences barely influenced the solute rejection rate for the *charged* solutes, whereas the *neutral* solutes were significantly influenced by the temperature difference. It was shown that raising the draw temperature (from 20 to 40°C) led to more neutral solute rejection, even more compared to the isothermal condition at base temperature (20°C) [27]. The reason being is that raising the draw temperature leads to increased water flux, which contributes to the increased solute rejection. At the same time, keeping the feed temperature low reduces the deposition of the solutes on to the membrane, thus preventing the neutral feed solutes from dissolving into the membrane and diffusing across the membrane [27].

5. Theoretical perspectives

To the best of our knowledge, effects of temperature and its gradient on the osmosis phenomena and FO processes have been investigated only phenomenologically without fundamental understanding. The theoretical research is currently in a burgeoning state in explaining the transmembrane temperature gradient effect on the FO performance. In this section, we first briefly review the conventional FO theories [37, 38] based on the solution-diffusion model and

van't Hoff's law. Then, we revisit statistical mechanics to identify the baseline of the osmosis-diffusion theories, where the isothermal condition was first applied. We then develop a new, general theoretical framework on which FO processes can be better understood under the influence of the system temperature, temperature gradient, and chemical potentials.

5.1. Revisit to the solution-diffusion model

The solution-diffusion model is widely used to describe the FO process, which was originally developed by Lonsdale et al. to explain the RO phenomena using isothermal-isobaric ensemble [39]. In the model, the chemical potential of water is represented as a function of temperature, pressure, and solute concentration, i.e. $\mu_w = \mu_w(T, P, C)$, and its transmembrane gradient is

$$\Delta\mu_w = \int \left(\frac{\partial\mu_w}{\partial C}\right)_{T,P} dC + \int \left(\frac{\partial\mu_w}{\partial P}\right)_{T,C} dP, \tag{5}$$

where the integration is over the membrane region. From the basic thermodynamic relationship,

$$\int \left(\frac{\partial\mu_w}{\partial P}\right)_{T,C} = \overline{V}_w \tag{6}$$

is used where $\overline{V}_w$ is the molar volume of water. In the isothermal-isobaric equilibrium $(\Delta\mu_w = 0)$, the applied pressure ΔP is balanced with the transmembrane difference of the osmotic pressure, i.e. $\Delta P = \Delta\pi$. This condition gives

$$0 = \int \left(\frac{\partial\mu_w}{\partial C}\right)_{T,P} dC + \overline{V}_w \Delta\pi \tag{7}$$

and hence we derive $\Delta\mu_w = \overline{V}_w(\Delta p - \Delta\pi)$. It is assumed that the water transport within the membrane is phenomenologically Fickian, having the transmembrane chemical potential difference of water as a net driving force. The water flux is given as

$$J_w = \frac{D_w C_w}{RT}\frac{d\mu_w}{dx} \simeq \frac{D_w C_w}{RT}\frac{\Delta\mu_w}{\delta_m}, \tag{8}$$

which becomes

$$J_w = A(\Delta p - \Delta\pi), \tag{9}$$

where $A\,(= D_w C_w / RT\delta_m)$ is the solvent permeability that can be obtained experimentally. The solute flux is similarly given as

$$J_s = -D_s\frac{dC'}{dx} \simeq D_s\frac{\Delta C'}{\delta_m} = D_s\left(\frac{\Delta C'}{\Delta C}\right)\frac{\Delta C}{\delta_m} = \frac{D_s K_m}{\delta_m}\Delta C = B\Delta C, \tag{10}$$

where $\Delta C'$ and ΔC are the concentration differences across the interior and exterior of the membrane, respectively, and $K_m = \Delta C'/\Delta C$ is the partition coefficient, which is assumed to be constant, and $B(= D_s K/\delta_m)$ is the solute permeability.

Figure 4(a) shows a schematic representing the PRO and FO modes altogether. Concentrations in the PRO and FO modes are denoted as C and n, respectively. In the PRO mode, C_1 and C_5 are the draw and feed concentrations, and C_2, C_3, and C_4 are concentrations at interfaces between the draw solution and the active layer, the active layer and the porous substrate, and the porous substrate and the feed solution, respectively. In the FO mode, n_1 and n_5 are the draw and feed concentrations, respectively, and similarly, n_2, n_3, and n_5 have the meanings corresponding to those in the PRO mode. To systematically compare the performances of the PRO and FO modes, we set $n_1 = C_1$ and $n_5 = C_5$, which are the draw (C_d) and feed (C_f) concentrations, respectively. Solvent and solute fluxes in the PRO mode are denoted as J_w^{PRO} and J_s^{PRO}, and those of the FO mode are J_w^{FO} and J_s^{FO}, respectively. In each mode, solvent and solute fluxes are oriented in opposite directions, influencing each other's driving forces. The active layer and porous substrate have thicknesses of δ_m and δ_s, respectively, as located in regions of $-\delta_m < x < 0$ and $0 < x < \delta_s$, respectively. Solute molecules migrate with molecular diffusivity D_0 in the porous substrate that is characterized using its thickness δ_s, porosity ε, and tortuosity τ.

In the PRO mode, the solvent flux (in magnitude) is

$$J_w = A(\pi_2 - \pi_3) \tag{11}$$

where π_2 and π_3 are osmotic pressures at concentration C_2 and C_3, respectively. In a steady state, the water flux J_w is constant in both the active and porous regions. The solute flux in the active layer is:

$$J_s = B(C_2 - C_3) \quad \text{for} \quad -\delta_m < x < 0 \tag{12}$$

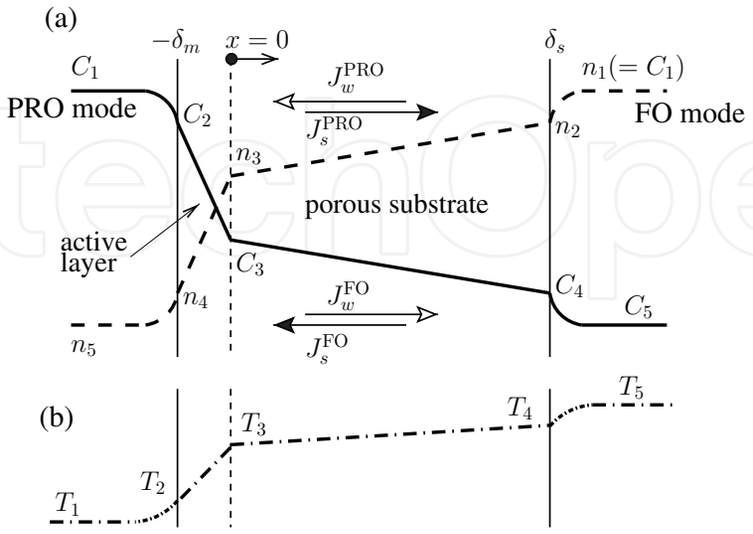

Figure 4. A schematic representation of (a) concentration polarization across a skinned membrane during FO process in the PRO and FO modes, represented using the solid and dashed lines, respectively and (b) arbitrary temperature profile increasing from the active layer to the porous substrate.

and that in the porous substrate:

$$J_s = -\frac{\epsilon}{\tau} D \frac{\mathrm{d}C}{\mathrm{d}x} - J_w C \quad \text{for} \quad 0 < x < \delta_s. \tag{13}$$

In a steady state, J_s of Eqs. (12) and (13) are equal to each other. Flux equations for the FO mode can be easily obtained by replacing subscript 2 by 4 in Eqs. (11) and (12) and replacing C by n in Eqs. (12), (13). Fluxes of the PRO and FO modes are calculated as

$$J_w^{\mathrm{PRO}} \simeq \frac{1}{K} \ln \left[\frac{B + A\pi_d - J_w^{\mathrm{PRO}}}{B + A\pi_f} \right] \tag{14}$$

and

$$J_w^{\mathrm{FO}} \simeq \frac{1}{K} \ln \left[\frac{B + A\pi_d}{B + A\pi_f + J_w^{\mathrm{FO}}} \right], \tag{15}$$

respectively, where π_d and π_f are the osmotic pressure of the draw and feed concentrations, respectively, and

$$K = \frac{\delta_s \tau}{D_0 \epsilon} = \frac{S}{D_0} \tag{16}$$

is interpreted as the characteristic mass transfer resistance, proposed by Lee et al. [37]. Following the convention of standard mass transfer theory, K^{-1} can be interpreted as the mass transfer coefficient of FO processes. In Eq. (16), $S\,(= \delta_s \tau / \epsilon)$, defined as the structural parameter having units in length, represents the actual path length of molecules passing through the tortuous porous substrate, which is by definition longer than the thickness δ_s. For mathematical simplicity, one can write the flux equation for both modes:

$$J_w = \frac{1}{K} \ln \left[\frac{B + A\pi_d - \varphi J_w}{B + A\pi_f + (1 - \varphi) J_w} \right] \tag{17}$$

where

$$\varphi = \begin{cases} 1 & \text{for PRO mode} \\ 0 & \text{for FO mode} \end{cases} \tag{18}$$

is an integer to toggle between the two modes. Any theoretical development can be initiated from Eq. (17) to consider universally both the FO and PRO modes, and then a proper value of φ can be chosen.

5.1.1. Underlying assumptions and approximations

In the theory, there are several key assumptions during derivations of Eqs. (14) and (15). These assumptions are summarized in the following for the PRO mode for simplicity, but conceptually are identical to those in the FO mode.

1. Mass transfer phenomena are described using the solution-diffusion model in which the solvent and solute transport are proportional to the transmembrane differences in the osmotic pressures and solute concentrations, respectively [39]. If one sees these combined phenomena as diffusion, the solvent transport can be treated as semibarometric diffusion. In other words, under the influence of pressure, the solute transport can be treated as Fickian diffusion, driven by the concentration gradient. In a universal view, the net driving forces of the solvent and solutes are their chemical potential differences.

2. In the flux equations, π_d and π_f are, respectively, overestimated and underestimated because their ture values are those at the draw-membrane and feed-membrane interfaces, i.e. π_2 and π_4, which are difficult to obtain. This approximation does not cause obvious errors if the flow velocities of the draw and feed solutions are fast enough to suppress formation of any significant external concentration polarizations. A necessary condition, which is less discussed in theories, is the high diffusivity or low molecular weight of solutes.

3. The osmotic pressure is presumed to be linear with the solute concentration C. In the PRO mode, one can indicate

$$\pi_2 - \pi_3 = \left(\frac{\pi_2 - \pi_3}{\pi_2 - \pi_4}\right)(\pi_2 - \pi_4) = \left(\frac{1 - C_3/C_2}{1 - C_4/C_2}\right)(\pi_2 - \pi_4) \tag{19}$$

using $\pi_2 - \pi_k = \pi_2(1 - C_k/C_2)$ for $k = 3, 4$. Eq. (19) can be erroneous if the draw concentration is extraordinarily high or pair-wise interactions between solutes are very strong so that the weak solution approach fails. A study on nonlinearity of π with respect to C can be found elsewhere [37, 38].

4. Rigorously saying, mass transport phenomena are assumed to be in a steady state and equilibrium thermodynamics are used to explain the filtration phenomena. Although the FO phenomenon occurs in an open system, transient behavior is barely described in the literature.

5. In the porous substrate, the bulk porosity is assumed to be uniform, which implies isotropic pore spaces. Moreover, the interfacial porosity between the active and porous layers is assumed to be equal to the bulk porosity. An in-depth discussion on the interfacial porosity can be found elsewhere [40]. In the same vein, the tortuosity is a characteristic geometric constant of the substrate, which is hard to measure independently. More importantly, tortuosity is included in the definition of the structural parameter S, which is used to fit the experimental data to the flux equations.

6. The solute diffusivity D_0 is assumed to be constant, that is, independent of the solute concentration such that the concentration profile is further implied to be linear within the porous substrate.

7. Finally, temperatures of the draw and the feed streams are assumed equal although hydraulic and thermal conditions of these two streams can be independently controlled. As a consequence, heat transfer across the membrane is barely discussed in the literature.

In practice, solvent and solute permeability A and B are measured experimentally in the RO mode using feed solution of zero and finite concentrations, respectively. The applied pressure is selected as a normal pressure to operate the RO, and the solute concentrations are usually in the range of that of a typical brackish water. Variations in A and B with C_d and C_f are

presumed to be negligible, similar to those of RO cases. In Eq. (17), J_w is directly related to the interfacial concentration, i.e. C_3 and n_3 in the PRO and FO modes, respectively, and therefore it can be predicted only if K is known. Mathematically, one FO flux equation has two unknowns, which are J_w and K. In most cases, the permeate flux J_w is measured experimentally and then used to back-calculate K. This experiment-based prediction often results in an imbalance of mass transfer [41, 42]. A recent study assumes that the interfacial porosity between the active and porous layers is different from the bulk porosity of the porous substrate, which successfully resolves the origin of the imbalance between theoretical and measured K values [40].

This chapter aims to explain how the temperature across the FO membrane, which consists of the active and porous layers, may affect the performance of the mass transfer at the level of statistical physics. The transmembrane temperature gradient prevents from using the abovementioned assumptions and approximations, which are widely used in the FO analysis. First, the SD model is purely based on isothermal-isobaric equilibrium in a closed system. Second, the external concentration polarizations in the draw and feed sides cannot be neglected at the same level because the temperature gradient causes a viscosity difference across the membrane. Third, the weighting factor connecting $\pi_2 - \pi_3$ and $\pi_2 - \pi_4$ cannot be represented only by concentrations but instead should include temperatures at the interfaces. Fourth, even if one can achieve a perfect solute rejection, i.e. $B = 0$, steady heat transfer across the membrane should be included since porous membrane is not a perfect thermal insulator. Fifth, the temperature gradient may change the (effective) properties of the active and porous layers such as A, B, ϵ, and τ in principle and the molecular diffusivity $D_0 \rightarrow D(T)$. Sixth, Fick's law should include additional thermal diffusion or temperature effects for determining the collective diffusion. Seventh, of great necessity is a novel, quantitative equation to calculate the osmotic pressure under the gradients of concentration as well as temperature, which generalizes van't Hoff's equation (1).

5.2. Heat transfer

Figure 4(b) shows an arbitrary temperature profile across the FO membrane, increasing from the active layer side to the porous layer side. In bulk phases of the active and porous sides, temperatures are maintained at T_1 and T_4, respectively. For simplicity, we set $T_1 < T_4$. Stream temperature on the active side increases to T_2, and within the membrane, temperature elevates from T_2 to T_3. Since the active layer is often made thin, a linear variation of temperature can be readily assumed. From the active-porous interface to the porous layer surface to the solution, the temperature increases from T_3 to T_4. A similar external temperature polarization occurs in the PL-side bulk phase, generating the temperature change from T_4 to T_5. The overall temperature profile is conceptually akin to the concentration profile in the FO mode. Having the same bulk temperatures, i.e. T_1 and T_5, the flow direction can noticeably change values from T_2 to T_4. For logical consistency, a steady state is assumed while investigating the heat transfer across the FO membrane in this chapter. Thus, heat fluxes of the four regions are

$$q_{BA} = h_{BA}(T_2 - T_1) \tag{20}$$

$$q_{AL} = h_{AL}(T_3 - T_2) \tag{21}$$

$$q_{PL} = h_{PL}(T_4 - T_3) \tag{22}$$

$$q_{BP} = h_{BP}(T_5 - T_4), \tag{23}$$

where subscripts BA and BP indicate bulk phases in the active and porous layer sides, respectively, and AL and PL mean the active layer and porous layer, respectively. The net temperature difference across the membrane is $T_4 - T_2$, which is to be approximated as $T_5 - T_1$. In the steady state, the heat flux q should be equal in each region, that is, $q = q_{BA} = q_{AL} = q_{PL} = q_{BP}$. Dividing each equation of (20)–(23) by the heat transfer coefficient $h's$, one derives

$$q = h_{\text{eq}}(T_5 - T_1) \tag{24}$$

$$\frac{1}{h_{\text{eq}}} = \frac{1}{h_{BA}} + \frac{1}{h_{AL}} + \frac{1}{h_{PL}} + \frac{1}{h_{BP}}. \tag{25}$$

Note that Eq. (24) assumes that the heat transfer is solely based on thermal conduction without thermal convection, that is, transfer rate of heat by solvent flux. In the FO process with the transmembrane thermal gradient, Eqs. (21) and (22) should be revised as

$$q_{AL} = h_{AL}(T_3 - T_2) \pm H_w J_w \tag{26}$$

$$q_{PL} = h_{PL}(T_4 - T_3) \pm H_w J_w, \tag{27}$$

where H_w and J_w are the enthalpy and flux of the solvent, respectively, and the sign is plus when the concentration and temperature profiles both increase and decrease together, otherwise it is negative. For example, for the temperature profile shown in **Figure 4**, the FO concentration profile has the same trend to that of the temperature, and therefore signs in Eqs. (26) and (27) are positive. In this case, Eq. (25) needs to be modified to

$$\frac{1}{h_{\text{eq}}} = \frac{1}{h_{BA}} + \frac{1}{h'_{AL}} + \frac{1}{h'_{PL}} + \frac{1}{h_{BP}}, \tag{28}$$

where

$$h'_{AL} = h_{\text{AL}} \pm \frac{H_w J_w}{T_3 - T_2} \tag{29}$$

$$h'_{LL} = h_{PL} \pm \frac{H_w J_w}{T_4 - T_3} \tag{30}$$

This heat balance analysis is very similar to that of membrane distillation [43, 44], but the FO process does not have any solvent phase transition so that the latent heat is not considered.

5.3. Mass transfer mechanisms

5.3.1. Anisothermal osmotic pressure

In statistical mechanics, Gibbs energy is the master function of the isothermal-isobaric ensemble. Consider a box in which two regions are separated by a semipermeable membrane. In

equilibrium, the maximum entropy condition requires that the chemical potential divided by the temperature should be constant, i.e.

$$\Delta\left(\frac{\mu(T,P,N)}{T}\right)=0, \tag{31}$$

which converts to the constant chemical potential for the isothermal environment, i.e. $\Delta\mu = 0$ for constant T. Note that in the conventional solution-diffusion model, the chemical potential of water μ_w in the external phase is assumed as a function of solute concentration C and pressure P. From Eq. (31), van't Hoff's osmotic pressure difference is derived as

$$\Delta\pi = RT\Delta C, \tag{32}$$

which can perhaps be extended intuitively to $\Delta\pi = R\Delta(CT)$ in the temperature gradient. Here we assume that the membrane properties do not change significantly with solute concentration C and local temperature T. In the presence of a concentration gradient only, van't Hoff's equation indicates that water (solvent) molecules tend to move from a lower solute concentration region to a higher solute concentration region. This is due to the water chemical potential being higher in the lower C region. Now we replace the concentration gradient by the temperature gradient. Diffusion of water molecules is purely based on their kinetic energy as proportional to T and the temperature gradient across the membrane, as shown in **Figure 4(a)**. For simplicity, we consider only the active layer of which A and B values are assumed to be insensitive to temperature. Therefore, similar to the direct contact membrane distillation, two solutions of high and low temperatures are in contact with the membrane surfaces. Since solutes are absent, the water motion is purely diffusive under the chemical potential gradient induced by the temperature gradient. Water molecules in the high temperature region move faster than those in the low temperature region. Therefore, water transfer must follow the direction of the temperature gradient. If one side of the membrane has a solution of both high temperature and concentration, then the net osmotic pressure must be less than that of the concentration gradient only, that is,

$$\Delta\pi = a\Delta C - b\Delta T \tag{33}$$

where a must be equal to RT and b is a positive constant. To the best of our knowledge, $a(T) = RT$ has not been rigorously proven, and $b(c)$ is so far unknown. The theoretical development of the anisothermal osmotic pressure, $\pi = \pi(C,T)$, as a natural extension from van't Hoff's equation is of urgent importance to the current literature in water transport theories, which are to be utilized not only in desalination and fresh water production but also in a broad applications of separation and filtration.

5.3.2. Anisothermal diffusion

Fick's law is a phenomenological equation based on experimental observations. The equation states that the diffusive flux J is proportional to the concentration gradient

$$\vec{J} = -D\,\vec{\nabla}\,C. \tag{34}$$

In the dilute limit, the diffusivity is independent of concentration C, i.e. $D \neq D(C)$, and if the solute molecules are Brownian, D is proportional to temperature T: $D \propto T$. If and only if the molecular motion is dragged by the viscous force, which is directly related to their relative velocity to the solvent (often stationary), then the drag force can be written as

$$\vec{F}_{\text{drag}} = -\beta\, \vec{v}\,, \tag{35}$$

where $\vec{v}$ is the molecular velocity relative to that of the solvent medium, and β is the drag coefficient independent of $\vec{v}$. The Brownian diffusivity is proven to be $D = k_B T/\beta$, where k_B is Boltzmann's constant. Stokes proved that $\beta = 3\pi\eta_w d_p$ where η_w is the solvent viscosity and d_p is the particle (molecule) diameter.

In the presence of the spatial variation of T, Eq. (34) is generalized as [45]

$$\vec{J} = \frac{D}{T}\,\vec{\nabla}\,(CT). \tag{36}$$

Thus, substitution of the Stokes-Einstein diffusivity into Eq. (36) gives

$$\vec{J} = \frac{k_B}{\beta}\,\vec{\nabla}\,(CT) = \frac{1}{\beta}\,\vec{\nabla}\,(\pi), \tag{37}$$

which is valid if the solvent viscosity η_w is a weak function of T such as water. For a homogeneous system, the diffusive flux may in general be

$$\vec{J} = -\alpha\,\vec{\nabla}\,\mu - \beta\,\vec{\nabla}\,T, \tag{38}$$

where one can write the chemical potential gradient as

$$\vec{\nabla}\,\mu = \left(\frac{\partial \mu}{\partial C}\right)_{P,T} \vec{\nabla}\,C + \left(\frac{\partial \mu}{\partial T}\right)_{C,P} \vec{\nabla}\,T + \left(\frac{\partial \mu}{\partial P}\right)_{C,T} \vec{\nabla}\,P. \tag{39}$$

Substitution of Eq. (39) into (38) gives

$$\vec{J} = -D\left(\vec{\nabla}\,C + k_T\,\vec{\nabla}\ln T + k_P\,\vec{\nabla}\ln P\right), \tag{40}$$

which defines the thermal diffusion coefficient $k_T D$, where k_T is the thermal diffusion ratio, which is a dimensionless quantity. The coefficient $k_P D$ is the barodiffusion coefficient. In the dilute limit, k_T vanishes as it is proportional to C. The barodiffusion is often negligible as the diffusion is characterized in a stationary fluid that will have finite velocity if the hydraulic pressure is applied.

5.3.3. Solute diffusivity matters

In the conventional isothermal theory of FO, one can write a conceptual relationship between the water flux and the transmembrane osmotic pressure difference as [33]

$$J_w \propto D \ln \Delta\pi, \tag{41}$$

which clearly indicates that J_w increases with both D and $\Delta\pi$, but $\Delta\pi$ increases much slower than D due to the logarithmic dependence. To double the flux J_w, there are two mathematical choices: $D \rightarrow 2D$ (linear) and $\Delta\pi \rightarrow (\Delta\pi)^2$ (geometric in a specific unit, or $\Delta C \rightarrow (\Delta C)^2$). The first way of increasing the solute diffusivity is related to finding or developing novel draw solutes, while the second option is practically challenging as it makes the draw recovery more energy consuming. Especially when selecting the draw solutes, their diffusivity is the most critical parameter in FO processes, as solutes of high diffusivity significantly decrease the ECP and ICP.

If we write intuitively the anisothermal osmotic pressure as

$$\Delta\pi = RT_m\Delta C - b\Delta T \tag{42}$$

across the membrane with $\Delta T = T_1 - T_2$ and $T_m = \frac{1}{2}(T_1 + T_2)$, it would be interesting to know the particular transmembrane temperature difference that can nullify the net osmotic pressure gradient:

$$\Delta T = b^{-1}R\overline{T}\Delta C. \tag{43}$$

As both T_1 and T_2 increase while keeping ΔT constant, $\Delta\pi$ increases. Moreover, increased T_m may noticeably enhance the solvent as well as solute diffusion. This thought process strongly supports the experimental literature in FO research, equivocally showing that the solvent flux is proportional to the system temperature. Note that Eq. (41) includes the permeability coefficients of solvent (A) and solute (B). As we discussed in the previous section, we know

$$\frac{\partial A}{\partial T} \quad \text{and} \quad \frac{\partial B}{\partial T} \gtrsim 0 \tag{44}$$

so that both the solvent and solute fluxes increase with the mean temperature T_m of the membrane where ΔT is maintained constant.

On the basis of our investigation, temperature effects on the osmotic phenomena are not as simple as expected from the linear van't Hoff equation, but highly correlated through the temperature-dependent material constants of solvent (η, A), solutes (D, B), and their strong linkage to the osmotic pressure: $\pi \rightarrow \pi(C, T)$.

6. Concluding remarks

This chapter provides a comprehensive review on the effect of temperature on the FO process. Although the motivation for studying the temperature effect comes from the fact that osmosis is a thermodynamically spontaneous process, changing the system temperature either locally or globally can offer more effective ways of engineering the FO process with lower energy consumption. However, as evidenced by the scattered data across the literature and a lack of theoretical descriptions, more robust and systematic studies are warranted for deeper understanding of the

phenomena. For example, most of the temperature-dependent FO studies relate the changes in the water and the solute flux to the change in the physical properties of the bulk solution only, neglecting any changes in the membrane properties such as water permeability *A*, solute permeability *B*, and mass transfer resistance *K*. Furthermore, a holistic theory accounting for the effect of transmembrane temperature gradient on the FO process is still missing, hence to be constructed in the near future.

Author details

Sangwoo Shin[1] and Albert S. Kim[2]*

*Address all correspondence to: albertsk@hawaii.edu

1 Department of Mechanical Engineering, University of Hawaii at Manoa, Honolulu, Hawaii, USA

2 Department of Civil and Environmental Engineering, University of Hawaii at Manoa, Honolulu, Hawaii, USA

References

[1] Batchelder GW. Process for the Demineralization of Water. Google Patents; 1965. US Patent 3,171,799

[2] Chekli L, Phuntsho S, Kim JE, Kim J, Choi JY, Choi JS, et al. A comprehensive review of hybrid forward osmosis systems: Performance, applications and future prospects. Journal of Membrane Science. 2016;**497**:430-449 https://doi.org/10.1016/j.memsci.2015.09.041

[3] Cath TY, Gormly S, Beaudry EG, Flynn MT, Adams VD, Childress AE. Membrane contactor processes for wastewater reclamation in space: Part I. Direct osmotic concentration as pretreatment for reverse osmosis. Journal of Membrane Science. 2005;**257**(1):85-98 https://doi.org/10.1016/j.memsci.2004.08.039

[4] Cath TY, Adams D, Childress AE. Membrane contactor processes for wastewater reclamation in space: II. Combined direct osmosis, osmotic distillation, and membrane distillation for treatment of metabolic wastewater. Journal of Membrane Science. 2005;**257**(1): 111-119 https://doi.org/10.1016/j.memsci.2004.07.039

[5] Kravath RE, Davis JA. Desalination of sea water by direct osmosis. Desalination. 1975;**16**(2): 151-155 https://doi.org/10.1016/S0011-9164(00)82089-5

[6] Kessler JO, Moody CD. Drinking water from sea water by forward osmosis. Desalination. 1976;**18**(3):297-306 https://doi.org/10.1016/S0011-9164(00)84119-3

[7] Moody CD, Kessler JO. Forward osmosis extractors. Desalination. 1976;**18**(3):283-295 https://doi.org/10.1016/S0011-9164(00)84118-1

[8] Cath TY, Childress AE, Elimelech M. Forward osmosis: Principles, applications, and recent developments. Journal of Membrane Science. 2006;**281**(1):70-87 https://doi.org/10.1016/j.memsci.2006.05.048

[9] Warczok J, Gierszewska M, Kujawski W, Güell C. Application of osmotic membrane distillation for reconcentration of sugar solutions from osmotic dehydration. Separation and Purification Technology. 2007;**57**(3):425-429 https://doi.org/10.1016/j.seppur.2006.04.012

[10] Ravindra Babu B, Rastogi NK, Raghavarao KSMS. Effect of process parameters on transmembrane flux during direct osmosis. Journal of Membrane Science. 2006;**280**(1):185-194 https://doi.org/10.1016/j.memsci.2006.01.018

[11] Wrolstad RE, McDaniel MR, Durst RW, Micheals N, Lampi KA, Beaudry EG. Composition and sensory characterization of red raspberry juice concentrated by direct-osmosis or evaporation. Journal of Food Science. 1993;**58**(3):633-637 https://doi.org/10.1111/j.1365-2621.1993.tb04344.x

[12] Theeuwes F, Yum SI. Principles of the design and operation of generic osmotic pumps for the delivery of semisolid or liquid drug formulations. Annals of Biomedical Engineering. 1976;**4**(4):343-353 https://doi.org/10.1007/BF02584524

[13] Wright JC, Johnson RM, Yum SI. DUROS® osmotic pharmaceutical systems for parenteral & site-directed therapy. Drug Delivery Technology. 2003;**3**(1):64-73

[14] Su YC, Lin L. A water-powered micro drug delivery system. Journal of Microelectromechanical Systems. 2004;**13**(1):75-82. DOI: 10.1109/JMEMS.2003.823215

[15] McGinnis RL, Elimelech M. Global challenges in energy and water supply: The promise of engineered osmosis. Environmental Science & Technology. 2008;**42**(23):8625-8629. DOI: 10.1021/es800812m

[16] Achilli A, Cath TY, Childress AE. Power generation with pressure retarded osmosis: An experimental and theoretical investigation. Journal of Membrane Science. 2009;**343**(1):42-52 https://doi.org/10.1016/j.memsci.2009.07.006

[17] Lutchmiah K, Verliefde ARD, Roest K, Rietveld LC, Cornelissen ER. Forward osmosis for application in wastewater treatment: A review. Water Research. 2014;**58**:179-197 https://doi.org/10.1016/j.watres.2014.03.045

[18] McCutcheon JR, McGinnis RL, Elimelech M. A novel ammonia–carbon dioxide forward (direct) osmosis desalination process. Desalination. 2005;**174**(1):1-11 https://doi.org/10.1016/j.desal.2004.11.002

[19] McCutcheon JR, McGinnis RL, Elimelech M. Desalination by ammonia–carbon dioxide forward osmosis: Influence of draw and feed solution concentrations on process performance. Journal of Membrane Science. 2006;**278**(1):114-123 https://doi.org/10.1016/j.memsci.2005.10.048

[20] Gray GT, McCutcheon JR, Elimelech M. Internal concentration polarization in forward osmosis: Role of membrane orientation. Desalination. 2006;**197**(1-3):1-8 https://doi.org/10.1016/j.desal.2006.02.003

[21] Traxler RN. The effect of temperature on rate of osmosis. Journal of Physical Chemistry A. 1928;**32**(1):127-141. DOI: 10.1021/j150283a010

[22] Wijmans JG, Baker RW. The solution-diffusion model: A review. Journal of Membrane Science. 1995;**107**(1-2):1-21 https://doi.org/10.1016/0376-7388(95)00102-I

[23] Garcia-Castello EM, McCutcheon JR, Elimelech M. Performance evaluation of sucrose concentration using forward osmosis. Journal of Membrane Science. 2009;**338**(1):61-66 https://doi.org/10.1016/j.memsci.2009.04.011

[24] Zhao S, Zou L. Effects of working temperature on separation performance, membrane scaling and cleaning in forward osmosis desalination. Desalination. 2011;**278**(1):157-164 https://doi.org/10.1016/j.desal.2011.05.018

[25] Petrotos KB, Quantick P, Petropakis H. A study of the direct osmotic concentration of tomato juice in tubular membrane–module configuration. I. The effect of certain basic process parameters on the process performance. Journal of Membrane Science. 1998;**150**(1): 99-110 https://doi.org/10.1016/S0376-7388(98)00216-6

[26] Phuntsho S, Vigneswaran S, Kandasamy J, Hong S, Lee S, Shon HK. Influence of temperature and temperature difference in the performance of forward osmosis desalination process. Journal of Membrane Science. 2012;**415**:734-744 https://doi.org/10.1016/j.memsci.2012.05.065

[27] Xie M, Price WE, Nghiem LD, Elimelech M. Effects of feed and draw solution temperature and transmembrane temperature difference on the rejection of trace organic contaminants by forward osmosis. Journal of Membrane Science. 2013;**438**:57-64 https://doi.org/10.1016/j.memsci.2013.03.031

[28] You SJ, Wang XH, Zhong M, Zhong YJ, Yu C, Ren NQ. Temperature as a factor affecting transmembrane water flux in forward osmosis: Steady-state modeling and experimental validation. Chemical Engineering Journal. 2012;**198**:52-60 https://doi.org/10.1016/j.cej.2012.05.087

[29] McCutcheon JR, Elimelech M. Influence of concentrative and dilutive internal concentration polarization on flux behavior in forward osmosis. Journal of Membrane Science. 2006;**284**(1):237-247 https://doi.org/10.1016/j.memsci.2006.07.049

[30] Ng HY, Tang W, Wong WS. Performance of forward (direct) osmosis process: Membrane structure and transport phenomenon. Environmental Science & Technology. 2006;**40**(7): 2408-2413 https://doi.org/10.1021/es0519177

[31] Cath TY, Elimelech M, McCutcheon JR, McGinnis RL, Achilli A, Anastasio D, et al. Standard methodology for evaluating membrane performance in osmotically driven membrane processes. Desalination. 2013;**312**:31-38 https://doi.org/10.1016/j.desal.2012.07.005

[32] Kim AS, Lee SW. Intrinsic flux inequality in forward osmosis (FO) and pressure-retarded osmosis (PRO) processes. Membrane Journal. 2015;**25**(4):367-372. http://db.koreascholar.com/article.aspx?code=306432

[33] Kim AS, Kim SW. Performance analysis of forward osmosis processes from the integral equation theory. Desalination and Water Treatment. 2013;**51**(25-27):5289-5297 http://dx.doi.org/10.1080/19443994.2013.768757

[34] Dale MC, Okos MR. Reverse osmosis membrane performance as affected by temperature and pressure. Industrial & Engineering Chemistry Product Research and Development. 1983;**22**(3):452-456 https://doi.org/10.1021/i300011a013

[35] Chanukya BS, Patil S, Rastogi NK. Influence of concentration polarization on flux behavior in forward osmosis during desalination using ammonium bicarbonate. Desalination. 2013;**312**:39-44 https://doi.org/10.1016/j.desal.2012.05.018

[36] Nayak CA, Rastogi NK. Forward osmosis for the concentration of anthocyanin from Garcinia indica Choisy. Separation and Purification Technology. 2010;**71**(2):144-151 https://doi.org/10.1016/j.seppur.2009.11.013

[37] Lee KL, Baker RW, Lonsdale HK. Membranes for power generation by pressure-retarded osmosis. Journal of Membrane Science. 1981;**8**(2):141-171 https://doi.org/10.1016/S0376-7388(00)82088-8

[38] Loeb S. Production of energy from concentrated brines by pressure-retarded osmosis. Journal of Membrane Science. 1976;**1**:49-63 https://doi.org/10.1016/S0376-7388(00)82257-7

[39] Lonsdale HK, Merten U, Riley RL. Transport properties of cellulose acetate osmotic membranes. Journal of Applied Polymer Science. 1965 Apr;**9**(4):1341-1362 https://doi.org/10.1002/app.1965.070090413

[40] Kang PK, Lee W, Lee S, Kim AS. Origin of structural parameter inconsistency in forward osmosis models: A pore-scale CFD study. Desalination. 2017;**421**:47-60 https://doi.org/10.1016/j.desal.2017.05.018

[41] Manickam SS, Gelb J, McCutcheon JR. Pore structure characterization of asymmetric membranes: Non-destructive characterization of porosity and tortuosity. Journal of Membrane Science. 2014;**454**:549-554 https://doi.org/10.1016/j.memsci.2013.11.044

[42] Manickam SS, McCutcheon JR. Model thin film composite membranes for forward osmosis: Demonstrating the inaccuracy of existing structural parameter models. Journal of Membrane Science. 2015;**483**:70-74 https://doi.org/10.1016/j.memsci.2015.01.017

[43] Khayet M, Matsuura T. Membrane Distillation: Principles and Applications. New York: Elsevier; 2011

[44] Kim AS. Cylindrical cell model for direct contact membrane distillation (DCMD) of densely packed hollow fibers. Journal of Membrane Science. 2014;**455**:168-186 https://doi.org/10.1016/j.memsci.2013.12.067

[45] Efros A. Theory of thermal diffusion of Brownian particles. Soviet Physics. Journal of Experimental and Theoretical Physics. 1966;**23**(3):536-541

Chapter 6

Pressure Dependency of the Membrane Structure Parameter and Implications in Pressure Retarded Osmosis (PRO)

Torleif Holt, Edvard Sivertsen, Willy R. Thelin and Geir Brekke

Additional information is available at the end of the chapter

http://dx.doi.org/10.5772/intechopen.72444

Abstract

Pressure retarded osmosis (PRO) can be used to exploit the mixing energy *e.g*. between river water and sea water. A PRO membrane must be highly permeable for water, whereas salt ions should be retained. Furthermore, the structure parameter of the membrane support and backing structure must be low. This paper summarises an assessment of the pressure dependency of the structure parameter for flat sheet membranes, and a transport model for PRO and procedures for determination of the pressure dependency of the structure parameter are presented. The results from laboratory experiments show that that the structure parameter increases significantly with increasing trans-membrane pressure. The increase in the structure parameter was observed to depend on both characteristics of the membrane and the fresh water spacer. Using a finely textured tricot spacer reduced the pressure dependency on the structure parameter, compared to a coarser spacer. Applying a non-woven backing material between the membrane and the fresh water spacer also reduced the impact of pressure. The results show that membranes suitable for river water/sea water PRO must have a sufficiently low structure parameter and additionally resist severe deformation at relevant operating pressures.

Keywords: osmotic power, pressure retarded osmosis, structure parameter, pressure dependence

1. Introduction

Pressure retarded osmosis (PRO) is one feasible technology that can be used to exploit the mixing energy from salt gradients which is commonly referred to as salinity gradient power or

osmotic power [1, 2]. In PRO the transport of water through the membrane is caused by the difference in osmotic pressure across the membrane skin, and the net volume increase on the high saline side due to mass transport against a pressure gradient can be utilised to run a turbine. It should be mentioned that indirect alternatives to exploit the osmotic power, such as osmotic energy recovery in desalination of sea water, have gained increasing attention recently [3–5].

The mass transport of salt and water in PRO can be characterised by three parameters, the water permeability, A, the salt permeability, B, and the structure parameter, S [1, 6]. The parameters must be optimised in order to maximise produced power, implying that the water permeability should be high, and both the salt permeability and the structure parameter should be low. Membrane development has been a prioritised research area for more than a decade, and significant improvements in PRO membrane performance have been achieved over the last years [6–11]. Membrane and element configuration has also been a focus area, and both flat sheet and hollow fibre configurations should be further investigated [12–14].

Resent research has showed that various transport models [14–17] fail to accurately model PRO performance as a function of pressure increase. Kim and Elimelech [18] have related the deviation between observed and modelled performance to adverse effects between the membrane support and the feed channel spacer. Both membrane deformation and obstruction of water permeation were proposed mechanisms to explain the reduced membrane performance at increasing pressures. In case of membrane obstruction, *i.e.* the spacer blocks part of the active membrane area This effect was referred to as the *spacer shadow effect*. Kim and Elimelech showed that the water permeability remained almost independent of the trans-membrane pressure when a diamond shaped feed spacer was applied. On the other hand, the salt permeability increased significantly when the trans-membrane pressure exceeded a certain value (in the range 9–12 bar).

She *et al*. [19] have also studied the impact of spacer characteristics on PRO performance. They showed that mechanical deformation of the PRO membrane did occur during PRO operation. Subsequently, they determined water and salt permeabilities obtained after deformation as a function of trans-membrane pressure in RO experiments, using the same types of feed spacers. Finally, the structure parameter was determined from calculations using the observed water fluxes from the PRO experiments. The variations in the estimated membrane parameters, as well as the mechanical deformation, were found to depend on spacer characteristics.

The interaction between the membrane and the feed spacer is found to reduce the PRO performance of flat sheet membranes. Hollow fibres are self-supporting structures, meaning that the use of spacers is avoided. Any pressure dependency of the PRO performance of hollow fibre membranes must therefore be related to other mechanisms than interactions between membrane and spacer. Chou *et al*. [7] observed a discrepancy between modelled and measured performances for fibres with the skin applied on the bore side. They determined the structure parameter at several pressure steps, and observed that this parameter decreased with increasing pressure. It was suggested that this was due to expansion of the polymer network resulting in reduced tortuosity of the membrane support when the inside of the fibres was pressurised.

The objective of this paper is to present a hypothesis for the interaction between the membrane and spacer which partly builds on the hypothesis of Kim and Elimelech [18]. Based on characterisation experiments we have demonstrated good correlation between measured and modelled membrane performances by applying a pressure dependent structure parameter.

Further, the implications of membrane and spacer interactions in PRO will be discussed and related to the need for optimisation of the characteristic parameters of PRO membranes.

2. Theory

2.1. PRO modelling

A simplified flow diagram indicating main components in a PRO process such as pre-treatment stage, membrane modules, and pressure exchanger, is given in **Figure 1**. In PRO, water will be transported against a pressure gradient due to the difference in osmotic pressure between the draw solution and the feed solution. The net volume increase on the high saline side, which are operated at elevated pressure, can *e.g.* be converted to power in a turbine. The produced power, P, equals the volume flux, J_v, through the membrane, multiplied with the hydraulic pressure difference over the membrane, Δp,

$$P = J_v \Delta p \tag{1}$$

Since the volume of salt transported through the membrane is negligible compared to the volume of water, the volume flux can be replaced by the water flux, J_w.

Different model frameworks describing the transport of salt and water through osmotic membranes have been developed by several authors [15, 20–24]. This paper is based on the stagnant boundary layer model presented by Thorsen and Holt [15], and the basic equations are given below.

Figure 2 shows the cross section of an osmotic membrane in a cross-flow cell, indicating the concentration profile of salt at a given position in the cell, from the fresh water side, through the membrane and to the sea water side.

The transport of water and salt (J_s) through the membrane skin is described by two flux equations, where the positive flux directions are indicated by the arrows in **Figure 2**

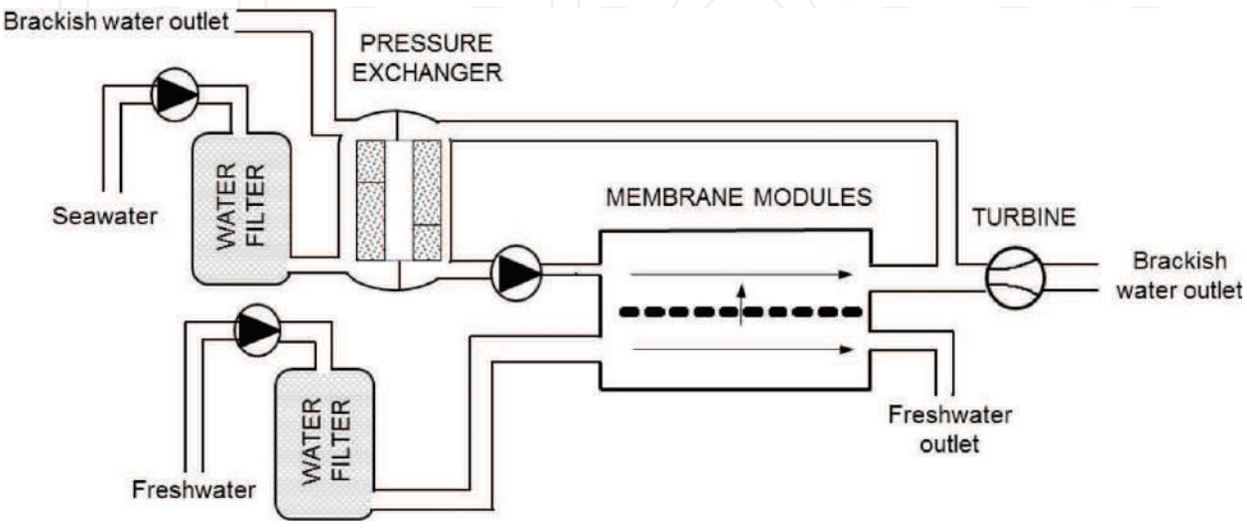

Figure 1. Simplified flow diagram of a PRO power plant.

$$J_w = A(\Delta\pi_{skin} - \Delta p) \tag{2}$$

and

$$J_s = B\Delta s_{skin} = B(c_{sm} - c_p) \tag{3}$$

A and B are the water and salt permeability of the skin, respectively. The osmotic pressure across the skin, $\Delta\pi_{skin}$, is related to the concentration difference $(c_{sm} - c_p)$ of salt over the skin by

$$\Delta\pi_{skin} = iRT(c_{sm} - c_p) = iRT\Delta c_{skin} \tag{4}$$

where i is the van't Hoff coefficient that equals 2.0 for ideal solutions of NaCl. A value of 1.9, which are based on published data for osmotic pressures in NaCl solutions, have been used in the present calculations [25]. R is the universal gas constant and T is the absolute temperature.

The coupled transport of salt in the support membrane and the boundary layers can be expressed by the mass balance

$$-J_s = \frac{\varphi}{\tau} D \frac{dc}{dx} - J_w c \tag{5}$$

where the porosity, φ, and the tortuosity, τ, in the boundary layers on the membrane surfaces equals unity. D is the diffusion coefficient of salt (NaCl). Inserting the water flux in Eq. (2) and the salt flux in Eq. (3) into the mass balance in Eq.(5) and evaluating the transport of water

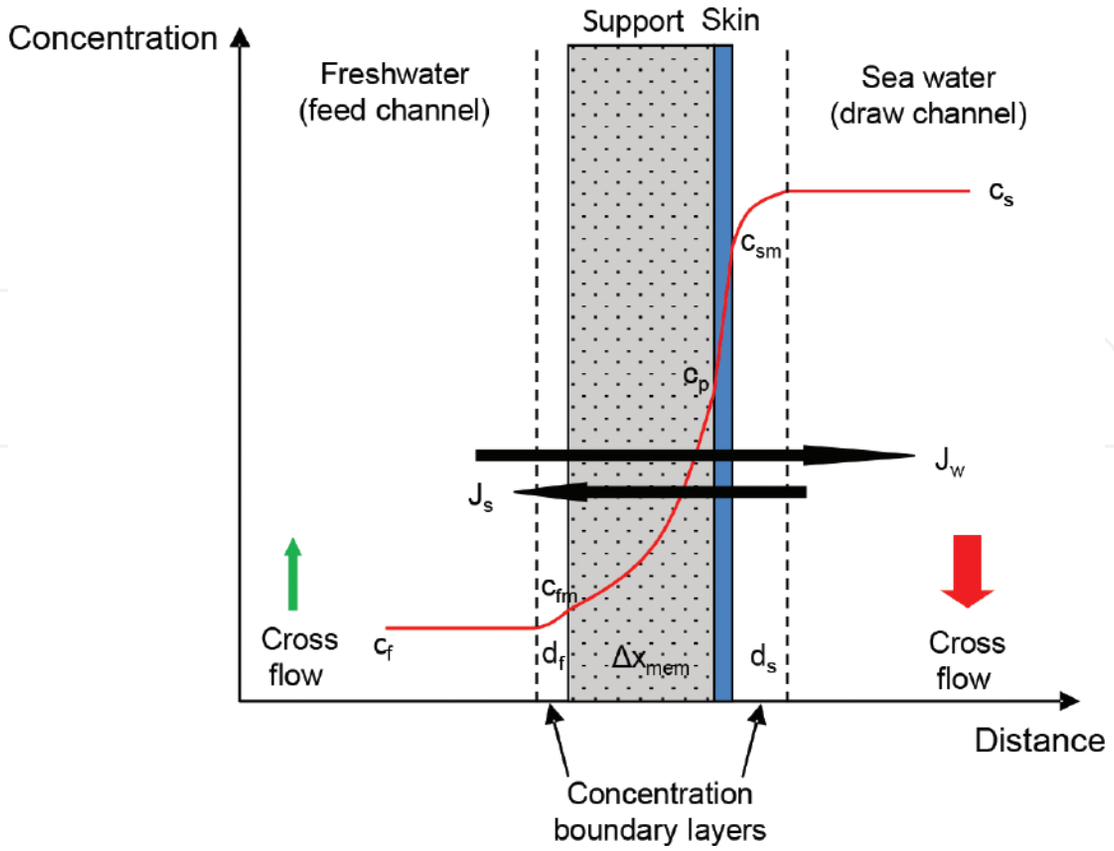

Figure 2. Concentration profile over the membrane and boundary layers.

http://dx.doi.org/10.5772/intechopen.72444

and salt in the different transport zones results in five equations containing five unknown parameters, J_s, J_w, c_{fm}, c_p and c_{sm}. After some rearrangement, the following expression for the concentration difference across the skin, Δc_s can be found:

$$\Delta c_{skin} = \frac{c_s - c_f e^{\left\{\frac{(S+d_s+d_f)J_w}{D}\right\}}}{e^{\left(\frac{dJ_w}{D}\right)} + \frac{B}{J_w}\left(e^{\left\{\frac{(S+d_s+d_f)}{D}\right\}} - 1\right)} \tag{6}$$

The equation relates the concentration difference of salt over the membrane skin to the bulk concentrations of salt, and furthermore to the characteristic membrane parameters, as well as the boundary layer thickness on each side, d_s and d_f, respectively. The structure parameter, S, of the membrane support is defined as

$$S = \frac{\tau}{\phi}\Delta x_{mem} \tag{7}$$

where Δx_{mem} is the thickness of the support membrane that for practical purpose will equal the measured membrane thickness. The salt flux can be found by multiplying Eq. (6) by B.

The water flux can be found by combining Eqs. (2), (4) and (6) giving

$$J_w = A\left(iRT\frac{c_s - c_f e^{\left\{\frac{(S+d_s+d_f)J_w}{D}\right\}}}{e^{\left(\frac{dJ_w}{D}\right)} + \frac{B}{J_w}\left(e^{\left\{\frac{(S+d_s+d_f)}{D}\right\}} - 1\right)} - \Delta p\right) \tag{8}$$

which is valid when the salt water faces the skin side of the membrane, *i.e.* PRO mode.

2.2. Pressure dependency of the structure parameter

The left sketch in **Figure 3** illustrates the cross section of a PRO membrane at zero trans-membrane pressure. The support membrane rests on the top of the filaments of the feed spacer. The contact area between the membrane and the spacer will in such case be low, and the presence of the spacer material has little or no impact on the mass transfer. An eventual impact will be included in the structure parameter determined by modelling of isobaric experiments.

When pressure is applied on the skin side in a PRO experiment the pressure will exert a force on the membrane, such that feed spacer will be squeezed into the support membrane. This situation is illustrated in **Figure 3** (right sketch). As a result, the membrane may be deformed, and the contact area between the membrane and the feed spacer might increase. Furthermore, the properties of the support structure, such as porosity and interconnections between pores, might be affected. The net effect of these phenomena can be modelled as an increased structure parameter.

A simple equation has been developed in order to illustrate the pressure dependency on the structure parameter and the implicit effect on the water flux:

$$S = S_0\frac{1}{1 - \left(F\Delta p/\Delta p_{ref}\right)} \tag{9}$$

where S_0 is the structure parameter at zero trans-membrane pressure, Δp. Arbitrarily values for the constant F were selected, and constant Δp_{ref} was set to 10.6 bar. As shown in **Figure 4**, the increase in the structure parameter is modest at low trans-membrane pressures, but increases rapidly at higher pressures. The water flux will be reduced when the structure parameter increases. The effect is more pronounced for higher F values.

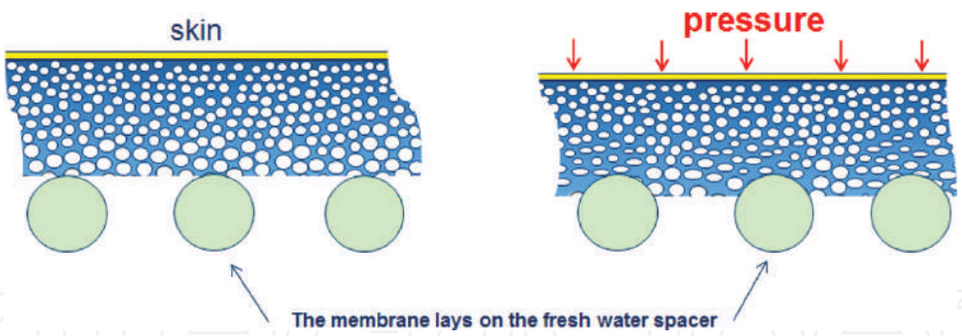

Figure 3. PRO membrane and spacer material at isobaric conditions (left) and pressurised conditions (right). The pores (illustrated by white circles) in the support membrane and possible reinforcement are interconnected giving continuous transport paths.

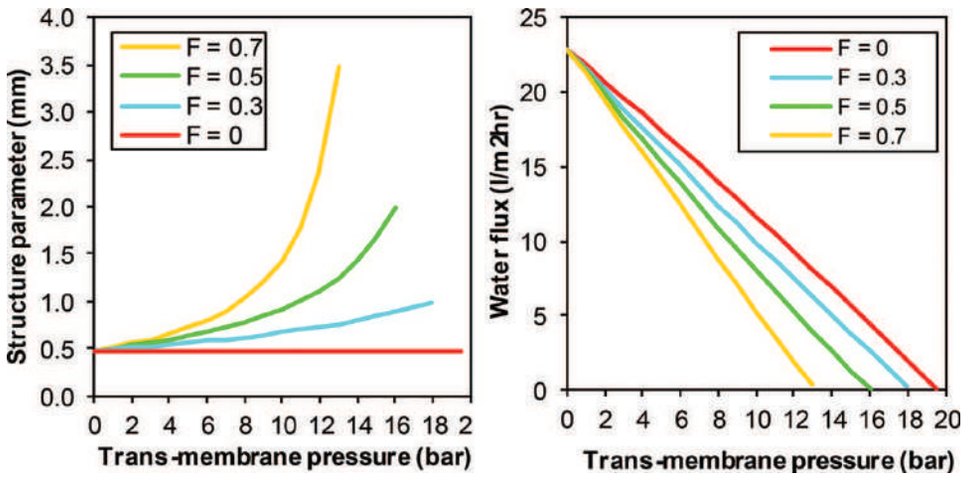

Figure 4. Structure parameters modelled as function of trans membrane pressure according to Eq. (9).

3. Experimental

3.1. Apparatus

All results presented in this work were obtained from measurements performed with two small cross-flow units as illustrated in **Figure 5**. Two membrane cells with different effective membrane area of 6.1 and 9.5 cm^2, respectively, were applied. The channel width was 1.1 cm and the depth of the draw channel was 0.07 cm for both cells. The depths of the feed channels for the two different cells were 0.1 and 0.05 cm, respectively. The draw channels were filled with a 0.07 cm thick diamond spacer, whereas different types of spacers were used in the feed channels.

Both feed and draw solution were pumped through the cross-flow cell using dual-piston pumps with displacement volumes of approximately 10 ml/stroke. The fluids were fed into the pumps from reservoirs placed on balances, and subsequently recycled back to the reservoirs. The cross-flow cells and up-stream tubing were immersed in temperature controlled water baths to maintain the temperature at 20°C during the experiments. The pressures, *p*, the

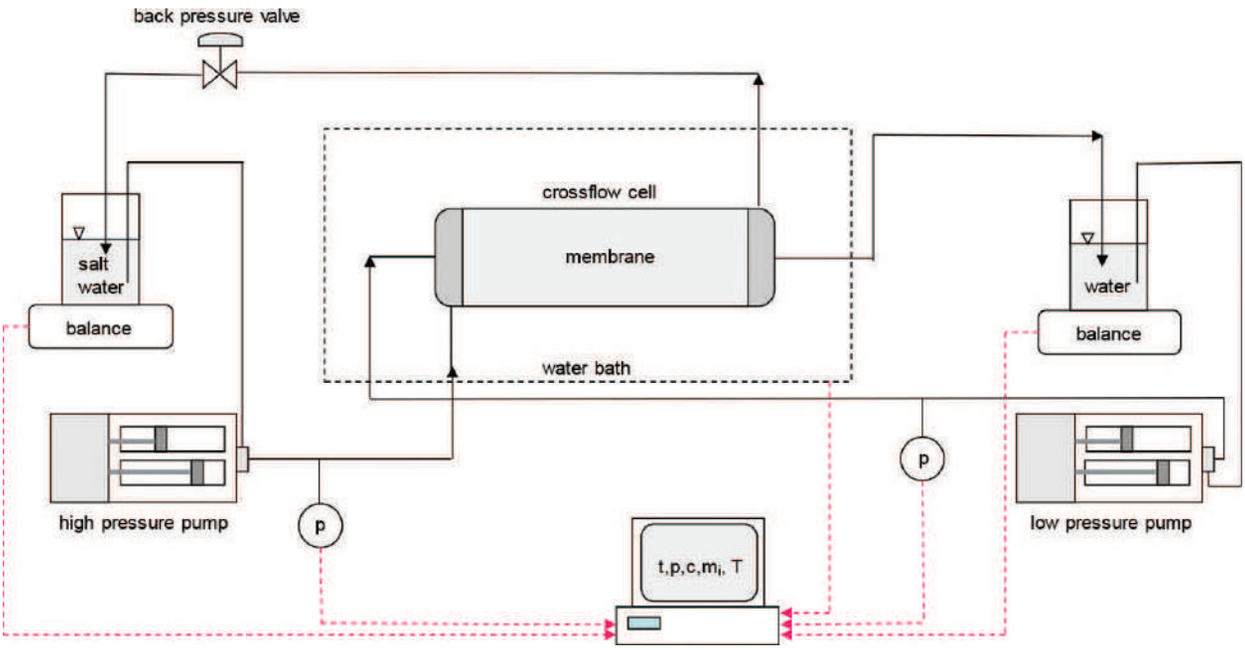

Figure 5. Simplified flow diagram for the two cross flow apparatuses used in the study.

temperature in the water bath, T, and the readings of the balances, m_i, were monitored and logged at regular intervals, t. An inline conductivity cell enabling the determination of the salt concentration in the fresh water, c, was not used in the present experiments.

3.2. Membranes and feed water spacers

The membranes used in this study include one CTA membrane and two TFC membranes (TFC1 and TFC2) from Hydration Technology Inc. and one TFC membrane (TFC3) from Nitto Denko. It should be noted that TFC1 and TFC2 are the first and second generation of the same membrane.

A relatively coarse tricot spacer with 0.5 mm thickness has been used as feed water spacer in our standard test protocols. In addition, some experiments were performed with a finer tricot spacer with 0.25 mm thickness. Photos of both types of spacers are shown in **Figure 4**.

3.3. Test protocol

The salt water solutions were made by dissolving NaCl (p.a.) in degassed (vacuum) and purified water. Degassed and purified water was also used as feed solution in the PRO experiments, and for all pre-treatment and rinsing steps.

If prescribed by the manufacturer, the membranes were pre-treated by immersion in a fluid of composition specified by the membrane manufacturer (often 50 vol. % methanol) for a prescribed time (typically 30 to 300 seconds). Subsequently, the samples were immersed in purified water for minimum 60 minutes prior to assembly in one of the membrane cells. The membranes that were not pre-conditioned were immersed in purified water prior to assembly in one of the membrane cells, in some cases combined with vacuum degassing of the sample.

After assembly, a hydraulic water permeability test was performed. The water flux was measured for minimum four pressure steps, ranging from 1 to 10 bar. Each pressure step lasted for minimum 1 hour. Subsequently, two independent osmotic flow experiments were performed at isobaric conditions. The first experiment was performed in FO mode, *i.e.* draw solution against the membrane support, followed by a second experiment in PRO mode, *i.e.* draw solution against the membrane skin. The cross-flow cell and tubing was flushed with purified water between each experiment.

3.4. Experimental conditions

For the osmotic experiments, the flow velocities (based on open channel) were 1.08 and 0.76 cm/s for the draw channel and the feed channel, respectively, unless stated otherwise. These flow velocities are in the same order as expected flow velocities in a full-scale membrane module for sea water/fresh water PRO. For the hydraulic water permeability experiments, purified water was supplied to both sides of the membrane.

During the osmotic experiments both sides of the membrane were conditioned at ambient pressure by bypassing the back-pressure valve shown in **Figure 5**. During the hydraulic water permeability experiments, and some of the PRO experiments, the back-pressure valve was used to regulate the applied pressure on the draw side. However, most PRO experiments were performed using a closed draw solution loop instead of the back-pressure valve. The closed draw solution loop was continuously pressurised by the volume increase in the draw solution loop.

4. Data analyses and modelling

4.1. Flux and permeability calculations

The water flux was determined based on mass changes in the feed reservoirs. The reported water fluxes were estimated based on the initial phase in each experiment, *i.e*. during the first 1 to 2 hours, before dilution of the draw solution and salt accumulation in the feed solution influenced the mass transport. Hydraulic water permeabilities were calculated from the hydraulic permeability experiments. The salt fluxes were determined by potentiometric analyses of Cl^- ions in a sample collected in the feed reservoir at the end of each experiment. The measured average salt fluxes were corrected to initial conditions using the ratio between initial and average salt concentration differences across the membrane.

4.2. Determination of A, B and S from isobaric osmotic flow experiments

A, *B* and *S* were determined for each membrane by modelling of two isobaric osmotic flow experiments ($\Delta p = 0$). The two experiments, one performed in FO mode and one in PRO mode, produced one water flux and one salt flux each that were used as input to the transport model described in Section 2. Further, *A*, *B* and *S* was determined as the combination of parameters resulting in the minimum sum of squared relative deviations between measured and modelled fluxes. Of the four fluxes that were obtained from the two osmotic flow experiments, three of them are independent, which corresponds to the minimum degrees of freedom required for the parameter estimation. All experiments were modelled by using a boundary layer thickness of 40 μm [26].

4.3. Modelling of PRO experiments

In order to assess the specific power production as function of applied pressure each experiment was divided into pressure steps. The water and salt fluxes, and the salt concentrations on both sides of the membrane, were calculated by mass balances for each pressure step, using the membrane parameters determined for the applied membrane, according to Section 4.2.

4.4. Determination of pressure dependency of the structure parameter

In order to assess the pressure dependency of the structure parameter, S was allowed to increase with pressure. Thus, the modelling procedure described in Section 4.2 was repeated for each pressure step. However, with the distinction that A and B were kept constant and equal to the values determined at isobaric conditions, whereas only the structure parameter was fitted to minimise the sum of squared relative deviations between measured and modelled fluxes.

5. Results and discussion

5.1. Modelling of PRO experiments with constant S

Figure 7 shows the water flux and specific power as function of trans-membrane pressure for two CTA membranes with imbedded reinforcement. The membranes originated from two different production batches. Symbols correspond to experimental data, whereas lines correspond to modelled values which are based on the characteristic membrane parameters determined from the osmotic flow experiments.

It can be observed from **Figure 7** that the measured water fluxes, and thus the specific power, were not very high, which is typical for asymmetric membranes. Furthermore, a significant deviation between measured and modelled performance was observed at increasing trans-membrane pressure.

5.2. Modelling of PRO experiments with pressure dependent S

Figure 8 shows the same experiments as presented in **Figure 7** with the distinction that the modelled values were obtained by using a pressure dependent structure parameter. The pressure dependent structure parameter obtained for the two CTA membranes is plotted as function of trans-membrane pressure in **Figure 9**.

It can be observed that the structure parameter increases significantly with increasing pressure for both membrane samples. Further, the observed variation in the structure parameter with trans-membrane pressure resembles the proposed behaviour given by Eq. (10).

Figure 10 shows the water flux and specific power as function of trans-membrane pressure for two parallel runs with a TFC membrane with imbedded reinforcement, denoted as TFC1. The modelled values were obtained by using a pressure dependent structure parameter. Note that the difference in salt concentration across the membrane skin at maximum specific power was 26.4 and 28.2 g/l for Experiment 1 and Experiment 2, respectively, which explains the observed difference in performance for the two experiments.

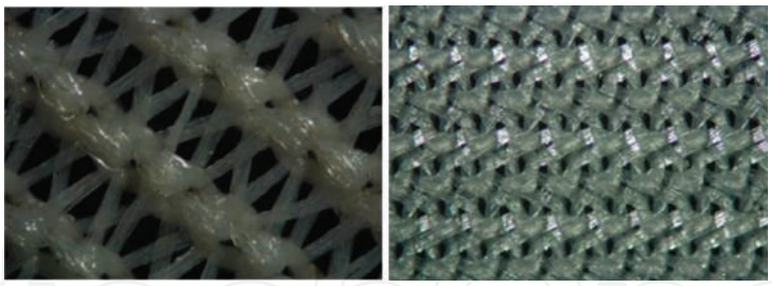

Figure 6. Top view of the tricot spacers used in the feed channel. Left: coarse spacer of 0.5 mm thickness. Right: Fine spacer of 0.25 mm thickness. Photos are shown at the same scale.

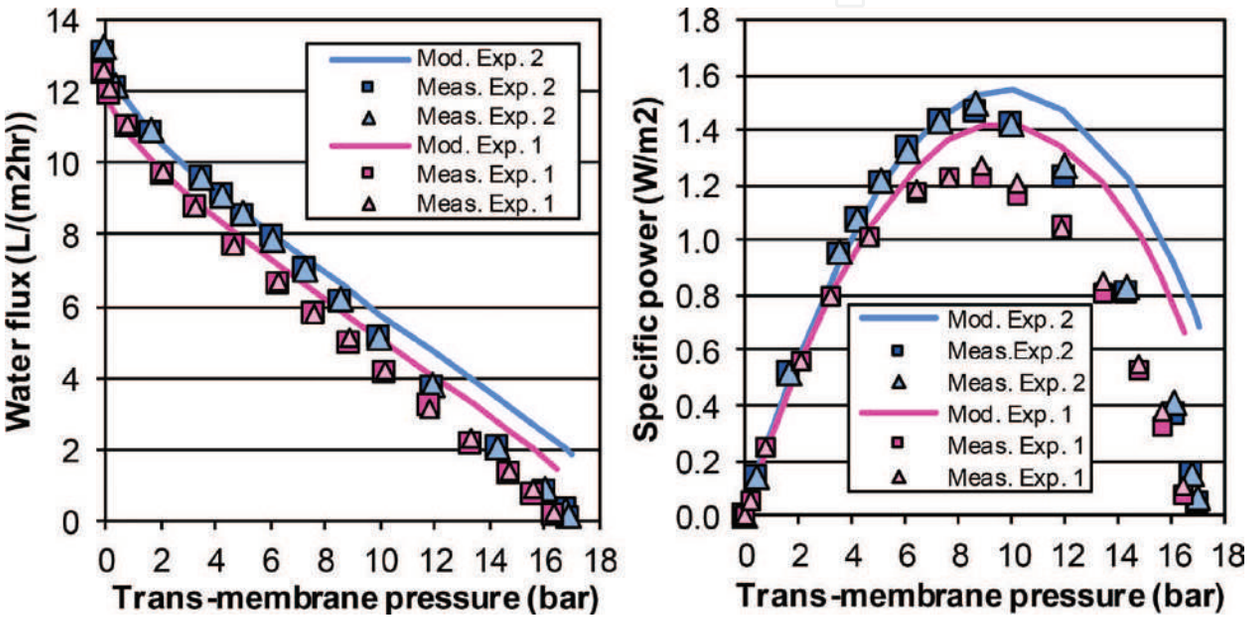

Figure 7. Water flux and specific power as function of trans-membrane pressure for CTA membranes. Modelled values were obtained by applying constant structure parameter determined at isobaric conditions.

Figure 11 shows the pressure dependency of the structure parameter for the two experiments performed with TFC1. Generally, it was observed that the structure parameter of the TFC1 membrane was less affected by pressure than the CTA membrane. *E.g.* at 10 bar the *S* value of the TFC1 membrane was doubled compared to isobaric conditions, whereas the increase in *S* value at 10 bar for the CTA membrane was in the range of 400%.

5.3. Impact of flow velocity on the pressure dependency of S

Table 1 summarises a series of PRO experiments, each performed with different cross-flow velocities and using the membrane denoted TFC2. Experiments 5 and 9 were both performed at standard conditions. The maximum specific power, P_{max}, and the difference in salt concentration across the membrane at maximum specific power, Δc at $P_{max,}$ are given in the table, as well as the pressure found by extrapolation of the water flux vs. the trans-membrane pressure curve to zero water flux, p_{osm}. The latter is commonly referred to as the practical osmotic pressure.

http://dx.doi.org/10.5772/intechopen.72444

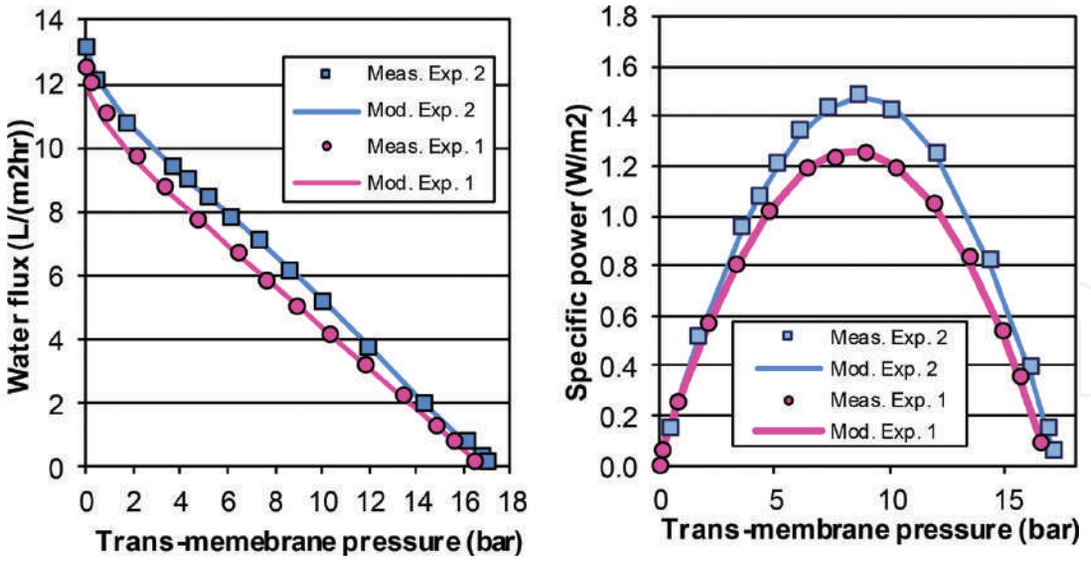

Figure 8. Water flux and specific power as functions of trans-membrane pressure for CTA membranes. Modelled values were obtained by applying a pressure dependent structure parameter.

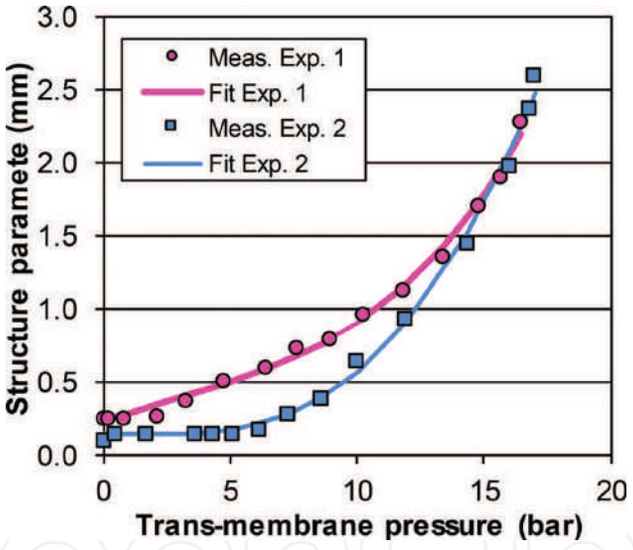

Figure 9. Modelled structure parameter as function of trans-membrane pressure for CTA membranes.

All experiments were modelled according to the procedure described in Section 4.4, and the respective pressure dependent structure parameters are shown in **Figure 12**.

From the reported specific power data in **Table 1** it was observed that the TFC2 membrane (second generation) performed significantly better than the TFC1 membrane (first generation). Further, the results from Experiment 5 and Experiment 9 performed at identical conditions are very similar and indicate good reproducibility.

Comparing the pressure dependency of the structure parameter for the two different TFC membranes in **Figure 12** and **Figure 11**, it was observed that the structure parameter of the TFC2 membrane was less influenced by increasing trans-membrane pressure. Further, the

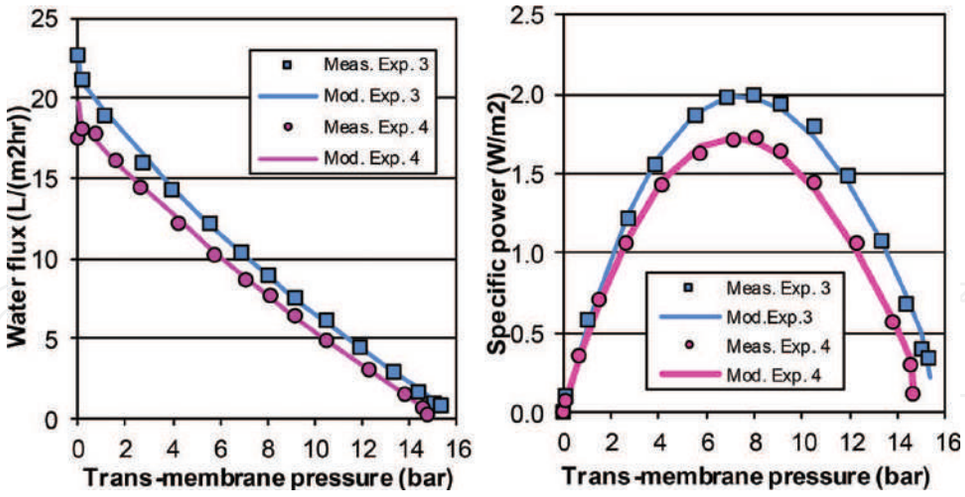

Figure 10. Water flux and specific power as functions of trans-membrane pressure for the TFC1 membrane. Modelled values were obtained by applying a pressure dependent structure parameter.

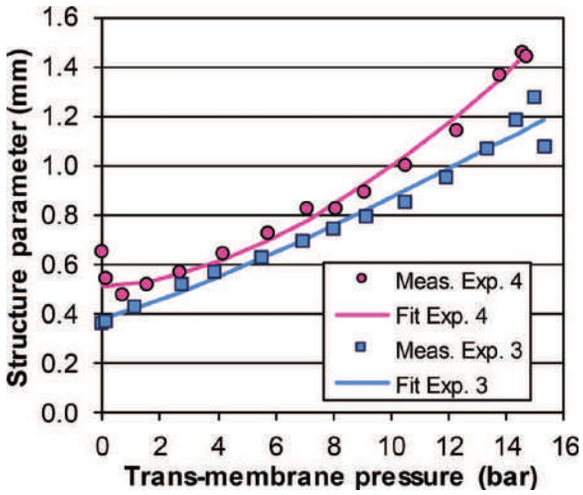

Figure 11. Structure parameters as functions of trans-membrane pressure for the TFC1 membrane.

Exp.	u_{draw} (cm/s)	u_{feed} (cm/s)	P_{max} (W/m²)	Δc at P_{max} (g/L)	p_{osm} (bar)
5	1.08	0.76	3.4	27.2	18.5
6	1.62	1.14	3.8	27.4	18.8
7	2.16	1.52	4.0	27.2	19.5
8	3.25	2.27	4.2	27.4	19.5
9	1.08	0.76	3.4	27.4	18.5

Table 1. Summary of PRO experiments performed with the TFC2 membrane and variable cross-flow velocities.

increase in structure parameter with increasing trans-membrane pressure was observed to have relatively identical slopes for all experiments performed with the TFC2 membrane. Additionally, the structure parameter was observed to decrease at increasing flow velocities.

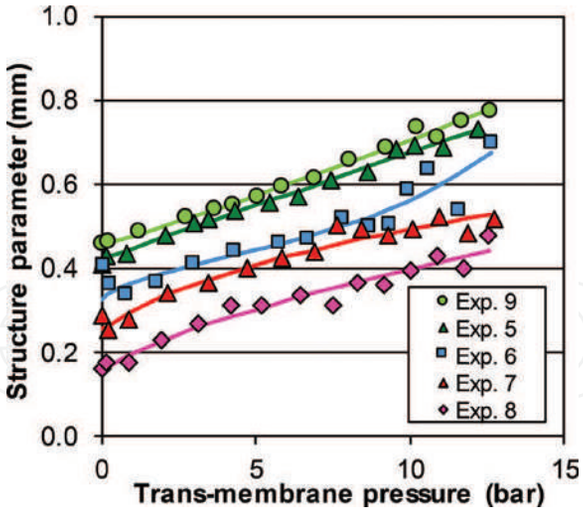

Figure 12. Pressure dependent structure parameters as functions of trans-membrane pressure for the TFC2 membrane.

Figure 13 illustrates the membrane and the feed channel in a cross-flow cell. Since the support membrane is a porous structure some water might be anticipated to flow in the longitudinal direction inside the support membrane as illustrated by the red arrows. The flow velocity inside the support membrane and the penetration depth for the longitudinal flow inside the support will depend on the cross-flow rate, as well as both the flow resistance in the spacer material and in the support membrane, respectively.

For low cross-flow rates and for feed spacers with low pressure drop, the pressure gradient in the feed channel will be small, and little or no water will flow in the longitudinal direction inside the support membrane. At higher cross-flow rates, the pressure gradient in the membrane support will increase, and a significant flow of water inside the support membrane may occur. This will reduce the magnitude of the structure parameter since the effective diffusion length will be reduced when the support structure become more saturated.

Even if high cross-flow velocities may improve mass transfer through the membrane by the effects discussed above, such measure will require increased pumping energy and additionally result in lower utilisation of the feed solution. It should be noted that large pressure losses are unacceptable in sea water/fresh water PRO, and sufficiently low pressure losses are important factors to be considered during development and design of membrane modules for application in PRO plants.

5.4. Impact of spacer selection on the pressure dependency of S

Table 2 summarises results from PRO experiments performed with the TFC3 membrane that was produced without fabric reinforcement.

Two different feed spacers having different thickness and structure were tested. Both spacers were of the tricot type. The feed spacer of 0.25 mm thickness had a much finer structure with smaller distance between the filaments (*cf.* **Figure 6**). Note that experiments 12–15 were performed with the same membrane sample, and between each experiment the membrane cell was opened in order to enable replacement of the feed spacer. Further, a Hirose Histar 15-TH48 (HH 15-TH48) non-woven fabric was placed between the membrane and the feed spacer in

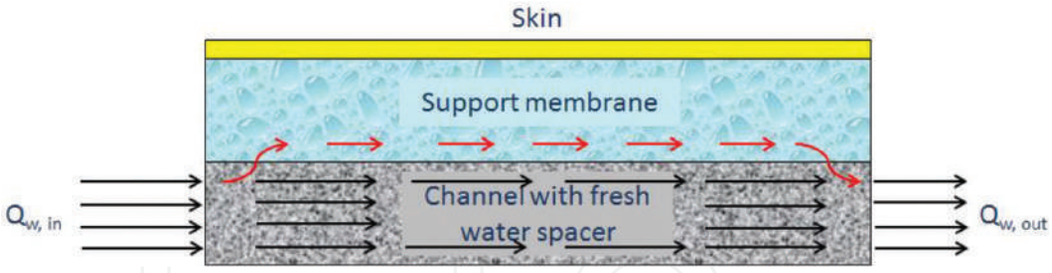

Figure 13. Flow conditions in the fresh water channel and support membrane.

Exp.	P_{max} (W/m²)	Δc at P_{max} (g/L)	p_{osm} (bar)	Feed water spacer	Extra fabric	Comment
10	3.5	28.1	14.7	0.50 mm	None	
11	4.5	27.4	18.0	2·0.25 mm	None	
12	4.6	27.1	19.0	2·0.25 mm	HH 15-TH48	
13	4.9	28.1	21.5	2·0.25 mm	HH 15-TH48	
14	4.3	28.3	20.0	0.50 mm	HH 15-TH48	
15	4.6	28.1	21.7	2·0.25 mm	HH 15-TH48	Spacer inv.

Table 2. Summary of PRO experiments with the TFC3 membrane.

order to assess if improved support to the membrane did influence membrane compaction, and the resulting increase in the structure parameter. Experiments 10 and 11 were performed with different membrane samples. The pressure dependent structure parameter was calculated for each experiment according to the procedure described in Section 4.4 and is shown in **Figure 14**.

The modelled structure parameter in the experiments performed with the 0.5 mm thick spacer was observed to increase more rapidly with increasing pressure compared to the experiments performed with the less coarse spacer of 0.25 mm thickness. Comparing the two experiments performed with the 0.5 mm spacer it was observed that the introduction of the extra non-woven fabric reduced the observed pressure dependency of the structure parameter. This indicates that improving the support for the membrane does influence the compaction of the membrane structure and the resulting increase in the structure parameter at elevated pressures.

The positive impact on the pressure dependency of the structure parameter by including the extra non-woven fabric was also observed for the experiments performed with the 0.25 mm feed spacer. The structure parameter of the fabric was estimated to 0.13 mm by performing independent salt diffusion experiments. The additional transport resistance exerted by the non-woven fabric can be recognised in the modelled structure parameter as the reinforcement layer ideally should add 0.13 mm to the isobaric structure parameter. This increment was not observed in Experiment 12; however, the deviation is within the expected uncertainty found in the pressure dependent structure parameters.

In Experiment 15, the feed spacer was inverted such that the "flat" side was facing the membrane, resulting in a slightly higher structure parameter compared to the experiments performed with normal orientation of the spacer.

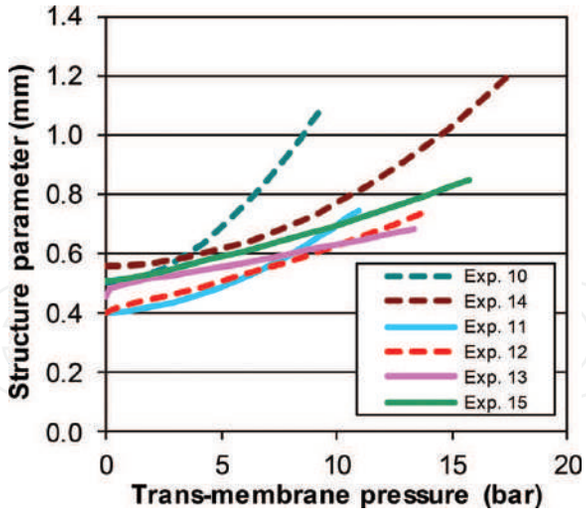

Figure 14. Structure parameter as function of trans-membrane pressure for the TFC3 membrane.

These results show that the extent of support for the membrane is crucial for the PRO performance. It was observed that the coarser spacer resulted in both a faster and a larger increase in the structure parameter at increasing pressure, compared to the more fine-structured spacer providing more support to the membrane. Similar behaviour has been observed in multiple experiments performed with different types of PRO membranes, and agrees well with recent literature [27]. The effect of introducing the extra reinforcement was observed to be larger for the coarser spacer.

5.5. Proposed measures to improve PRO performance at elevated pressures

In order to promote a high specific power in sea water/fresh water PRO, the structure parameter must be low, preferably less than 0.5 mm. The isobaric structure parameters measured for many existing membranes are well below this value. However, when pressurised, an excessive increase in the structure parameter have been observed for many potentially good PRO membranes. An improved strength of the support membrane which is more resistant to compression will therefore be required.

The results in **Figure 14** suggest that one approach to reduce the pressure dependency of the structure parameter might be to apply fine textured feed spacers. However, this will result in increased pressure drop in the feed channel, which might drastically reduce the net produced power in a PRO plant. Even the relatively coarse 0.5 mm feed spacer used in the present work will result in an unacceptable pressure loss. Thus, it should be investigated if it is possible to cast the support membrane directly on a feed spacer, possibly a fine textured tricot type. Supposing that this is viable, two membrane sheets may be separated by *e.g.* a simple diamond type spacer ensuring reasonable low frictional losses.

5.6. Uncertainty in experiments and modelling

The calculation of pressure dependent structure parameters in this paper were based on the assumption that the water and salt permeability were independent of the applied pressure, which may appear to be somewhat contradictory to part of the literature [18, 19]. Nevertheless, our assumption is based on several arguments. (1) In the presented work, the

Exp.	A_{leak}/A (%)	Exp.	A_{leak}/A (%)	Exp.	A_{leak}/A (%)
1	4.9	6	0.1	11	−3.1
2	4.2	7	−0.5	12	0.1
3	5.7	8	−0.6	13	−0.3
4	2.8	9	−1.0	14	0.1
5	0.2	10	−2.5	15	−0.1

Table 3. Hydraulic leakage relative to water permeability.

PRO experiments were performed with a tricot type feed spacer that has been found to result in the lowest variation in the modelled membrane parameters due to variations in trans-membrane pressures [19], and (2) initial water permeability tests using pressures up to 10 bar were performed prior to all PRO experiments. Thus, any membrane deformation that could be expected to influence the skin properties of the membrane as a result of pressurisation should have occurred during the water permeability tests. And (3) the obtained water permeability that were calculated at several pressure steps for each membrane were found to be independent of trans-membrane pressure.

At the end of each PRO experiment the amount of salt on the feed side was determined and compared with the amount of salt calculated by using the transport model. If an excess of salt was determined this was attributed to a hydraulic leakage, and subsequently a leakage volume was calculated by assuming zero salt rejection for the leakage. A leakage permeability, A_{leak}, was calculated based on the leakage volume, duration of the experiment, and average pressure during the experiment. The leakage permeabilities determined for the various experiments are given in **Table 3**. The total leakage volume was distributed for each pressure step based on the duration and average pressure of the step. The salt concentrations on each side of the membrane were subsequently recalculated resulting in new water and salt fluxes, and finally an updated value of excess salt was determined. The calculations converged quickly, and the excess salt was normally low, indicating no (negative leakage volume and thus negative ratio) or only minor leakages.

6. Conclusions

The pressure dependency of the structure parameter in PRO has been investigated for flat sheet membranes, and a transport model including procedures for determination of the pressure dependency of the structure parameter have been presented.

The results from laboratory experiments show that the structure parameter increases significantly with increasing trans-membrane pressure. This was the case both for the CTA membrane and the three TFC membranes that were tested, however, the impact of pressure on the structure parameter was found to be larger for the CTA membrane. Furthermore,

the increase in the structure parameter was observed to depend on the type of feed spacer. Using a finely textured spacer of the tricot type reduced the impact of pressure on the structure parameter in comparison to a coarser spacer material. Applying a non-woven backing material between the membrane and the fresh water spacer was also observed to reduce the impact of pressure on the structure parameter. These results show that developing membranes with sufficiently low structure parameter for pressures relevant for PRO will rely on the membrane's ability to resist deformation during compression. The type of feed spacer is another factor which is crucial to avoid deformation and the resulting increase in the structure parameter at elevated pressures.

The results also showed that increased flow velocities in the feed channel and the draw channel, respectively, will improve the mass transfer of water through the membrane. This might be partly ascribed to reduced concentration polarisation on the membrane surfaces. It is also suggested that high pressure gradients in the feed channel may result in convective flow in parts of the support membrane, improving the mass transfer conditions further. However, large frictional losses in the flow channels, will drastically reduce the net produced power in a sea water/fresh water PRO plant, and must be avoided. This will limit the choice of feed spacers that can be used for PRO.

Nomenclatures

A	water permeability (m/s/Pa)
A_{leak}	hydraulic leakage permeability (m/s/Pa)
B	salt permeability (m/s)
c_f	bulk concentration at the fresh water side (g/l)
c_{fm}	surface concentration at the fresh water side (g/l)
c_p	concentration at the interface between the skin and the porous support (g/l)
c_s	bulk concentration at the salt water side (g/l)
c_{sm}	surface concentration at the salt water side (g/l)
Δc_{skin}	concentration difference across the membrane skin (= $c_{sm} - c_p$) (g/l)
D	diffusion coefficient (m^2/s)
d_s	salt water film thickness (m)
d_f	freshwater film thickness (m)
F	constant in Eq. (10)
i	corrected van't Hoff coefficient (−)

J_V volume flux (m/s)

J_w water flux (m/s)

J_s salt flux (mol/m^2/s)

P specific power (W/m^2)

P_{max} maximum specific power (W/m^2)

p_{osm} practical osmotic pressure (bar)

Δp trans-membrane pressure (bar)

Δp_{max} maximum trans-membrane pressure (bar)

Δp_{ref} reference pressure in Eq. (10) (bar)

$Q_{water,in}$ volumetric flow of water entering a module (−)

$Q_{water,out}$ volumetric flow of water exiting a module (−)

R universal gas constant (J/K/mol)

S structure parameter (m)

S_0 isobaric structure parameter (m)

T absolute temperature (K)

u_{draw} empty channel velocity at draw side (cm/s)

u_{feed} empty channel velocity at feed side (cm/s)

x direction perpendicular to the membrane surface (m)

Δx_{mem} membrane thickness (m)

Greek letters

τ tortuosity (−)

φ porosity (−)

$\Delta\pi_{skin}$ osmotic pressure difference across the membrane skin (bar)

Author details

Torleif Holt[1]*, Edvard Sivertsen[2], Willy R. Thelin[2] and Geir Brekke[3]

*Address all correspondence to: Torleif.Holt@sintef.no

1 SINTEF Petroleum, Trondheim, Norway

2 SINTEF Building and Infrastructure, Trondheim, Norway

3 Statkraft AS, Oslo, Norway

References

[1] Skilhagen SE, Dugstad JE, Aaberg RJ. Osmotic power—Power production based on the osmotic pressure difference between waters with varying salt gradients. Desalination. 2008;**220**:476-482. DOI: 10.1016/j.desal.2007.02.045

[2] Logan BE, Elimelech M. Membrane-based processes for sustainable power generation using water. Nature. 2012;**488**:313-319. DOI: 10.1038/nature11477

[3] Touati K, Tadeo F, Elfil H. Osmotic energy recovery from reverse osmosis using two-stage pressure retarded osmosis. Energy. 2017;**132**:213-224. DOI: 10.1016/j.energy.2017.05.050

[4] Bajraktari N, Helix-Nielsen C, Madsen HT. Pressure retarded osmosis from hypersaline sources—A review. Desalination. 2017;**413**:65-85. DOI: 10.1016/j.desal.2017.02.017

[5] Attarde D, Jain M, Singh PK, Gupta SK. Energy-efficient seawater desalination and wastewater treatment using osmotically driven membrane processes. Desalination. 2017; **413**:86-100. DOI: 10.1016/j.desal.2017.03.010

[6] Sivertsen E, Holt T, Thelin WR, Brekke GM. Iso-watt diagrams for evaluation of membrane performance in pressure retarded osmosis. Journal of Membrane Science. 2015;**489**:299-307. DOI: 10.1016/j.memsci.2015.04.042

[7] Chou S, Wang R, Fane AG. Robust and high performance hollow fiber membranes for energy harvesting from salinity gradients by pressure retarded osmosis. Journal of Membrane Science. 2013;**448**:44-54. DOI: 10.1016/j.memsci.2013.07.063

[8] Yip YN, Tiraferri A, Phillip WA, Schiffman JD, Hoover LA, Kim YC, Elimelech M. Thin-film composite pressure retarded osmosis membranes for sustainable power generation from salinity gradients. Environmental Science & Technology. 2011;**45**:4360-4369. DOI: 10.1021/es104325z

[9] Han G, Zhang S, Li X, Chung TS. High performance thin film composite pressure retarded osmosis (PRO) membranes for renewable salinity-gradient energy generation. Journal of Membrane Science. 2013;**440**:108-121. DOI: 10.1016/j.memsci.2013.04.001

[10] Han G, Wang P, Chung TS. Highly robust thin-film composite pressure retarded osmosis (PRO) hollow fiber membranes with high power densities for renewable salinity-gradient energy generation. Environmental Science and Technology. 2013;**47**:8070-8077. DOI: 10.1021/es4013917

[11] Zhang S, Sukitopaneenit P, Chung TS. Design of robust hollow fibre membranes with high power density for osmotic energy production. Chemical Engineering Journal. 2014; **241**:457-465. DOI: 10.1016/j.cej.2013.10.063

[12] Kim YC, Elimelech M. Potential of osmotic power generation by pressure retarded osmosis using seawater as feed solution. Analysis and experiments. Journal of Membrane Science. 2013;**429**:330-337. DOI: 10.1016/j.memsci.2012.11.039

[13] Sivertsen E, Holt T, Thelin WR, Brekke GM. Pressure retarded osmosis efficiency for different hollow fibre membrane module flow configurations. Desalination. 2013;**312**:107-123. DOI: 10.1016/j.desal.2012.11.019

[14] She QH, Jin X, Tang CY. Osmotic power production from salinity gradient resource by pressure retarded osmosis: Effects of operating conditions and reverse solute diffusion. Journal of Membrane Science. 2012;**401**:262-273. DOI: 10.1016/j.memsci.2012.02.014

[15] Thorsen T, Holt T. The potential for power production from salinity gradients by pressure retarded osmosis. Journal of Membrane Science. 2009;**335**:103-110. DOI: 10.1016/j.memsci.2009.03.003

[16] Yip NY, Elimelech M. Thermodynamic and energy efficiency analysis of power generation from natural salinity gradients by pressure retarded osmosis. Environmental Science & Technology. 2012;**46**:5230-5239. DOI: 10.1021/es300060m

[17] Tiraferri A, Yip NY, Phillip WA, Schiffman JD, Elimelech M. Relating performance of thin-film composite forward osmosis membranes to support layer formation and structure. Journal of Membrane Science. 2011;**367**:340-352. DOI: 10.1016/j.memsci.2010.11.014

[18] Kim YC, Elimelech M. Adverse impact of Feed Channel spacers on the performance of pressure retarded osmosis. Environmental Science & Technology. 2012;**46**:4673-4681. DOI: 10.1021/es3002597

[19] She Q, Hou D, Liu J, Tan KH, Tang CY. Effect of feed spacer induced membrane deformation on the performance of pressure retarded osmosis (PRO): Implications for PRO process operation. Journal of Membrane Science. 2013;**445**:170-182. DOI: 10.1016/j.memsci.2013.05.061

[20] McCutcheon JR, Elimelech M. Modeling water flux in forward osmosis: Implications for improved membrane design. AICHE Journal. 2007;**53**:1736-1744. DOI: 10.1002/aic.11197

[21] McCutcheon JR, Elimelech M. Influence of concentrative and dilutive internal concentration polarization on flux behavior in forward osmosis. Journal of Membrane Science. 2006;**284**:237-247. DOI: 10.1016/j.memsci.2006.07.049

[22] McCutcheon JR, Elimelech M. Forward (direct) osmosis desalination using polymeric membranes. Abstracts of Papers of the American Chemical Society. 2004;**228**:261

[23] Tang CY, She QH, Lay WCL, Wang R, Fane AG. Coupled effects of internal concentration polarization and fouling on flux behavior of forward osmosis membranes during humic acid filtration. Journal of Membrane Science. 2010;**354**:123-133. DOI: 10.1016/j.memsci.2010.02.059

[24] Tang WL, Ng HY. Concentration of brine by forward osmosis: Performance and influence of membrane structure. Desalination. 2008;**224**:143-153. DOI: 10.1016/j.desal.2007.04.085

[25] Dytnerskij JI. Membranprozesse—Theorie und Berechnung. Moskau: Verlag Chimija; 1986. p. 254

[26] Sivertsen E, Holt T, Thelin WR, Brekke GM. Modelling mass transport in hollow fibre membranes used for pressure retarded osmosis. Journal of Membrane Science. 2012;**417-418**: 69-79. DOI: 10.1016/j.memsci.2012.06.014

[27] Sim J, Koo J, Nam S, Kim E, Hwang TM. Effect of combined positions of feed spacer-type tricot on the performance in pressure retarded osmosis (PRO). Desalination and Water Treatment. 2017;**77**:63-68. DOI: 10.5004/dwt.2017.20667

Chapter 7

Nonideal Solution Behavior in Forward Osmosis Processes Using Magnetic Nanoparticles

Jimmy D. Roach, Mandy M. Bondaruk and Zain Burney

Additional information is available at the end of the chapter

http://dx.doi.org/10.5772/intechopen.72474

Abstract

Despite the tremendous progress made toward the realization of wider application for forward osmosis (FO) technologies, lack of suitable draw solutes that provide high water flux, low reverse solute flux, and facile recovery has hindered commercial development. An extensive variety of osmotic agents have been investigated during the past decade, and while simple inorganic salts remain the most widely used, organic-coated magnetic nanoparticles (MNPs) offer exploitable properties that hold great promise. In addition to size-mitigated reverse flux and low-cost recovery via magnetic separation, devitalized MNPs provide enhanced osmotic performance when compared to that of the ungrafted coating material at similar concentration levels, a consequence of greater nonideal solution behavior. This nonideality has been assessed using a simple, semiempirical model and is largely attributable to the increased solvent-accessible surface area and enhanced hydration. When attached to MNPs, polymers appear to behave osmotically as much smaller molecules, providing higher osmotic pressures and improved FO performance.

Keywords: forward osmosis, nonideality, draw solute, magnetic nanoparticles, counterion binding

1. Introduction

Forward osmosis (FO) exploits the natural osmotic pressure gradient between two fluids separated by a semi-permeable membrane to induce the net transport of solvent from a solution of lower osmotic pressure to that of higher osmotic pressure. The FO process appears to provide a low-energy, low-cost alternative to more conventional membrane-based separation methods and offers a myriad of potential applications in industries as diverse as desalination, oil and gas, and food processing [1, 2]. Despite advances made in FO during the past

decade, several challenges must still be overcome before more widespread relevance of the technology can be realized [3]. Recently, Shaffer et al. [4] provided a thermodynamic argument showing that FO-reverse osmosis (RO) desalination schemes cannot provide energy savings when compared to standalone RO. Although FO technology has been applied to a variety of water treatment strategies, draw solute inadequacies restrict its wider application [5, 6]. Mitigation of these inadequacies requires identification of draw solutions that achieve high osmotic pressure while minimizing reverse solute flux and also providing ease of recovery; the need for osmotic agents that allow for facile, inexpensive recovery remains paramount [7].

During the past decade, researchers have primarily focused their efforts in two areas, FO membrane production and draw solute identification. While considerable progress has been made toward the development of inexpensive and more robust membranes [8, 9], few commercially viable osmotic agents have been identified [10]. Desirable properties of the ideal osmotic agent are that it be nontoxic, inexpensive, stable, and highly water-soluble. In addition, the agent should have limited reverse draw solute flux, reduce internal concentration polarization (ICP), and be easily recoverable. Some osmotic agents and recovery schemes investigated to date include using inorganic salts with recovery by RO [11]; using poly(sodium acrylate) with recovery by ultrafiltration (UF) [12]; using thermoresponsive chitosan derivatives with recovery by aggregation at elevated temperature [13]; using ammonia-carbon dioxide with recovery by thermal separation [14]; using poly(N-isopropylacrylamide-co-acrylic acid) with recovery by heating and centrifugation [15]; using surfactants with recovery by UF [16]; and, using polyelectrolyte-based hydrogels with recovery by elevated temperature and pressure [17]. A critical review of what the authors term non-responsive and responsive draw solutes was recently provided by Cai and Hu [7].

Because they meet several of the aforementioned criteria, low reverse draw flux and easy recovery in particular, functionalized magnetic nanoparticles (MNPs) have garnered much attention as potential osmotic agents [18]. These MNPs typically incorporate a superparamagnetic core of Fe_3O_4, with a magnetization value of 75.0 emu g^{-1} [19], onto which organic content is coated. Among the grafting agents that have been affixed to MNPs and investigated in FO processes are 2-pyrrolidine, triethylene glycol, and poly(acrylic acid) [20]; dextran [21]; poly(ethylene glycol) diacid [22]; poly(sodium acrylate) [23–25]; poly(sodium styrene-4-sulfonate) and poly(N–isopropylacrylamide) [26]; citrate [27]; hyperbranched polyglycerol [28]; and, citric acid and oxalic acid [19]. A primary advantage of using MNPs is their ease of recyclability through magnetic separation, although particle aggregation has been shown to diminish FO water flux values after multiple regeneration cycles [10]. Another benefit of derivatized MNPs is that they have been shown to provide higher osmotic pressures when compared to solutions of the organic grafting agents alone [20], an enhancement attributable to increased solution nonideality.

A solution behaves ideally when: (1) solute/solute, solvent/solvent, and solvent/solute interactions are identical and (2) all solute and solvent molecules occupy the same volume. Real solutions deviate from ideality due to an energetic nonequivalence in one or more of these interactions and/or volume occupancies are not identical. In aqueous solution, water molecules exhibit particularly strong hydrogen bonding with various organic functional groups, carboxylate moieties in particular [29]. Factors such as hydration, ion-pairing, and dimerization can

be significant contributors to thermodynamic nonideality [30] and can dramatically impact the osmotic performance of FO draw solutions.

A variety of models have been developed to explain the interesting osmotic behavior of concentrated solutions of proteins and other biological molecules [31–34]. The nonideal solution behavior of large biological molecules can lead to extreme changes in osmotic pressure. As an example, at a fixed protein concentration, the osmotic pressures of bovine serum albumin (BSA) solutions display greater than fivefold changes in the range $3 < pH < 8$ [32]. Such nonideality is generally attributable to variations in solvent-accessible surface area and polymeric segmental motion [35]. Models that adequately describe nonideal behavior in BSA and other polymer solutions provide a basis for explaining the unique osmotic properties of MNPs used in FO.

2. Osmotic theory

In order to function effectively as a draw agent in FO, the osmotic pressure of the draw solution must far exceed that of the feed solution. In terms of desalination, the draw must have an osmotic pressure significantly in excess of 7.7 atm in the case of a brackish feed, and in excess of 27 atm in the case of a seawater feed [4]. Because of their abilities to achieve high osmotic pressures while maintaining low solution viscosities, simple inorganic salts remain the most widely used draw agents. In addition, small ions tend to have greater diffusivity values thus moderating the effect of concentrative ICP. The strong affinity of small inorganic ions for water is revealed in their highly exothermic enthalpies of hydration [36]. This strong affiliation serves to significantly lower the chemical potential of water in draw solutions. Strong solvent/solute interactions provide high solution osmotic pressures while paradoxically making the regeneration of draw solute more difficult. Resolving this paradox has spurn interest in the development of easily removable draw agents that allow for regeneration through exploitation of solute size, thermal sensitivity, or magnetic properties. Of course, to be effective in FO processes these solutes must still provide appreciable osmotic pressure. Interestingly, structural features of various macromolecular species and molecular aggregates that allow for easy removal from aqueous solution can also serve to enhance osmotic pressure through nonideal solvent/solute interactions.

2.1. Osmotic pressure and FO water flux

The effects of osmotic pressure, solution viscosity, and molecular/ionic diffusivity on water flux (J_w) are shown in Eq. (1),

$$J_w = \frac{D\varepsilon}{t\tau} \ln \frac{B + A\pi_{D,m} - J_w}{B + A\pi_{F,b}} \tag{1}$$

where D is the diffusion coefficient of the solute (which decreases with solution viscosity); ε, t, and τ are the porosity, thickness, and tortuosity of the membrane support layer, respectively; B is the salt permeability coefficient of the membrane active layer; A is the pure water permeability coefficient; $\pi_{D,m}$ is the osmotic pressure of the draw solution at the membrane surface; and, $\pi_{F,b}$ is the osmotic pressure of the feed solution in the bulk [37]. Water flux increases with

increasing osmotic pressure difference ($\pi_{D,m} - \pi_{F,b}$), however the relationship is nonlinear because of ICP. As Eq. (1) demonstrates, draw solution osmotic pressure is the principal driving force in FO processes.

2.2. Thermodynamic basis of osmotic pressure

Consider an FO process using a polymer solution as the osmotic agent. If a polymer solution is separated from pure water by a semipermeable membrane the movement of water through the barrier is explained in terms of the chemical potential of the water, μ_w, under isothermal conditions, as given in Eq. (2),

$$\mu_w(P, X) = \mu_w^o(P, X^o) + RTln(\alpha_w) \tag{2}$$

where P is pressure, X is solution composition, R is the gas constant, T is temperature, α_w is the activity of water in the solution, and the superscript "o" denotes standard conditions. For the derivation that follows α_w will be replaced with the mole fraction of water in solution, X_w. In **Figure 1**, water spontaneously moves from the left side to the right side because $\mu_{w,left} > \mu_{w,right}$. Alternatively, it is possible to prevent net water flow by increasing the external pressure on the polymer solution such that $\mu_{w,left} = \mu_{w,right}$. The amount by which the external pressure is increased to prevent net flow is termed the osmotic pressure, π, of the draw solution.

As Eq. (2) implies, it is reasonable to differentiate μ_w in terms of P and X_s (the mole fraction of solute) to obtain Eq. (3).

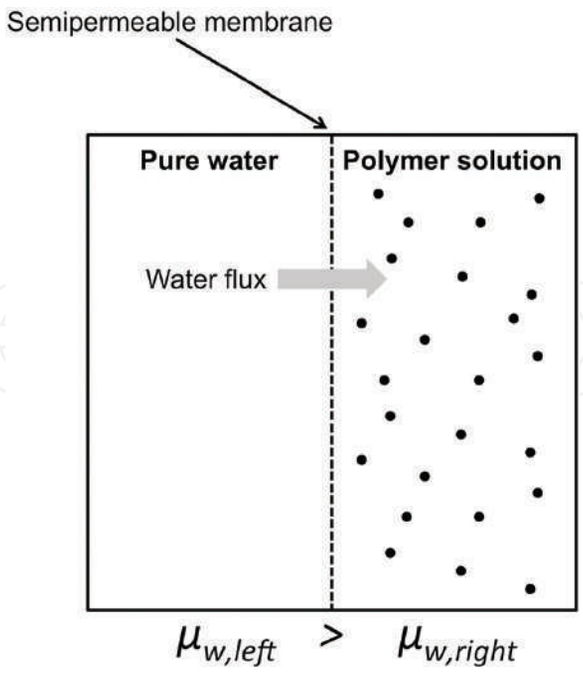

Figure 1. Osmotic behavior of an aqueous polymer solution.

$$d\mu_w = \left(\frac{\partial \mu_w}{\partial P}\right)_{T, X_s} dP + \left(\frac{\partial \mu_w}{\partial X_s}\right)_{T, P} dX_s \tag{3}$$

The definitions of Gibbs free energy and chemical potential are given by Eqs. (4) and (5), respectively,

$$G = H - TS \tag{4}$$

$$\mu_w = \left(\frac{\partial G}{\partial n_w}\right)_{T, P, n_s} \tag{5}$$

where H is enthalpy, S is entropy, n_w is moles of water, and n_s is moles of solute. Application of fundamental thermodynamics to a two-component solution of water and polymer solute, s, provides Eq. (6), in which V is the volume of solution.

$$dG = -SdT + VdP + \left(\frac{\partial G}{\partial n_w}\right)_{T, P, n_s} dn_w + \left(\frac{\partial G}{\partial n_s}\right)_{T, P, n_w} dn_s \tag{6}$$

Eq. (6) reveals that under conditions of constant temperature and solution composition, the derivative of Gibbs free energy with respect to pressure is given by Eq. (7).

$$\left(\frac{\partial G}{\partial P}\right)_{T, X} = V \tag{7}$$

By differentiating Eq. (5) with respect to pressure, while holding other variables constant, Eq. (8) is obtained.

$$\left(\frac{\partial \mu_w}{\partial P}\right)_{T, X} = \frac{\partial^2 G}{\partial P \partial n_w} \tag{8}$$

Similarly, by differentiating Eq. (7) with respect to amount of water Eq. (9) is obtained, in which V_{m_w} is the partial molar volume of water.

$$\frac{\partial^2 G}{\partial n_w \partial P} = \left(\frac{\partial V}{\partial n_w}\right) = V_{m_w} \tag{9}$$

Because of the symmetry of second derivatives, meaning the order of differentiation is inconsequential, the partial molar volume of water is also given by Eq. (10).

$$V_{m_w} = \left(\frac{\partial \mu_w}{\partial P}\right)_{T, X} \tag{10}$$

Next, differentiation of an analogous form of Eq. (2) with respect to X_w provides Eq. (11).

$$\left(\frac{\partial \mu_w}{\partial X_w}\right)_{T,P} = \frac{RT}{X_w} \tag{11}$$

Because $X_w = 1 - X_s$ and therefore $\frac{dX_w}{dX_s} = -1$, Eq. (12) can be obtained.

$$\left(\frac{\partial \mu_w}{\partial X_s}\right)_{T,P} = \left(\frac{\partial \mu_w}{\partial X_w}\right)_{T,P} \frac{dX_w}{dX_s} = -\frac{RT}{1 - X_s} \tag{12}$$

If there is no net flow of water in an apparatus like that depicted in **Figure 1**, $d\mu_w = 0$ providing Eq. (13).

$$\left(\frac{\partial \mu_w}{\partial P}\right)_{T,X_s} dP = -\left(\frac{\partial \mu_w}{\partial X_s}\right)_{T,P} dX_s \tag{13}$$

Substituting Eqs. (10) and (12) into Eq. (13) and then integrating provides Eq. (14).

$$\int_{P_o}^{P_o+\pi} V_{m_w} dP = RT \int_0^{X_s} \frac{dX_s}{1 - X_s} \tag{14}$$

Assuming the solution is incompressible (meaning that partial molar volume is independent of pressure) allows for simple integration providing Eq. (15).

$$\pi = -\frac{RT}{V_{m_w}} \ln (1 - X_s) = -\frac{RT}{V_{m_w}} \ln (X_w) \tag{15}$$

For dilute solutions ($X_s \ll 1$ and $n_s \ll n_w$) the approximations in Eqs. (16) and (17) are justified,

$$\ln (1 - X_s) \approx -X_s \tag{16}$$

$$X_s = \frac{n_s}{n_s + n_w} \approx \frac{n_s}{n_w} \tag{17}$$

which upon substitution into Eq. (15) provides the familiar van't Hoff equation, Eq. (18).

$$\pi V = n_s RT \tag{18}$$

Deviations of solution osmotic pressure data from Eq. (18) are generally attributable to nonideal solvent-solute and solute-solute interactions. One way of expressing the extent to which a solution deviates from ideality is through the osmotic coefficient, ϕ, which is defined on an amount fraction basis in Eq. (19).

$$\phi = \frac{\mu_w^o - \mu_w}{RTlnX_w} \tag{19}$$

The osmotic coefficient is analogous to the activity coefficient and can be defined in terms of other concentration units. It is often used in conjunction with *i*, which accounts for dissociation/ion-pairing, to provide Eq. (20), where C_s is the molar concentration of associated solute.

$$\pi = i\varphi C_s RT \tag{20}$$

Alternatively, and in particularly for polymer solutions, solution osmotic pressure is often expressed as a power series expansion in C_s as in Eq. (21),

$$\pi = RT\left(\frac{C_s}{M_r} + A_2 C_s^2 + A_3 C_s^3 + \ldots\right) \tag{21}$$

where M_r is molar mass and A_2 and A_3 are the second and third virial coefficients, respectively. These coefficients are temperature dependent, empirically determined constants for a given solvent system. In terms of the activity of water, α_w, osmotic pressure is perhaps best expressed as shown in Eq. (22).

$$\pi = -\frac{RT}{V_{m_w}} \ln(\alpha_w) \tag{22}$$

An empirical, semi-empirical, or theoretical methodology can then be used to relate α_w in Eq. (22) to X_w in Eq. (15). Given the significance of Eqs. (15) and (22), it is important to discuss the factors that effectively reduce the mole fraction of *free* water through hydration of solute species. The hydration number of a solute, h, influences X_w as shown in Eq. (23).

$$X_w = \frac{n_w - hn_s}{n_w - hn_s + in_s} \tag{23}$$

In terms of solute molality (C_{sm}), a concentration unit often reported in FO studies, the hydration number of a solute, h, can be incorporated as shown in Eq. (24),

$$C_{sm} = \frac{n_s}{M_w - (hn_s \times 0.018015)} \tag{24}$$

where M_w is the total mass of water in the solution in kg. Solutes with greater h values produce solutions with higher osmotic pressures at a given concentration and are potentially better draw agents in FO processes, though viscosity considerations are also very important.

2.3. Osmotic pressure of aqueous solutions of inorganic salts

Wilson and Stewart [38] have provided a good discussion of how solution osmotic pressure is affected by the hydration of simple ionic compounds. The short range interactions between electron pairs in water molecules and cations lead to h values that can range from, for example, 1.8 for NH_4^+ to 13 for Mg^{2+} [39]. To illustrate the influence of hydration, consider the comparison of aqueous solutions of NaCl and KCl as osmotic agents. Achilli et al. [11] determined the concentrations of NaCl and KCl required to achieve a solution osmotic pressure of 44 atm and also the corresponding J_w values for these solutions. **Table 1** provides the results of using Eqs. (15) and (23), with literature values [40] for h and i, to calculate osmotic pressures. The sodium ion's smaller size and corresponding higher charge density impart a larger h value,

Compound	Molarity	h	i	X_w	π (atm)	J_w (m/s)
NaCl	0.869	3.9	1.84	0.968	44	3.38×10^{-6}
KCl	0.943	1.7	1.85	0.968	44	3.74×10^{-6}

Table 1. Osmotic properties of aqueous solutions of NaCl and KCl [11, 40].

allowing NaCl solutions to achieve a given osmotic pressure at a lower concentration than KCl solutions.

In terms of osmotic pressure and corresponding FO performance there are diminishing returns on using ever-higher concentrations of ionic compounds, especially when increased solution viscosity is also considered. While hydration numbers tend to increase with increasing cation charge density, they decrease with increasing concentration, owing in part to increased ion-pairing, effectively reducing *i*. The hydration of molecular aggregates or macromolecular species and its corresponding effect on solution osmotic pressure has also been extensively studied, especially for systems consisting of poly(ethylene glycol) (PEG), DNA, chondroitin sulfate, and BSA [31–35, 41, 42]. These studies provide valuable insights into FO processes using molecular aggregates or macromolecular species as draw agents, especially those incorporating MNPs.

2.4. Osmotic properties of aqueous solutions of large organic molecules

In their studies of BSA, Kanal et al. [32] observed that osmotic pressure decreases as solution pH increases from 3 to approximately 4.6 and then increases with pH. Increases in osmotic pressure on either side of the minimum are attributed to increased electrostatic repulsive interactions. At pH values below the isoelectric point (pI_{BSA} = 5.4), the protein adopts a net positive charge along its surface. At pH values above pI_{BSA}, it is net negative. Electrostatic repulsion leads to a less compact protein conformation, greater segmental motion, more effective hydration, and higher osmotic pressures. Near the isoelectric point, the net-neutral protein strands adopt a more compact configuration, are less hydrated, and even tend to aggregate due to reduced intermolecular repulsion. The osmotic nonideality of BSA solutions is generally attributable to two sources: (1) large solvent/solute interactions that effectively increase polymer hydration (*h*) and (2) segmental motion of small portions of the polymer chains that effectively increase the number of particles in solution (*i*). Similar sources of nonideal behavior were also used to describe the osmotic properties of aqueous solutions of PEG [31, 43, 44].

The hydration of PEG of molecular weight 2000 Da (PEG^{2000}), both unattached and attached to distearoyl phosphoethanolamine liposomes ((DSEP)-PEG^{2000}), was investigated by Tirosh et al. [43]. Using differential scanning calorimetry, PEG^{2000} was found to bind 136 $\pm$ 4 water molecules, while (DSEP)-PEG^{2000} binds 210 $\pm$ 6 water molecules. In terms of hydration number per monomeric unit (approximately 46 units in 2000 Da PEG), these binding values correspond to hydration numbers of 3.0 and 4.6 for PEG^{2000} and (DSEP)-PEG^{2000}, respectively. The increase in water molecule binding is attributed to conformational changes, a coil configuration in PEG^{2000} and a brush configuration in (DSEP)-PEG^{2000}. When grafted to the liposome surface, the close

proximity of the polymeric strands causes them to repel each other and to adopt a more extended, easily hydrated, form. Such behavior has been exploited in the development of draw agents that incorporate superparamagnetic magnetite (Fe_3O_4) onto which polymers were grafted [19–28].

3. MNPs as FO draw agents

A summary of some recent applications of derivatized MNPs as draw agents in FO processes is provided in **Table 2**, which includes approximate concentrations of the repeating (monomeric) units used as capping agents on the MNPs. Other researchers have demonstrated that the osmotic properties of aqueous polymer solutions are perhaps best interpreted in terms of monomer concentration [31, 45].

Coating agent	Size (nm)	[Monomer] (M)	J_w (LMH)	π (atm)	Ref.
2-Pyrrolidine	28	0.15	4.6	17	[20]
TREG	24	0.20	5.8	23	
PAA^{1800}	21	1.0	7.6	36	
Dextran	10	11	8.9	N/A	[21]
PEG^{250}-$(COOH)_2$	11.7	0.37	N/A	73	[22]
PEG^{600}-$(COOH)_2$	13.5	0.88	9.1	66	
PEG^{4000}-$(COOH)_2$	17.5	5.9	N/A	55	
PAA^{1800}	5	1.5	11.2	70	[46]
PAA^{1800}	20	N/A	N/A	18	[23]
$PNaAA^{1800}$	20	N/A	2.1	32	
$PCaAA^{1800}$	20	N/A	1.8	27	
PNaSS-PNIPAM	5	2.3	14.9	55.0	[26]
	9	2.5	9.9	40.8	
Citrate	3–8	0.015	16	N/A	[27]
HPG	20.9	2.1	6.7	15	[28]
$PNaAA^{2100}$	9	0.0083	5.3	11.4	[24]
Citric acid	40	0.52	12.7	64	[19]
Oxalic acid	35	0.84	10.3	47	
PNaAA	160	12.4	N/A	19.5	[25]
Si-COOH	12.7	0.046	1.7	6.3	[47]
$Si\text{-}PEG^{530}$	13.6	0.43	2.0	7.6	

Abbreviations: TREG: triethylene glycol; PAA: poly(acrylic acid); PEG-$(COOH)_2$: poly(ethylene glycol) diacid; PNaAA: poly(sodium acrylate); PCaAA: poly(calcium acrylate); PNaSS-PNIPAM: poly(sodium styrene-4-sulfonate) and poly(N-isopropylacrylamide) [15% PNaSS, 85% PNIPAM]; HPG: hyperbranched polyglycerol; Si-COOH: N-(trinethoxysilylpropyl)ethylenediamine triacetic acid; Si-PEG: 2-[methoxy- (polyethyleneoxy)propyl]trimethoxysilane. Superscripts represent the average molecular weights of polymeric stands.

Table 2. Summary of MNP-based draw agents used in FO processes.

3.1. Osmotic behavior of draw agents alone vs. grafted onto MNPs

Some investigators have studied the FO properties of osmotic agents that are both alone in aqueous solution and grafted onto MNPs [20, 24]. Ling et al. [20] compared 2-pyrrolidine, TREG, and PAA as draw solutes. When grafted onto MNPs, 2-pyrrolidine exhibited a near sixfold increase in osmolality when compared to the ungrafted solute. TREG and PAA exhibited approximately threefold and thirtyfold increases in osmolalities, respectively, at similar concentrations when grafted onto MNPs. Dey and Izake [24] found that 3.5 wt.% PNaAA provided a FO-water flux value of 1.72 LMH while only 0.078 wt.% PNaAA grafted onto MNPs provided a flux value of 5.32 LMH. These results indicate that anchoring polymers onto nanoparticles serves to significantly improve their osmotic performance.

The tremendous enhancement to osmotic pressure and water flux values associated with polymeric solutes anchored to MNPs can be attributed to improved hydration of the polymeric strands. The dense packing of polymer chains around MNPs leads to a more extended, brush-like, conformation due to excluded volume interactions [48, 49]. In addition, Ling et al. [20] ascribe a reduced interaction between PAA-MNPs and the FO-membrane surface as also contributing to the improved performance; carboxyl groups interacting with ester moieties on the membrane surface are not interacting with water and thereby reducing its chemical potential.

3.2. A semiempirical model

While h values can serve as a good assessment of changes in solution ideality, simply using Eqs. (15) and (23) to calculate h requires highly precise measurements of amount and osmotic pressure. Such measurements are likely not practical for osmotic systems incorporating macromolecular species or derivatized MNPs in FO. Fortunately, Fullerton et al. [50] proposed using Eq. (25) to model the osmotic behavior of proteins,

$$\frac{M_w}{M_s} = S \times \frac{1}{\pi} + I \tag{25}$$

where M_w is the mass of water, M_s is the mass of solute, and the two fitting parameters, S and I, are assessments of nonideality. The slope is given by Eq. (26),

$$S = \frac{RT\rho}{A_e} \tag{26}$$

where ρ is the density of water at temperature, T, and A_e is the effective osmotic molecular weight. Parameter I is a measure of solvent/solute interactions and is interpreted as varying directly with solvent-accessible surface area. The model and fitting parameters have been shown to adequately explain the solution properties of macromolecular solutes like BSA [32, 35] and PEG [31]. A free-solvent model proposed by Yousef et al. [51] that uses mole fraction as a measure of composition may also prove useful in analyzing nonidealities and has been shown effective particularly at high solute concentrations.

Figure 2 depicts the application of Eq. (25) to data for TREG [20, 31, 52] both alone in solution and grafted to MNPs. The ungrafted TREG molecules display little deviation from ideality,

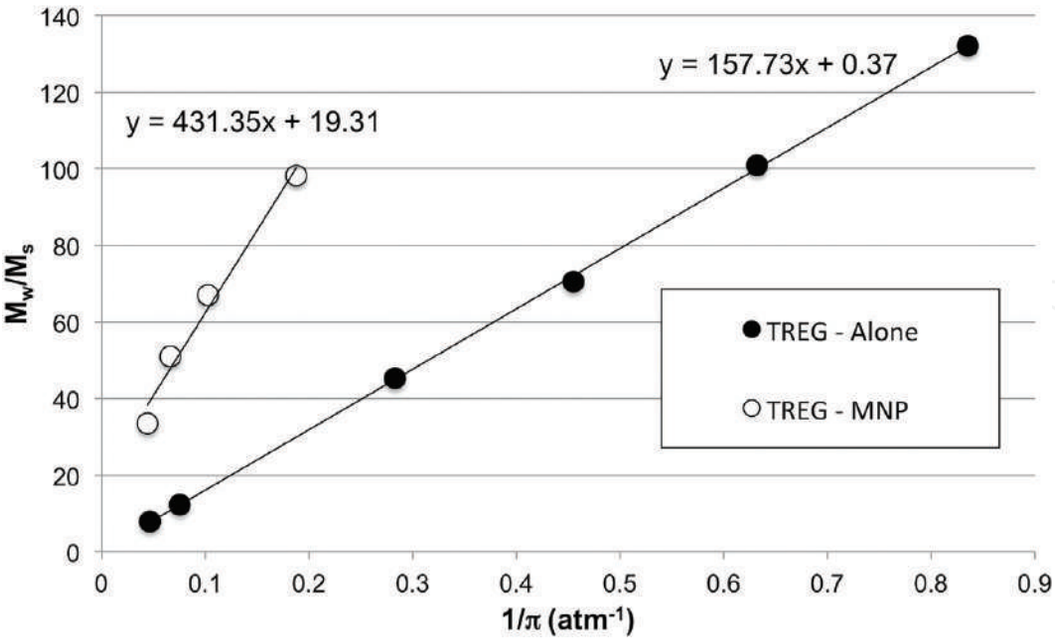

Figure 2. Nonideality analyses for TREG, using data from [20, 31, 52].

with a relatively small I value (0.37) and an effective osmotic molecular weight (153 g mol^{-1}) that is very close to the true molecular weight (150 g mol^{-1}). Though available data is somewhat limited, when grafted, nonideality appears to increase significantly. The value for I (19.3) is quite large when compared to values typically obtained for BSA (~4–12) [35] and for PEG (~1–4) [31], likely resulting from an increase in the amount of water in hydration shells around MNPs when compared to ungrafted TREG. The value for A_e (56.1 g mol^{-1}) is significantly lower than the value for the anchored trimer (149 g mol^{-1}), indicating that the grafted molecule behaves in solution as much smaller molecules.

The application of Eq. (25) to data for which 2-[methoxy-(polyethyleneoxy)$_{6–9}$propyl] trimethoxysilane (MW: 459–591 g mol^{-1}) was used as the grafting agent [47] is provided in **Figure 3**. When compared to TREG data, the greater number of monomers per polymeric strand results in a smaller I value (5.8) and a larger A_e value (101 g mol^{-1}). Although there are differences in particle size and attachment group, these data seem to demonstrate that polymer molar mass affects osmotic performance. Ge et al. [22] found that MNPs coated with PEG^{250}-(COOH)$_2$ provided the best FO performance when compared to similar grafting agents of larger molar mass, observing lower osmotic pressures per monomer concentration as polymer length increased. This difference is perhaps attributable to limited interactions between shorter grafted polymeric strands when compared to longer. Because of the close proximity of individual strands when attached to MNPs, longer strands may be more likely to become intertwined with neighboring strands, thus reducing the surface area available for hydration. Interestingly, the opposite trend has been observed for ungrafted PEGs in the range 200 Da to 10,000 Da, with I values generally increasing with molecular weight before leveling off [31]. Ge et al. [22] also found that MNP-dispersibility increases with polymer length. Optimizing FO performance requires balancing the competing effects of polymer size on dispersibility, osmotic pressure, and viscosity.

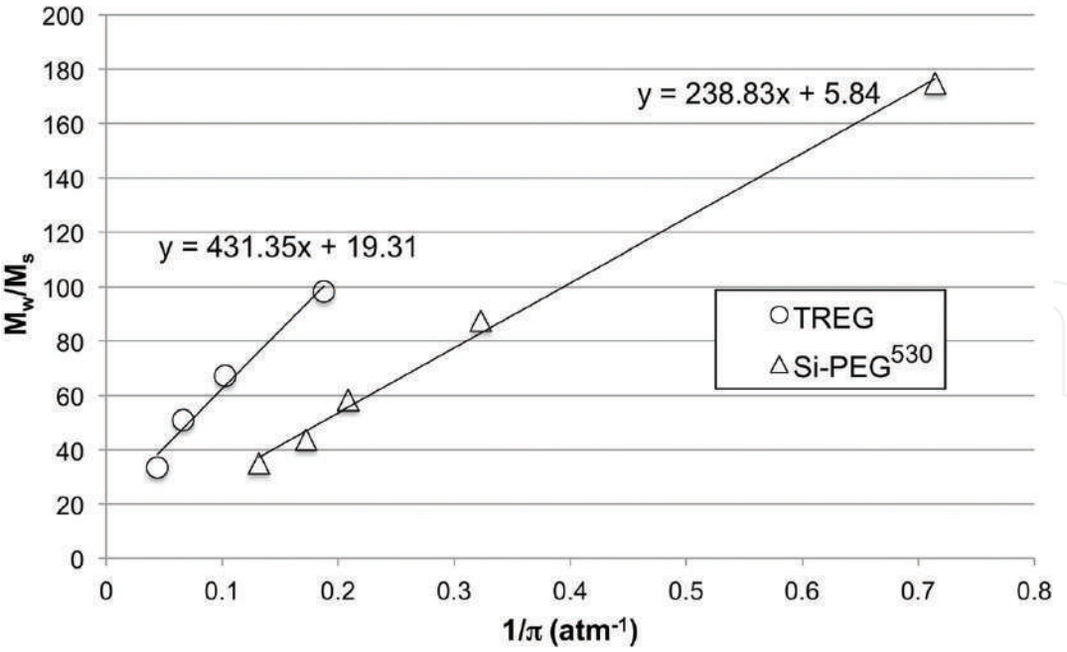

Figure 3. Nonideality analyses for TREG and Si-PEG^{530}, using data from [20, 31, 47, 52].

In **Figure 4**, data for MNPs coated with PAA [20] and HPG [28] are depicted. These results again demonstrate the significant nonideal solution behavior of derivatized MNPs. The large A_e and small I values associated with HPG seem to indicate that the sprawling network of ether linkages may hinder hydration on a per gram of grafting agent basis. By comparison, the long, filamentous PAA^{1800} strands provide an A_e value of 111 g mol^{-1}, which is intermediate between the

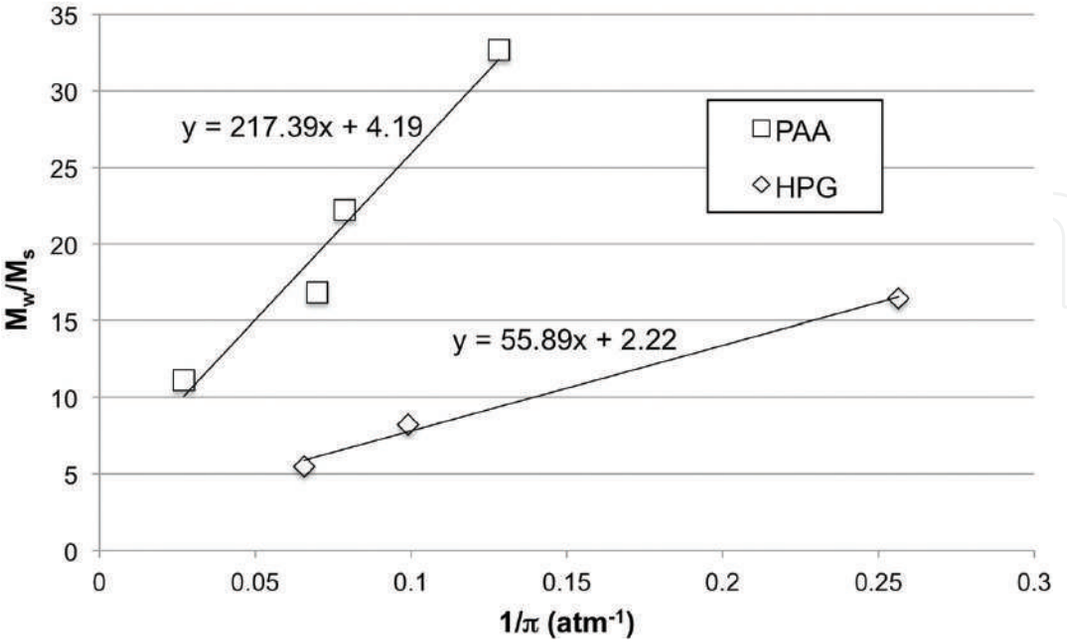

Figure 4. Nonideality analyses for HPG and PAA^{1800}, using data from [20, 28].

Osmotic agent	I	A_e	Ref.
TREG–alone	0.37	153	[20, 31, 52]
TREG–MNP	19.3	56.1	[20]
Si-PEG^{530}–MNP	5.8	101	[47]
PAA^{1800}–MNP	4.2	111	[46]
HPG–MNP	2.2	433	[28]

Table 3. Summary of I and A_e values.

repeating monomer (72 g mol^{-1}) and the full polymer molecular weight (1800 g mol^{-1}). Several researchers [23–25] have also explored PNaAA as an MNP coating agent. Polyelectrolytes exploit greater i values to reduce X_w, however, the extent of ion-pairing between monomer units and counterions greatly influences solution osmotic pressure (**Table 3**).

3.3. Counterion binding

Another significant contributing factor to the osmotic potential of draw solutions incorporating polyelectrolytes is counterion binding. Oosawa was among the first to introduce the concept of counterion condensation around a polyion [53]. His model considers a fraction of counterions that is *bound* to the polyelectrolyte and the remainder is *unbound* in the bulk aqueous phase. Oosawa's expression, provided in Eq.(27), relates the degree of polyelectrolyte dissociation, β; the apparent volume fraction in which counterions are located, ϕ; the absolute value of charge on the counterion, z; and, the intensity of the potential at the polymer surface, Q.

$$\ln\left(\frac{1-\beta}{\beta}\right) = \ln\left(\frac{\phi}{1-\phi}\right) + \beta z Q ln\left(\frac{1}{\phi}\right) \tag{27}$$

Using this model, bound counterions would not contribute to osmotic pressure while unbound ions would. Polymeric structural features that influence the magnitude of Q would therefore significantly impact the osmotic properties of solutions containing that polymer, either alone or grafted onto MNPs. Gwak et al. [54] demonstrated that poly(sodium aspartate) (PNaAsp) provided better osmotic performance than PNaAA, a result attributed to greater polyelectrolyte dissociation (larger β) in the case of PNaAsp. The larger spacing between charged moieties on PNaAsp strands results in a lower surface potential and therefore a higher degree of unbound counterions. Tian et al. [55] investigated the use of ungrafted PNaSS as a draw solute in FO, observing that conductivity and osmotic pressure increase with increasing PNaSS molecular weight, particularly at higher molecular weights. These results indicate that β and Q vary with polymer molecular weight.

3.4. Particle size

Data also indicate that MNP particle size influences their osmotic performance because smaller particles have a larger surface area per volume, thus allowing for more effective grafting-agent coverage and increased nonideality. Ling et al. [20] demonstrated the inverse relationship

between nanoparticle size and osmolality using PAA-MNPs. However, Kim et al. [56] found that particles smaller than 11 nm were difficult to separate from solution even with the application of a strong magnetic field, while the removal of particles larger than about 20 nm from the magnetic separator column was problematic. Additionally, the larger the mass percentage of coating material on a Fe_3O_4 core, the lower the saturated magnetization value on a per gram of particle basis. More coating material likely imparts greater osmotic pressure, but it reduces the efficacy of separation. Another significant challenge associated with MNP draw agents is particle aggregation following magnetic separation.

Ge et al. [22] observed a flux decline to approximately 80% of its original value after 9 recycles; this flux decline was accompanied by a particle size increase to 141% of the original value. That study used MNPs with an initial diameter <20 nm. Mino et al. [25] used much larger particles, with diameters of approximately 160 nm, and observed no aggregation even after 10 recycles, though the larger particles achieved only modest osmotic pressures. Park et al. [47] demonstrated that Si-PEG^{530}-MNPs ($diameter_{initial}$ = 13.6 nm) showed no significant aggregation or FO performance decline after 8 recycles, while Si-COOH-MNPs displayed considerable aggregation after only 5 recycles. Aggregation of the Si-COOH-MNPs was attributed to strong hydrogen bonding between carboxylate groups on adjacent particles when brought into close proximity during magnetic separation and subsequent drying. The oxalic acid- and citric acid-coated MNPs studied by Ge et al. [19] showed no significant particle agglomeration during regeneration, likely the result of strong electrostatic repulsion between particles. Zhao et al. [26] also observed only a slight decline in water flux (<10%) following recycles of their negatively charged PNaSS-PNIPAM-coated particles. In addition, Na et al. [27] demonstrated that small MNPs (3–8 nm) penetrate pores within the FO-membrane support layer (10–40 nm) and become lodged leading to a decline in flux values with time.

4. Summary

While it is now generally accepted that FO processes do not offer an overall energy cost savings when compared to RO for seawater desalination, the prospects of niche applications for FO where RO is unsuitable are numerous. A major challenge for the wider use of FO technology is the development of draw agents that provide high water flux, low reverse solute flux, and facile recovery. Organic-coated superparamagnetic nanoparticles provide properties that address these requirements. The FO performance of MNPs is a function of coating material, particle size, and concentration; with mitigation of particle aggregation during recovery being an essential consideration. The osmotic performance of organic compounds improves significantly when grafted onto MNPs, likely resulting from increased solvent-accessible surface area and enhanced hydration. Application of a simple semiempirical model provides assessments of the nonideality associated with MNPs through calculation of a solvent/solute interaction parameter (I) and the effective osmotic molecular weight (A_e). When attached to MNPs, polymers behave osmotically as much smaller molecules. MNPs derivatized with filamentous, charged molecules (i.e. PNaAA) seem to provide the best results, both in terms of water flux and recoverability. Other significant contributing factors to the overall efficacy of

MNP-based draw solutions are particle size and the extent of counterion binding, with particles in the range 10–20 nm, coated with polyelectrolytes demonstrating high degrees of dissociation, proving most favorable. While the search for the *ideal* draw solute will certainly continue, organic-coated MNPs, because of their enhanced nonideal behavior, offer an encouraging avenue of possibility and opportunity.

Acknowledgements

Support for this work was provided by the Qatar Foundation and was made possible in part by a grant from the Qatar National Research Fund under its Undergraduate Research Experience Program award no. UREP13-018-1-001. Its contents are solely the responsibility of the authors and do not necessarily represent the official views of the Qatar National Research Fund.

Author details

Jimmy D. Roach*, Mandy M. Bondaruk and Zain Burney

*Address all correspondence to: jar2038@qatar-med.cornell.edu

Pre-Medical Education Unit, Weill Cornell Medicine-Qatar, Doha, Qatar

References

[1] Zhao S, Zou L, Tang CY, Mulcahy D. Recent developments in forward osmosis: Opportunities and challenges. Journal of Membrane Science. 2012;**396**:1-21

[2] Klaysom C, Cath TY, Depuydt T, Vankelecom IF. Forward and pressure retarded osmosis: Potential solutions for global challenges in energy and water supply. Chemical Society Reviews. 2013;**42**:6959-6989

[3] Phuntsho S, Sahebi S, Majeed T, Lotfi F, Kim JE, Shon HK. Assessing the major factors affecting the performances of forward osmosis and its implications on the desalination process. Chemical Engineering Journal. 2013;**231**:484-496

[4] Shaffer DL, Werber JR, Jaramillo H, Lin S, Elimelech M. Forward osmosis: Where are we now? Desalination. 2015;**356**:271-284

[5] Akther N, Sodiq A, Giwa A, Daer S, Arafat HA, Hasan SW. Recent advancements in forward osmosis desalination: A review. Chemical Engineering Journal. 2015;**281**:502-522

[6] Qasim M, Darwish NA, Sarp S, Hilal N. Water desalination by forward (direct) osmosis phenomenon: A comprehensive review. Desalination. 2015;**374**:47-69

[7] Cai Y, Hu X. A critical review on draw solutes development for forward osmosis. Desalination. 2016;**391**:16-29

[8] Cath TY, Elimelech M, McCutcheon JR, McGinnis RL, Achilli A, Anastasio D, Brady AR, Childress AE, Farr IV, Hancock NT, Lampi J, Nghiem LD, Xie M, Yip NY. Standard methodology for evaluating membrane performance in osmotically driven membrane processes. Desalination. 2013;**312**:31-38

[9] Wei J, Qiu C, Tang CY, Wang R, Fane AG. Synthesis and characterization of flat-sheet thin film composite forward osmosis membranes. Journal of Membrane Science. 2011;**372**:292-302

[10] Alejo T, Arruebo M, Carcelen V, Monsalvo VM, Sebastian V. Advances in draw solutes for forward osmosis: Hybrid organic-inorganic nanoparticles and conventional solutes. Chemical Engineering Journal. 2017;**309**:738-752

[11] Achilli A, Cath TY, Childress AE. Selection of inorganic-based draw solutions for forward osmosis applications. Journal of Membrane Science. 2010;**364**:233-241

[12] Ge Q, Su J, Amy GL, Chung T-L. Exploration of polyelectrolytes as draw solutes in forward osmosis processes. Water Research. 2012;**46**:1318-1326

[13] Lecaros RLG, Syu Z-C, Chiao Y-H, Wickranasinghe SR, Ji Y-L, An Q-F, Hung W-S, Hu C-C, Lee K-R, Lai J-Y. Characeterization of a thermoresponsive chitosan derivative as a potential draw solute for forward osmosis. Environmental Science & Technology. 2016;**50**:11935-11942

[14] McCutcheon JR, McGinnis RL, Elimelech M. Desalination by ammonia–carbon dioxide forward osmosis: Influence of draw and feed solution concentrations on process performance. Journal of Membrane Science. 2006;**278**:114-123

[15] Wang Y, Yu H, Xie R, Zhao K, Ju X, Wang W, Liu Z, Chu L. An easily recoverable thermosensitive polyelectrolyte as draw agent for forward osmosis process. Chinese Journal of Chemical Engineering. 2016;**24**:86-93

[16] Roach JD, Al-Abdulmalek A, Al-Naama A, Haji M. Use of micellar solutions as draw agents in forward osmosis. Journal of Surfactants and Detergents. 2014;**17**:1241-1248

[17] Li D, Zhang XY, Yao JF, Simon GP, Wang HT. Stimuli-responsive polymer hydrogels as a new class of draw agent for forward osmosis desalination. Chemical Communications. 2011;**47**:1710-1712

[18] Li D, Wang H. Smart draw agents for emerging forward osmosis application. Journal of Materials Chemistry A. 2013;**1**:14049-14060

[19] Ge Q, Yang L, Cai J, Xu W, Chen Q, Liu M. Hydroacid magnetic nanoparticles in forward osmosis for seawater desalination and efficient regeneration via integrated magnetic and membrane separations. Journal of Membrane Science. 2016;**520**:550-559

[20] Ling MM, Wang KY, Chung T-S. Highly water-soluble magnetic nanoparticles as novel draw solutes in forward osmosis for water reuse. Industrial & Engineering Chemistry Research. 2010;**49**:5869-5876

[21] Bai H, Liu Z, Sun DD. Highly water soluble and recovered dextran coated Fe_3O_4 magnetic nanoparticles for brackish water desalination. Separation and Purification Technology. 2011;**81**:392-399

[22] Ge Q, Su J, Chung T-S, Amy G. Hydrophillic supermagnetic nanoparticles: Synthesis, characterization, and performance in forward osmosis. Industrial & Engineering Chemistry Research. 2011;**50**:382-388

[23] Ling MM, Chung T-S. Surface-dissociated nanoparticle draw solutions in forward osmosis and the regeneration in an integrated electric field and nanofiltration system. Industrial & Engineering Chemistry Research. 2012;**51**:15463-15471

[24] Dey P, Izake EL. Magnetic nanoparticles boosting the osmotic efficiency of a polymeric FO draw agent: Effect of polymer conformation. Desalination. 2015;**373**:79-85

[25] Mino Y, Ogawa D, Matsuyama H. Functional magnetic particles providing osmotic pressure as reusable draw solutes in forward osmosis membrane process. Advanced Powder Technology. 2016;**27**:2136-2144

[26] Zhao Q, Chen N, Zhao D, Lu X. Thermoresponsive magnetic nanoparticles for seawater desalination. ACS Applied Materials & Interfaces. 2013;**5**:11453-11461

[27] Na Y, Yang S, Lee S. Evaluation of citrate-coated magnetic nanoparticles as draw solute for forward osmosis. Desalination. 2014;**347**:34-42

[28] Yang H-M, Seo B-K, Lee K-W, Moon J-K. Hyperbranched polyglycerol-coated magnetic nanoparticles as draw solute in forward osmosis. Asian Journal of Chemistry. 2014;**26**: 4031-4034

[29] Beaman DK, Robertson EJ, Richmond GL. From head to tail: Structure, solvation, and hydrogen bonding of carboxylate surfactants at the organic–water interface. Journal of Physical Chemistry C. 2011;**115**:12508-12516

[30] Wills PR, Scott DJ, Winzor DJ. Thermodynamics and thermodynamic nonideality. In: Roberts GK, editor. Encyclopedia of Biophysics. Springer; 2013. pp. 2583-2589

[31] Zimmerman RJ, Chao H, Fullerton GD, Cameron IL. Solute/solvent interaction corrections account for non-ideal freezing point depression. Journal of Biochemical and Biophysical Methods. 1993;**26**:61-70

[32] Kanal KM, Fullerton GD, Cameron IL. A study of the molecular sources of nonideal osmotic pressure of bovine serum albumin solutions as a function of pH. Biophysical Journal. 1994;**66**:153-160

[33] Minton AP. A molecular model for the dependence of the osmotic pressure of bovine serum albumin upon concentration and pH. Biophysical Chemistry. 1995;**57**:65-70

[34] Yousef MA, Datta R, Rodgers VGJ. Understanding nonidealities of the osmotic pressure of concentrated bovine serum albumin. Journal of Colloid and Interface Science. 1998;**207**: 273-282

[35] Zimmerman RJ, Kanal KM, Sanders J, Cameron IL, Fullerton GD. Osmotic pressure method to measure salt induced folding/unfolding of bovine serum albumin. Journal of Biochemical and Biophysical Methods. 1995;**30**:113-131

[36] Yamada S, Tanaka M. Softness of some metal ions. Journal of Inorganic and Nuclear Chemistry. 1975;**37**:587-589

[37] Loeb S, Titelman L, Korngold E, Freiman J. Effect of porous support fabric on osmosis through a Loeb-Sourirajan type asymmetric membrane. Journal of Membrane Science. 1997;**129**:243-249

[38] Wilson AD, Stewart FF. Deriving osmotic pressures of draw solutes used in osmotically driven membrane processes. Journal of Membrane Science. 2013;**431**:205-211

[39] Zavitsas AA. Properties of water solutions of electrolytes and nonelectrolytes. Journal of Physical Chemistry B. 2001;**105**:7805-7817

[40] Marcus Y. Ions in Solution and their Solvation. Wiley; 2015. p. 140

[41] Bathe M, Rutledge GC, Grodzinsky AJ, Tidor B. Osmotic pressure of aqueous chondroitin sulfate solution: A molecular modeling investigation. Biophysical Journal. 2005;**89**:2357-2371

[42] Carrillo J-MY, Dobrynin AV. Salt effect on osmotic pressure of polyelectrolyte solutions: Simulation study. Polymer. 2014;**6**:1897-1913

[43] Tirosh O, Barenholz Y, Katzhendler J, Priev A. Hydration of polyethylene glycol-grafted liposomes. Biophysical Journal. 1998;**74**:1371-1379

[44] Hansen PL, Cohen JA, Podgornik R, Parsegian VA. Osmotic properties of poly(ethylene glycols): Quantitative features of brush and bulk scaling laws. Biophysical Journal. 2003;**84**:350-355

[45] Essafi W, Lafuma F, Baigl D, Williams CE. Anomalous counterion condensation in salt-free hydrophobic polyelectrolyte solutions: Osmotic pressure measurements. Europhysics Letters. 2005;**71**:938-944

[46] Ling MM, Chung TS. Desalination process using super hydrophilic nanoparticles via forward osmosis integrated with ultrafiltration regeneration. Desalination. 2011;**278**:194-202

[47] Park S–Y, Ahn H–W, Chung J–W, Kwak S–Y. Magnetic core-hydrophilic shell nanosphere as stability-enhanced draw solute for forward osmosis (FO) application. Desalination. 2016;**397**:22-29

[48] Achilleos DS, Vamvakaki MV. End-grafted polymer chains onto inorganic nano-objects. Materials. 2010;**3**:1981-2026

[49] Milner ST. Polymer brushes. Science. 1991;**251**:905-914

[50] Fullerton GD, Zimmerman RJ, Cantu C, Cameron IL. New expressions to describe solution nonideality: Osmotic pressure, freezing-point depression and vapor pressure. Journal of. Biochemistry and Cell Biology. 1992;**70**:1325-1331

[51] Yousef MA, Datta R, Rodgers VGJ. Free–solvent model of osmotic pressure revisited: Application to concentrated IgG solution under physiological conditions. Journal of Colloid and Interface Science. 1998;**1997**:108-118

[52] Sun T, Teja A. Density, viscosity, and thermal conductivity of aqueous ethylene, diethylene, and triethylene glycol mixtures between 290 K and 450 K. Journal of Chemical & Engineering Data. 2003;**48**:198-202

[53] Oosawa F. A simple theory of thermodynamic properties of polyelectrolyte solutins. Journal of Polymer Science. 1957;**23**:421-430

[54] Gwak G, Jung B, Han S, Hong S. Evaluation of poly (aspartic acid sodium salt) as a draw solute for forward osmosis. Water Research. 2015;**80**:294-305

[55] Tian E, Hu C, Qin Y, Ren Y, Wang X, Wang X, Xiao P, Yang X. A study of poly (sodium 4–styrenesulfonate) as draw solute in forward osmosis. Desalination. 2015;**360**:130-137

[56] Kim YC, Han S, Hong S. A feasibility study of magnetic separation of magnetic nanoparticle for forward osmosis. Water Science and Technology. 2011;**64**:469-476

IntechOpen

Chapter 8

Fouling in Forward Osmosis Membranes: Mechanisms, Control, and Challenges

Amira Abdelrasoul, Huu Doan, Ali Lohi and Chil-Hung Cheng

Additional information is available at the end of the chapter

http://dx.doi.org/10.5772/intechopen.72644

Abstract

Continuously escalating global water demand places a substantial burden on the available water and energy resources. Forward osmosis (FO) is an evolving membrane desalination technology that has recently raised interest as a promising low-energy process. FO is a unique method since it utilizes natural osmosis as the driving force, and hence, it ensures that the energy consumption is significantly reduced, in comparison to other pressure-driven membrane processes that are constrained by their excessive energy consumption and unsustainable cost. Therefore, the growing interest in FO from various disciplines and industrial sectors calls for a better understanding of the FO process and further advances in the FO technology management. This chapter aims to provide an in-depth assessment of the water transport phenomenon in FO membranes by focusing on the influence of internal concentration polarization, membrane structure/material, and membrane orientation on the permeate flux. This chapter offers critical insight that can lead to the potential development of new FO membranes with reduced internal concentration polarization and higher water permeability. In addition, key strategies for FO membrane development, some of its challenges, and the perspectives for future investigations of FO membrane fouling and effective FO fouling control methods are explored in this chapter.

Keywords: forward osmosis, fouling, concentration polarization, mass transfer, water filtration

1. Introduction

As the fossil fuels are depleted and the world population continues to rapidly increase, energy and water became two of the most vital global resources. Energy emergencies and the lack of

water have severely affected communities worldwide [1–3]. Reports indicate that more than 1.2 billion people do not have access to safe and clean drinking water sources, while 2.6 billion do not have adequate levels of sanitation [1, 4, 5]. In fact, the overall annual financial loss in Africa caused by the lack of access to basic sanitation and clean water is valued at $28 billion, or 5% of Africa's gross domestic product [5]. While oceans are covering the majority of the planet's surface, only 0.8% of the world's water can be defined as potable [6]. Moreover, the recent world energy outlook report [2] indicates that the world's marketed energy use is predicted to rise by 49% from 2007 to 2035. Data such as this reflects a dangerous trend, especially since currently 1.5 billion people, or more than 1/5 of the world's population, still do not have access to reliable electricity.

Interdisciplinary research groups need to remain aware of the explicit connection that exists between energy and water. The process of making freshwater accessible is a highly energy-demanding process, while the production of the required power frequently necessitates substantial amounts of water [7, 8]. A relatively new technology, forward osmosis (FO), shows a lot of potential in energy production and water supply, especially for applications in controlled-release–type drug medication, medical product enrichment, and food processing. Over the last decade, FO has incited substantial interest in the areas of seawater/brackish desalination [9–11], food processing [12–15], power generation [16–19], and wastewater treatment [20–22]. In terms of its methodology, FO is an osmotically driven membrane process that relies on the osmotic pressure gradient and that moves water across a semipermeable-type membrane from the feed solution side, with the low osmotic pressure, to the draw solution side, featuring high osmotic pressure. Because of its lower hydraulic pressure demands, FO provides multiple benefits, such as lower fouling tendency, easier fouling removal [20, 22, 23], smaller energy input [24], and greater water recovery [25, 26], if compared to pressure-driven processes such as ultrafiltration (UF), nanofiltration (NF), and reverse osmosis (RO).

2. Advantages of forward osmosis

There are numerous potential benefits offered by FO, especially because of the lower hydraulic pressure values necessary for this osmotically driven–type process. FO's benefits are reflected by its various water treatment applications. First, FO can help obtain smaller energy consumption potentials and as a consequence lower the overall costs and contribute to the production of technically and economically innovative solutes and their respective regeneration methodologies [3, 18, 24]. Arguably, this is one of the key advantages of FO, considering the ongoing global energy crisis. Research studies have shown that membrane fouling in FO is comparatively small [20], somewhat more reversible [23, 27], and may be lowered using hydrodynamics optimization [28]. Furthermore, a number of contaminants may be successfully filtered out with the aid of the FO process [29, 30]. FO can likewise feature greater water recovery and improved water flux because of the higher osmotic pressure gradient occurring across the membrane. Greater water recovery can help reduce the desalination brine volume, especially as it is a substantial environmental concern when it comes to desalination plants and inland desalination facilities [9]. Moreover, in the industries like pharmaceutical and food processing,

FO offers the benefits of preserving the physical properties of the feed, such as color, aroma, nutrition, and taste, without diminishing the overall quality, as it is not heated or pressurized [14, 31, 32]. When it comes to medical uses, FO can help with the release of drugs featuring low oral bioavailability, or poor solubility, in a controlled way and implementing osmotic pumps [33, 34].

3. Modeling of water transport in forward osmosis

The general equation for water flux in forward osmosis (FO), reverse osmosis (RO), or pressure-retarded osmosis (PRO) is [16]:

$$J_w = A(\sigma\Delta\pi - \Delta P) \tag{1}$$

where J_w is the water flux, A is the membrane's water permeability constant, σ is the reflection coefficient, $\Delta\pi$ is the osmotic pressure difference across the membrane, and ΔP is the applied hydraulic pressure variance. In Eq. (1), the term ($\sigma\ \Delta\pi\ -\ \Delta$P) signifies the effective driving force necessary for the water molecules' transport across the membrane. In the FO desalination process, there is no hydraulic pressure applied and the change in osmotic pressures is the sole driving force; Eq. (1) can be expressed as:

$$J_w = A\sigma\Delta\pi_{Bulk} = A\sigma(\Delta\pi_{Draw} - \Delta\pi_{Feed}) \tag{2}$$

where $\Delta\pi_{Feed}$ stands for the feed solution's bulk osmotic pressure, and $\Delta\pi_{Draw}$ is the draw solution's bulk osmotic pressure. Eq. (2) is restricted by the assumption that the membrane does not permit draw solute permeation [35, 36]. Furthermore, Eq. (2) is applicable for dense symmetric membranes, in which the driving force for water molecules is the difference between the osmotic pressures of the bulk feed and draw solutions, as reflected in **Figure 1**.

If it can be assumed that the difference between the bulk osmotic pressure of the feed and the draw solution is the driving force responsible for water permeation through membranes in FO, then Lee et al. [37] proposed the following model for low water flux cases:

$$J_w = \frac{1}{K} ln\left(\frac{\pi_{Draw}}{\pi_{Feed}}\right) \tag{3}$$

where K stands for the resistance to diffusion of solute within the porous support layer of the FO membrane, and π_{Draw} and π_{Feed} are the respective bulk osmotic pressures of the draw and the feed solution. K can be estimated using Eq. (4) [16]:

$$K = \frac{t\tau}{\varepsilon D} = \frac{S}{D} \tag{4}$$

where t is the membrane's thickness, τ is tortuosity, ε is membrane porosity, S is membrane's structural parameter, and D is the solute's diffusion coefficient.

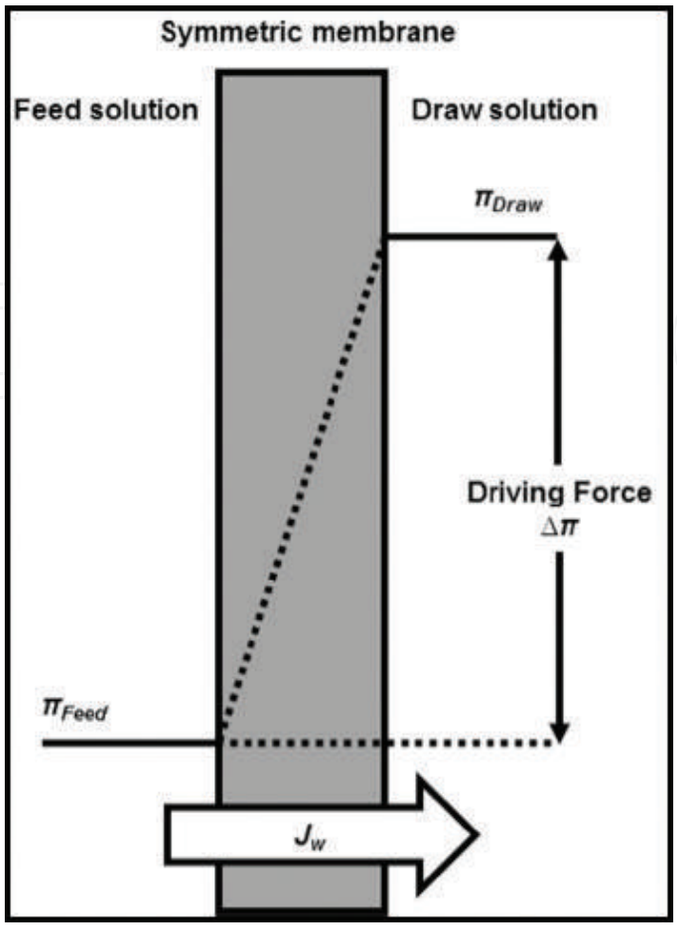

Figure 1. Ideal osmotic pressure driving force in the case of symmetric membranes.

4. Challenges in forward osmosis

FO applications are still facing some critical challenges even though the osmotically driven membrane processes have been extensively researched in relation to a range of applications and environments. FO's primary issues are connected to aspects such as membrane fouling, reverse solute diffusion, further membrane development, concentration polarization, and the improvement of the draw solute design.

4.1. Concentration polarization mechanism in forward osmosis

When it comes to the osmotically driven and pressure-driven membrane processes, the concentration polarization is an inevitable and frequent phenomenon [11, 38–42]. As illustrated in **Figure 2**, in the osmotically driven membrane processes, the concentration polarization is produced by the overall concentration variance occurring between the draw solution and the feed solution through the asymmetric FO membrane. The internal concentration polarization (ICP) and external concentration polarization (ECP) can happen during the FO processes. In general, ICP happens within the membrane's porous support layer, and ECP happens at the surface of the membrane's dense active layer. The sections below further describe both ECP and ICP.

http://dx.doi.org/10.5772/intechopen.72644

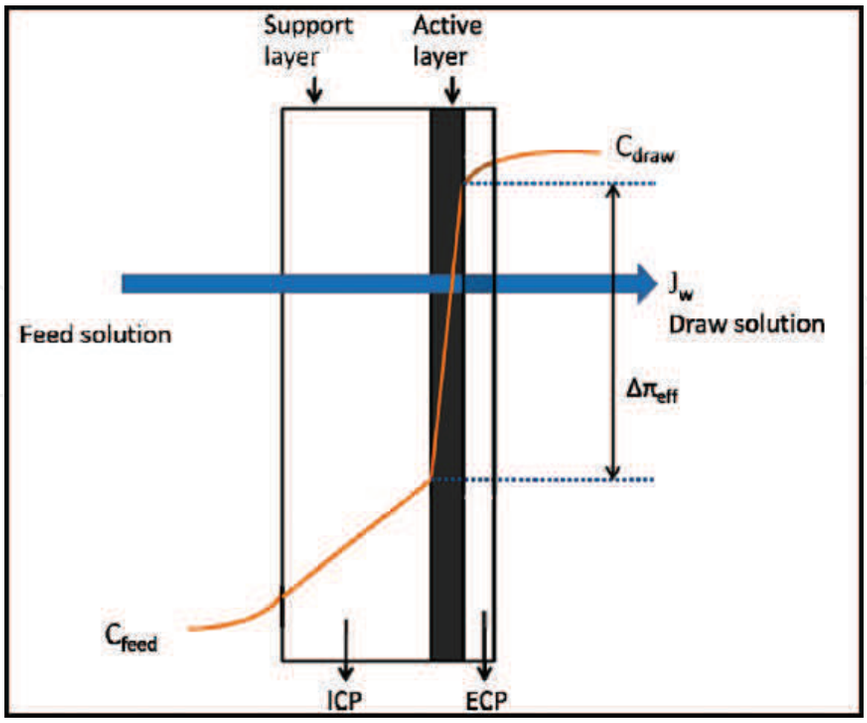

Figure 2. Internal concentration polarization (ICP) and external concentration polarization (ECP) through an asymmetric FO membrane [16].

4.1.1. External concentration polarization: modeling and mechanism

ECP in FO occurs at the surface of the membrane's active layer, similar to the other pressure-driven membrane processes. Their distinction is due to the fact that only concentrative ECP can occur in a pressure-driven membrane process, and both dilutive ECP and concentrative ECP can happen in an osmotically driven membrane process, conditional on the membrane's orientation with regard to the feed and the draw solutions. The dilutive ECP happens when the membrane's support layer is facing the feed solution, while the concentrative ECP occurs in instances where the membrane's support layer is facing the draw solution. ECP lowers the overall driving force due to the higher osmotic pressure at the membrane's active layer interface located on the membrane's feed side, or the lowered osmotic pressure at the membrane's active layer surface located on the draw solution side. The unfavorable effects of ECP on the permeate flux can be alleviated by optimizing the water flux and raising the flow's velocity or turbulence [11]. With the application of the boundary-layer film theory McCutcheon and Elimelech have successfully modeled ECP in FO [38, 43]. The generalized equation for concentration polarization modulus in pressure-driven membrane processes may be expressed in Eq. (5), as follows.

$$\frac{C_m}{C_b} = exp\left(\frac{J_w}{k}\right) \tag{5}$$

where J_w is the water flux, k is the mass transfer coefficient value, and C_m and C_b are the concentrations of the feed solution at the membrane's surface and in the bulk, respectively. The mass transfer coefficient (k) is related to the Sherwood number (Sh) by:

$$k = \frac{ShD}{D_h} \tag{6}$$

where D is the solute diffusion coefficient value, and D_h is the hydraulic characteristic length. When the feed solution concentration is relatively low in FO, the concentrations in Eq. (5) can be substituted by the osmotic pressures. As a result, the concentrative ECP modulus can be expressed as follows:

$$\frac{\pi_{m-feed}}{\pi_{b-feed}} = exp\left(\frac{J_w}{k_{feed}}\right) \tag{7}$$

where k_{feed} is the mass transfer coefficient on the feed side, π_{m-feed} and π_{b-feed} are the osmotic pressures of the feed solution at the membrane's surface and in the bulk, respectively. Similarly, the dilutive ECP modulus in FO can be expressed as:

$$\frac{\pi_{m-draw}}{\pi_{b-draw}} = exp\left(-\frac{J_w}{k_{draw}}\right) \tag{8}$$

where k_{draw} is the mass transfer coefficient on the draw side, and π_{m-draw} and π_{b-draw} are the osmotic pressures of the draw solution at the membrane's surface and in the bulk, respectively. Eqs. (1) and (2) reflect the water transport in RO, FO, and pressure-retarded osmosis (PRO), as indicated in Eqs. (1) and (2), as shown in Section 3. Both π_{draw} and π_{feed} should be the effective osmotic pressures at the membrane's surfaces, specifically.

$$J_w = A\left(\pi_{m-draw} - \pi_{m-feed}\right) \tag{9}$$

By substituting Eqs. (7) and (8) into Eq. (9), Eq. (10) can be obtained as below:

$$J_w = A\left[\pi_{b-draw}\ exp\left(-\frac{J_w}{k_{draw}}\right) - \pi_{b-feed}\ exp\left(\frac{J_w}{k_{feed}}\right)\right] \tag{10}$$

Although the dilutive ECP and concentrative ECP have been examined in Eq. (10) [43], there are multiple key points that have to be noted in Eq. (10). First of all, the mass transfer coefficient values on the feed and draw solution sides are not the same because of the varying hydraulic conditions between the draw solution side and the feed side. Next, this model relies on multiple assumptions, including that the solute permeability's coefficient is zero (i.e., the reflection coefficient σ = 1 [44]) and that the draw and feed solution concentration values are reasonably low, since only in this case can it be accepted that the concentration is equal to the corresponding osmotic pressure values. Finally, it must be noted that this model is adequate only in instances with a dense symmetric film, instead of an asymmetric-type membrane. As a result, the uses for this model can be somewhat limited. It is necessary to examine the dynamic where an asymmetric FO membrane is applied in a manner that would replicate its real-world practical uses and where the ICP effects become more significant.

4.1.2. Internal concentration polarization: modeling and mechanism

ICP is a critical aspect of the osmotically driven membrane-type processes. Research indicates that the water flux decline in FO is primarily produced by ICP [38, 44–46]. The early research

projects that looked at FO suggested that ICP might lower the water flux by more than 80% [45, 47]. As indicated in **Figure 3**, there are two types of ICP, concentrative ICP and dilutive ICP, occurring within the membrane's support layer, and they depend on the membrane's orientation [48]. Once the draw solution is situated against the membrane's support layer, dilutive ICP can successfully happen within the membrane's support layer since the water permeates across the membrane, from the feed solution to the draw solution. In a different membrane orientation where the feed solution is opposite the membrane support layer, concentrative ICP happens when the solute properly accumulates within the membrane's support layer located on the feed side. The ICP process is happening in the support layer and, as a result, it cannot be weakened through a change in the hydrodynamic conditions, including higher turbulence or flow rate.

The effects of ICP on FO water flux have been modeled using an adaptation of the classical solution-diffusion theory [38, 43]. The dilutive ICP dominates the water flux (Jw) when the draw solution is placed against the membrane support layer (i.e., FO mode) and can be expressed [49] as follows:

$$J_w = \frac{1}{K} ln \frac{A\pi_{draw} + B}{A\pi_{feed} + B + J_w} \tag{11}$$

where B is the membrane's solute permeability coefficient, and K is the solute resistivity value, a measure of solute transport in the membrane's support layer. K is used to quantify the solute's capacity to diffuse into or out of the membrane's support layer, and it can reflect the degree of ICP available in the support layer. Lower K values indicate less ICP and cause greater pure water flux (J_w). K is defined earlier in Eq. (4). It should be noted that the structural parameter S, in Eq. (4), is an essential membrane quality since it governs ICP in the membrane's support by establishing membrane's tortuosity, porosity, and thickness values. As a

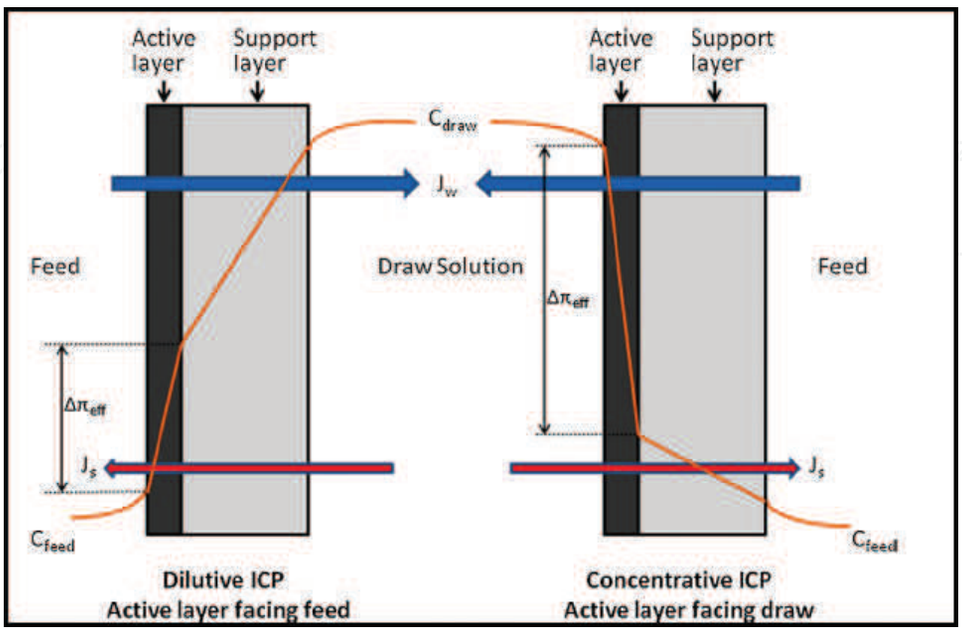

Figure 3. Dilutive ICP and concentrative ICP across an asymmetric FO membrane [48].

result, when it comes to the newly developed membranes, it is crucial to describe the membrane's structural parameter S. The value of S can be calculated based on Eqs. (4) and (11) and by fitting FO test results [50, 51]. On the other hand, in a specific membrane orientation, both ICP and ECP happen concurrently rather than occurring separately. Researchers McCutcheon and Elimelech have designed models that consider the characteristics and influences of both ECP and ICP. For the FO mode, the analytical model capturing the effects of both concentrative ECP and dilutive ICP on permeate flux may be conveyed [38, 43] by:

$$J_w = A\left[\pi_{draw}\ exp\left(-J_w K\right) - \pi_{feed}\ exp\left(\frac{J_w}{k}\right)\right] \tag{12}$$

As seen in Eq. (4), it appears that ICP in the membrane's support layer is formed based on the membrane properties, such as membrane's tortuosity, porosity, and thickness, as well as the diffusion solute properties, like the diffusion coefficient of the solute. A research project by Zhao and Zou has connected ICP to additional properties of the solution, like viscosity and diffusion solute size, by considering the idea of constrictivity [48]. The equation that corresponds to this dynamic is embodied in the following:

$$K = \frac{t\tau}{\delta\varepsilon_{eff}D} \tag{13}$$

In this case, a new parameter δ is expressed as the constrictivity factor, and ε_{eff} is the effective transport through porosity, as it can be lower than the overall membrane porosity if certain small pores are not available to the larger solute. In particular, the constrictivity parameter relies on the ratio of the pore diameter to the solute molecule diameter:

$$\lambda = \frac{molecule\ diameter}{pore\ diameter} < 1 \tag{14}$$

Tang et al. researched the cumulative effect of fouling and ICP on FO flux behavior. [50]. Tang et al. noted two critical phenomena during the experimental runs. The first phenomenon was that the water flux was comparatively stable and its decrease was minor during the FO mode, whereas during the PRO mode, the flux decrease was substantial and especially prominent when membrane fouling happened. The second phenomenon had to do with the fact that the effects of ICP on FO flux were more distinct at greater draw solution concentration values [48]. A number of new modeling techniques have been used to research the concentration polarization (CP) phenomenon, such as the computational fluid dynamics (CFD) [52], numerical simulation [53], and the finite element method (FEM) [54, 55]. A project spearheaded by Li et al. used FEM to interrogate the relationship between the membrane's porous structure and ICP [54]. The mathematical models that came out of this project can serve as a valuable toolkit for improving FO performance and optimizing the membrane's support construction [54].

4.2. Membrane fouling mechanism in forward osmosis

Like concentration polarization, membrane fouling is an unavoidable as well as essential phenomenon influencing all types of membrane processes [28, 56–63]. As a consequence,

smaller membrane fouling potential ensures that there is less cleaning, longer membrane life, and more water produced, which effectually decreases capital and operational costs. On the other hand, the membrane-type fouling happening in osmotically driven membrane processes is distinct from the types of fouling present in pressure-driven membrane processes, as a result of the low hydraulic pressure being used in the former case. Initially, Cath et al. researched membrane fouling in FO in relation to systems used in long-term space missions [64, 65]. Cath et al. suggested that FO could have the capacity to reduce membrane fouling, since there was no flux decrease due to fouling detected during the experimental runs [65]. During the last few years, FO has been applied in osmotic membrane bioreactors (OMBR) primarily for wastewater treatment because of its lower energy consumption and lower fouling needs [20, 22], both of which are two challenges for membrane bioreactors [59, 66]. In a research project by In addition, the OMBR system was used to treat activated sludge. The results report that neither irreversible nor reversible fouling was seen whenever the membrane's active layer was positioned in a way facing the activated sludge [22]. An experiment conducted by Achilli et al. relied on a submerged OMBR so as to treat domestic wastewater over the prolonged period of up to 28 days, indicating that the decrease of water flux was primarily due to membrane fouling [20]. On the other hand, the flux of the initial values could be recovered by roughly 90% through the process of osmotic backwashing. This experimental result suggests that membrane fouling in OMBR may in fact be reversible. Similarly, the data reflect that membrane fouling does exist in FO and is apparent during long-term operational runs. Mi and Elimelech interrogated the inorganic and organic fouling in FO [23, 27, 62]. Mi and Elimelech determined that, first of all, the intermolecular adhesion and organic fouling were connected and that foulant-foulant interactions had an important role in organic cleaning and fouling. Second, Mi and Elimelech found out that FO fouling was controlled by the coupled effects of chemical, for example, calcium binding, and hydrodynamic, for instance permeation drag and shear force, interactions. They likewise noted that membrane materials had a key role in organic fouling and cleaning, which was later verified with the help of atomic force microscope (AFM) measurements. Mi and Elimelech also found that both inorganic and organic types of fouling in FO were nearly fully reversible using water rinsing. This could be attributed to the less compact fouling layer created by the applied low hydraulic pressure, which suggests that chemical cleaning could be prevented. Moreover, researchers comparing membrane fouling in FO and RO suggested that it could be diverse from one case to another with respect to water cleaning efficiency and reversibility [23, 27, 28]. Although it was irreversible in RO, Lee et al. observed that membrane fouling in FO was almost entirely reversible [28]. Alternatively, Lee et al. linked the FO fouling to the accelerated cake-enhanced osmotic pressure (CEOP) created by the reverse solute (salt) diffusion process in the draw solution. **Figure 4** outlines the mechanics of this process [31]. Once the draw solution faces the membrane's support layer, using the reverse diffusion, the draw solute collects on the active layer's surface located on the feed side, lowering the net osmotic driving force and improving the concentration polarization layer. The draw solute featuring a less hydrated radius value (e.g., NaCl) is more easily capable of initiating CEOP, when compared to the ones with a greater hydrated radius values, like dextrose. In an experiment by Lay et al., it was noted that the reverse diffusion of the draw solute could worsen the CEOP effect as well as intensify FO fouling [67]. Alternatively, new research suggests that FO fouling could be substantially lowered if the cross flow velocity is increased [28].

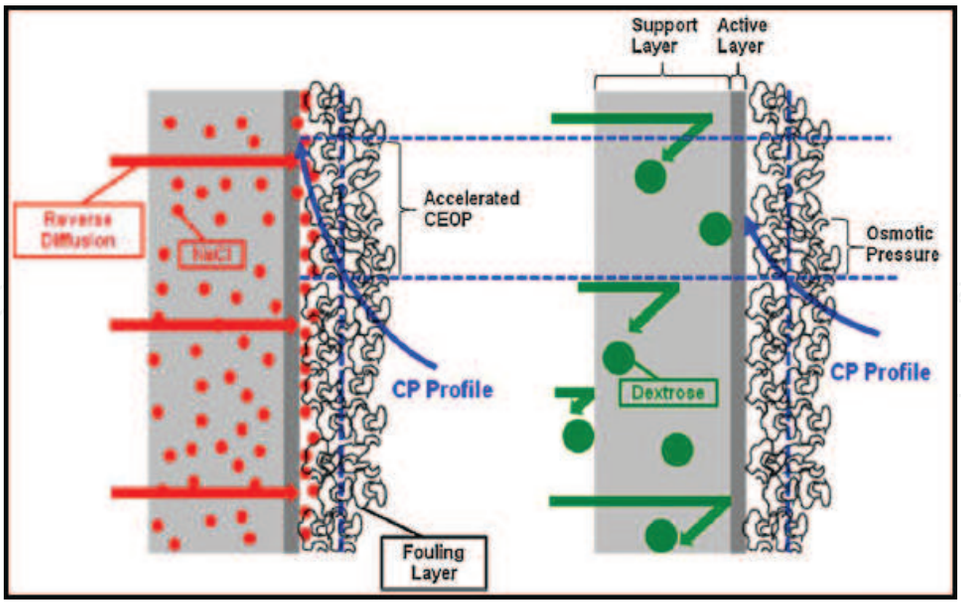

Figure 4. The effects of draw solute reverse diffusion on cake-enhanced osmotic pressure (CEOP) in FO for two different draw solutions: (a) NaCl and (b) dextrose [31].

In a recent experimental attempt, Tang's group used direct microscopic observation to study FO fouling and its mechanisms. They determined that the critical flux concept could also be relevant to osmotically drive the types of processes [63]. Direct microscopic observation has been implemented to research the production of fouling in pressure-driven membrane processes and currently remains one of the primary membrane fouling characterization methodologies [68–71]. Admittedly, direct microscopic observation is relevant only for the cases with large foulants in colloidal or biofouling fouling, such as microbes or particles. Thus, direct microscopic observation can likewise be implemented in the research of membrane fouling if visible fouling layers or large foulants are present in FO.

Usually defined as the level of permeate flux where membrane fouling becomes noticeable, critical flux has been widely used in pressure-driven membrane processes [72–75]. Critical flux can also be applied to osmotically driven membrane processes. A recent study by Zhao et al. confirms its presence in FO [76]. It is necessary to note that the critical flux identified by Zhao et al.'s FO research study, as well as by Tang and coworkers, was detected when the membrane's surface was partially covered with visible foulant [63, 76]. As a consequence, the critical flux in FO could have an implicit connection to the visible fouling layer. This particular connection must be investigated in greater depth. Research suggests that greater working temperatures can have various negative influences on FO cleaning and scaling in brackish water desalination processes, potentially because of the change of HCO_3^- into CO_3^{2-} at high temperature values [26]. The report indicates that, caused by the polymerization of dissolved silica, the silica scaling of FO membranes was the primary inorganic type of fouling in real-case seawater desalination examples [77]. The silica polymerization might likewise quicken the organic fouling, which is removed much easier using water rinsing if compared to the silica scaling [77].

Alternatively, membrane fouling could improve the FO membrane's solute rejection potential. It was also detected that organic foulants located on the membrane's surface, or its active layer,

could improve the negative charge property and surface hydrophilicity, and this in turn can raise the hydrophilic compound absorption capacity [78]. Changes like these can increase the critical rejection potential for many new contaminants, including trace organic compounds, as well as hydrophobic neutral compounds and hydrophilic ionic compounds [78]. Once the FO tests were run continuously for prolonged periods of time at the pilot scale, the rejection performance values improved even further as more substantial fouling happened [79]. In a project by Jin et al., it was determined that organic fouling can likewise have substantial consequences for the elimination of inorganic contaminants, like arsenic and boron [80]. In particular, their influences relied on the membrane's orientation. For instance, in the FO mode, where the membrane's support layer is facing the draw solution, the organic fouling on the membrane's active layer can improve the sieving influence and essentially increase the arsenic rejection in the feed. Alternatively, in the PRO mode, where the membrane's support layer is facing the feed, the organic fouling in the membrane's support structure can lower the boron rejection [80]. Membrane fouling and concentration polarization remain critical phenomena in FO processes since they have the capacity to heighten the additional membrane resistance and lower membrane permeability potential. Researchers must continue to further examine their functions and mechanisms if they want to improve the FO process and its performance capacity. Successful application of FO in real settings will remain problematic until a more comprehensive analysis becomes available.

4.3. Reverse solute diffusion

In membrane processes that are osmotically driven, the solute's reverse diffusion, from the draw solution and through the membrane toward the feed solution, is likewise almost certainly due to the concentration variances. Cath et al. (2009) state that the draw solute reverse diffusion has to be carefully studied as it could endanger the success of the process [11, 81]. Some research studies have linked draw solute reverse diffusion with the membrane fouling phenomenon. Lay et al. and Lee et al. have shown that the draw solute reverse diffusion can, on the one hand, improve the CEOP influence and, on the other hand, intensify FO fouling [28, 67]. Thus, multivalent ion solutions featuring smaller diffusion coefficient values are better for certain uses in which higher rejection potentials are required [11]. Alternatively, in other cases, multivalent ions, like Ca^{2+} and Mg^{2+}, could impede the foulants in the feed solution following reverse diffusion, a dynamic that can worsen the overall membrane fouling [82]. Furthermore, multivalent ions could likewise incite a more substantial ICP due to their smaller diffusion coefficients and bigger ion sizes [48]. Defined as the ratio of the reverse solute flux to the forward water flux, specific reverse solute flux has been added as another potential measure of membrane's selectivity [81, 82]. Specific reverse solute flux parameter offers a third dynamic for the proper FO performance evaluation, together with the salt rejection and the permeate flux parameters. A greater specific reverse solute flux suggests reduced membrane selectivity potential, as well as an inferior FO efficiency value. Although the specific reverse solute flux depends on the membrane's active layer selectivity, it is independent of the structure of the membrane support layer and the draw solution concentration values [51]. This key outcome grants another standard for the production of a new type of FO membrane, that is, greater selectivity of the membrane's active layer. Moreover, engaging a multivalent ion solution as the draw solution could reduce membrane fouling [28, 67] and lower the reverse solute

diffusion [81], but in this case, there is also a potential to have a higher ICP [48] and a greater risk of fouling [82]. To sum up, reverse solute diffusion remains one of the main challenges in osmotically driven membrane processes and as a result must be reduced during the production and design of draw solutes and FO membranes.

4.4. Membrane development

Based on the available membrane fabrication methodologies, newly produced and designed membranes can be organized into three categories: the thin film composite (TFC) membranes, the chemically modified membranes, and the phase inversion-formed cellulosic membranes. Reverse solute diffusion, membrane fouling, and ICP are three of the crucial concerns that exist with respect to the osmotically driven membrane processes, since they effectually direct the FO performance. As a result, when considering innovative FO membrane development, it is essential to characterize its salt rejection, antifouling, and anti-ICP characteristics. When compared with other types of processes, FO could be viewed as more competitive when treating challenging waters with higher fouling potential or solid content, since ICP and fouling are frequently much more serious. When it comes to FO, the water flux is affected by the water permeability, while the reverse solute flux is shaped by the membrane solute permeability. In this instance, there is a type of trade-off between salt rejection and water permeability [83]. Higher water permeability values are desirable, as well as lower salt rejection potential. In most cases, FO membrane featuring higher water permeability potential likewise offers higher salt flux, and the reverse relationship holds true as well. As a consequence, defined as the ratio of the reverse solute flux to the forward water flux, specific reverse solute flux can be a superior parameter to evaluate when considering the FO performance [81]. In fact, it might be better to assess the FO performance with the aid of the osmotic water flux and specific reverse solute flux when membrane fouling and ICP are present. Thus, the characterization and design of new FO membrane in the forthcoming future must reflect on the antifouling and the anti-ICP properties, as well as salt rejection (solute permeability), structural parameters, and water permeability.

4.4.1. Phase inversion-formed cellulosic membranes

Asymmetric cellulosic osmotically driven membranes developed through phase inversion have been created specifically for osmotic drug delivery before they were used for water treatment purposes [33, 84, 85]. Most of these membranes were created using conventional phase inversion and with the help of cellulose acetate as the dip-coating polymer. A research breakthrough in Loeb and Sourirajan's method occurred when they prepared RO membranes through phase inversion based on cellulose acetate polymer. Cellulose acetate offers a variety of desirable properties, such as a comparatively high hydrophilicity favoring lower fouling propensity and greater water flux, wide availability, improved mechanical strength, as well as enhanced resistance to degradation by chlorine and other types of oxidants [86, 87]. This particular form of cellulosic membrane is implemented in energy generation, such as osmotic power, and through a PRO process [88]. Recently, Chung's research group has produced a number of cellulose ester-based membranes specifically for FO applications and containing flat sheet modules and hollow fiber [89–91]. In this case, the methods for creating these cellulose derivative membranes are relatively similar, in the form of phase inversion that is followed by hot water annealing at 60–95°C. Chung's research group determined that the resulting

membrane could have two selective skin layers that are capable of lowering ICP in the membrane support layer [87, 90]. A more recent study modeled this type of double-skinned FO membrane [92]. Chung's research group likewise noted that the relationship between the casting substrate and the polymer had an important role during phase inversion for the development of the membrane's structure [87, 91]. Furthermore, Sairam et al. implemented this phase inversion approach in order to create flat sheet FO membranes using cellulose acetate [93]. Specifically, they applied maleic acid, zinc chloride, and lactic acid as pore-forming agents, while casting the membrane onto nylon fabric at a range of annealing temperature values. Sairam et al. noted that the membrane developed with zinc chloride as the pore-forming agent allowed for a reasonably effective FO performance. On the other hand, the disadvantages of cellulose acetate have to be examined before it is used in FO membranes. While cellulose acetate membranes are more resistant to chloride degradation and more hydrophilic, if compared to the TFC polyamide RO membranes, they have lower resistance potential to biological attachments and hydrolysis [86, 94, 95]. To reduce the hydrolysis of cellulose acetate membranes, it is crucial to modify the pH of the feed and draw solutions within the ranges of 4–6 and to sustain the working temperature that does not rise above 35°C [86, 94].

4.4.2. Thin film composite membranes

It has been noted that there is a key trade-off dynamic occurring between salt rejection and water permeability potential. For instance, the raising of the trimesoyl chloride (TMC) concentration or the reduction of the m-phenylenediamine (MPD) concentration caused greater membrane permeability potential but lower salt rejection values [83]. Research likewise indicates that greater hydrophilicity of the support layer may prefer water diffusion across the FO membrane [96, 97]. Wang et al. prepared polyethersulfone (PES)/sulfonated polysulfone (PSF)-alloyed–type membranes as the substrates of interfacial polymerization and produced high-performance FO membranes. On the other hand, Yu et al. developed a nonporous polyethersulfone (PES) FO-type membrane with the aid of phase inversion, however, without using interfacial polymerization [98]. In this case, the polyester nonwoven fabrics were implemented for backing support. This membrane creation approach was comparable to the one used by Elimelech's group, with the exception of the additional interfacial polymerization phase. According to the report, the membrane produced by this method featured an active layer formed on top of the support layer, high water flux value, and low reverse solute flux potential [98].

Song et al. reported the creation of a nanofiber TFC FO-type membrane using electrospinning, which was followed by interfacial polymerization (ES-IP) [99]. Song et al. noted that the nanocomposite FO membrane allowed for an improved FO performance mostly because of high porosity and low tortuosity that significantly decreased the structural parameters of the membrane. If compared to the TFC FO membrane made using phase inversion followed by interfacial polymerization (PI-IP), the electrospinning-formed nanofiber support layer offers a porous structure resembling a scaffold with interlocked pores between individual nanofibers [99]. Due to this structure, the water flux value of the ES-IP–formed FO membrane was found to be three times as high as the water flux potential of the PI-IP–formed membrane. In this instance, the performance of the FO membrane was enhanced with respect to osmotic water flux, while salt rejection was obtained as well as confirmed by Bui et al. research group [100]. The majority of the approaches used for preparing TFC FO membranes and asymmetric

cellulose acetate FO membranes are indistinguishable from the original traditional RO membrane methods, like phase inversion followed by interfacial polymerization, or phase inversion and annealing.

When it comes to a TFC FO membrane, the membrane support layer made using phase inversion governs the ICP, water flux in FO, and the membrane's active layer controls reverse solute flux potential and salt rejection values. A high salt rejection can be obtained when the TFC membranes are developed with the help of interfacial polymerization. In fact, FO's performance is shaped by the membrane's support layer. Next-generation FO membrane production must pay attention to the membrane's support layer and its role. All in all, an effective FO membrane has to provide a design that appears sufficiently porous and offers improved hydrophilic support combined with lower tortuosity capable of decreasing ICP, as well as a selective active layer that can lower reverse solute diffusion and augment salt rejection potential.

4.4.3. Chemically modified membranes

Over the course of the last several years, chemical modification methodologies have been implemented during the development of innovative FO membranes. Arena et al. research group (2011) applied polydopamine (PDA) as a new bioinspired hydrophilic polymer for the modification of the support layers in commercial TFC RO membranes catering to engineered osmosis applications [101]. This modified membrane showed improved water flux and lower ICP during the conducted FO tests. Furthermore, Setiawan et al. created a hollow-type fiber FO membrane featuring a positively charged NF-like selective layer using a polyelectrolyte posttreatment of a polyamide-imide (PAI) microporous substrate with polyethylenimine (PEI) [102]. Setiawan et al. indicated that the final FO membrane produced could be applied in heavy metal removal processes due to its unique positively charged characteristic. This research group likewise designed a flat sheet–type membrane offering a positively charged NF-like selective layer on top of a woven fabric–embedded substrate and implementing a similar methodology. The reported results suggest that the overall thickness of the substrate was reduced to 55 μm when the PAI microporous substrate was successfully embedded within a woven fabric. Moreover, Tang and coworkers relied on a creative layer-by-layer assembly approach in order to produce FO membranes with desirable properties [103, 104]. In Tang's research studies, polyacrylonitrile (PAN) substrate was prepared with the aid of phase inversion and then posttreated by sodium hydroxide so as to improve surface negative charge density and hydrophilicity potential. Poly(sodium 4-styrene-sulfonate) (PSS) and poly(allylamine hydrochloride) (PAH) were implemented as the polyanion and polycation, respectively. Arguably, the majority of the present approaches to the FO membrane preparation are established methods that have been applied during the last few decades for the creation of pressure-driven–type membranes, such as RO and NF. The production and design of innovative high-performance FO membranes are still in their early stages. As a result, the process of relying on the older methodologies for RO or NF membrane preparation is a sensible and practical direction. Forthcoming research may expand the recently developed techniques for the production of high-performance FO membranes, including layer-by-layer assembly [103, 105–112], UV-photographing [113–116], and polyelectrolyte dip-coating [117, 118]. In addition, membranes featuring polyelectrolyte multilayers, charged properties, or double selective layers can provide exciting avenues for specific real-life FO applications.

4.5. Draw solute/solution developments

Despite preexisting setbacks, key innovative approaches for draw solute selection have been suggested [119, 120]. Specifically, there are three conditions for successful selection of a suitable draw solution in FO applications. To begin, the draw solution must offer a reasonably high osmotic pressure values [11]. Next, the diluted draw solution needs to be economically and effortlessly reconcentrated and recovered [11, 121]. Finally, the draw solute has to showcase lowered ICP during the FO processes. A research study by Zhao and Zou indicates that ICP in FO is seriously influenced by draw solution viscosity, draw solution's ion/molecule size of the solute, and solute diffusion coefficient values [48]. Increased diffusion coefficients, coupled with lowered ion/molecule sizes and smaller solution viscosities, will minimize ICP and allow for resulting in improved permeate fluxes [48]. Moreover, additional parameters like low reverse solute permeability [11], zero toxicity, low cost, absence of membrane damage, inertness and stability at or near natural pH, and good biofouling-resistance should be considered when the draw solute/solution is selected.

During the last few decades, numerous draw solutes/solutions have been examined during osmotically driven–type processes. The primary benefit of implementing volatile gases as draw solutes in FO is that the final thermolytic draw solution may be separated or recovered with the help of heating/or distillation. In a separate project, sugars were likewise tested as draw solutes since there is no necessity to separate the diluted nutrient solutions further, and the diluted solutions may be reconcentrated in decreased pressures with loose RO membranes. After the 2000s, Elimelech and coworkers suggested a new draw solution for the purposes of FO desalination, that is, a water-soluble mixture of NH_3 and CO_2 including ammonium bicarbonate (NH_4HCO_3) [9, 10, 24]. The proposed draw solution can offer improved water fluxes as a result of the higher driving forces created by the greater solubilities of the solutes. These types of draw solutes may be effortlessly recovered or recycled using moderate heating (~60°C) [9]. As a result, this innovative draw solution could find a potential application in large-scale desalination, even though the removal the ammonia (NH_3) smell from the produced water could be a concern. Furthermore, various other chemicals have been assessed for the role of the draw solutes [119].

For instance, synthetic materials, like organic compounds [121] and magnetic and/or hydrophilic nanoparticles [122–124], have been proposed for the application as the draw solutes. In the case of the laboratory-designed magnetic nanoparticles, data suggest that the particle size and surface hydrophilicity of the particles had critical roles for the FO separation performance [123]. It was also noted that particle agglomeration happened during draw solute recycling process using magnetic separators [124]. Such an accumulation of magnetic nanoparticles may be reduced with the aid of ultrasonication. When using this method, the particles' magnetic characteristics and the recovery efficacy were threatened by ultrasonication as well. In order to transcend the issue of accumulation during draw solute recycling, the thermal-responsive properties were integrated into the magnetic nanoparticles using the one-step thermal decomposition [125]. UF could likewise be used to recover diluted draw solutes featuring big particle or molecule sizes. Wang's research group has produced a stimuli-responsive polymer hydrogel as another draw solute for FO desalination [126]. Polymer hydrogels such as these have the capacity to pull water from the saline feed during swelling and after that release the water while deflating, the latter being caused by heating and hydraulic pressure. So as to enhance the

capacity of swelling ratios and drawing water, a type of light-absorbing carbon particles was introduced into the polymer hydrogels, and as a consequence an improved performance was obtained [127]. A new draw solute separation system simulating the "destabilization" phenomenon was suggested for the process of generating drinking water [128]. In this particular system, $Al_2(SO_4)_3$ was chosen as the draw solute, while the diluted $Al_2(SO_4)_3$ solution pH was attuned using CaO, finally resulting in the creation of a white gel-like mixture made out of positively charged $Al(OH)_3$ and $CaSO_4$. In the following step, negatively charged superparamagnetic nanoparticles were added so as to enable the sedimentation. To accelerate the sedimentation process and enhance separation efficiency, an external magnetic field was introduced. Such an innovative draw solution separation technique can make FO a more economical and eco-sustainable process for efficient drinking water production [128].

The selection criteria for the draw solutes and solutions need to be addressed for the process to be effective and sustainable. An effective draw solute option for FO must offer easy and economical recovery, lower tendency to cause ICP, zero toxicity, reasonable costs, higher solubility, and greater osmotic pressure. The diffusion coefficient, viscosity of the draw solution, and the solute particle size need to be examined as they are directly connected to ICP [48] effectually dominating the water flux in FO [38, 46].

4.6. Forward osmosis fouling control

In this chapter, the focus was on discussing and reviewing the primary five issues that exist in FO. Certainly, these challenges do not exist in isolation but are rather interconnected. To sum up some of these issues, the membrane's support layer needs to be as porous as possible for the lower ICP, and the membrane's active layer needs to be more selective for a lower reverse solute diffusion potential. The smaller reverse solute diffusion can then decrease the membrane fouling. When it comes to the draw solute, small ion or molecule sizes could minimize ICP [48]; however, they can likewise increase membrane fouling and reverse solute diffusion. All of these correlations and criteria make the creation of advantageous draw solutes much more problematic. In most cases, higher reverse solute diffusion may lead to substantial membrane fouling, and this correlation holds the other way as well [28, 67]. In addition, ICP and membrane fouling could lead to multiple adverse properties for water flux in FO [50]. Furthermore, reverse solute diffusion, membrane fouling, and ICP are at their core determined by draw solute properties and membrane qualifications.

5. Conclusion

The membrane processes based on osmosis are new technological directions that have exhibited a lot of promise for a range of applications, and especially water purification, food processing, desalination, wastewater treatment, power generation, and pharmaceutical product dehydration. While FO is not likely to fully replace RO as the primary desalination technology in the foreseeable future, it remains an appealing alternative as an effective desalination approach offering many benefits over pressure-driven–type membrane processes. In order to transfer FO from the laboratory stages of research into hands-on industrial applications, a set of advances in terms of FO membrane and draw solute development needs to happen. In fact, the membranes

need to offer critical properties of minimizing ICP, higher mechanical strength, stability, improved water permeability, and better selectivity. To sum up, this chapter examined five essential challenges for FO in the form of membrane fouling, reverse solute diffusion, further membrane development, concentration polarization, and enhanced draw solute design. The innovative draw solutes must be capable of producing higher osmotic pressure, remain easily and economically regenerated/or recycled, and provide minimal ICP. Draw solutes must also offer compatibility with the FO membranes and zero toxicity. A successful draw solute has a vital role in the popularization and efficacy of FO applications. The next level of draw solute development will allow for a much wider use of FO in a range of industrial-scale applications and fields.

Nomenclature

A	water permeability constant of the membrane
B	solute permeability coefficient of the membrane
C_m	concentrations of the feed solution at the membrane surface
C_b	concentrations of the feed solution at the bulk
D	diffusion coefficient of the solute
D_h	hydraulic diameter
J_w	water flux
k	mass transfer coefficient
k_{feed}	mass transfer coefficient on the feed side
k_{draw}	mass transfer coefficient on the draw side
t	thickness of the membrane
τ	tortuosity
σ	reflection coefficient
ε	membrane porosity
S	membrane structural parameter
Sh	Sherwood number
ΔP	applied hydraulic pressure difference
$\Delta\pi$	osmotic pressure difference across the membrane
$\Delta\pi_{Feed}$	bulk osmotic pressure of the feed solution
π_{m-draw}	osmotic pressures of the draw solution at the membrane surface
π_{b-draw}	osmotic pressures of the draw solution in the bulk
$\Delta\pi_{Draw}$	bulk osmotic pressure of the draw solution

Abbreviations

AFM	atomic force microscope
CEOP	cake-enhanced osmotic pressure
CFD	computational fluid dynamics
ECP	external concentration polarization
ES-IP	electrospinning followed by interfacial polymerization
FEM	finite element method
FO	forward osmosis
ICP	internal concentration polarization
MPD	m-phenylenediamine
NF	nanofiltration
OMBR	osmotic membrane bioreactor
PAH	poly(allylamine hydrochloride)
PAI	polyamide-imide
PAN	polyacrylonitrile
PDA	polydopamine
PEI	polyethylenimine
PES	polyethersulfone
PRO	pressure-retarded osmosis
PSF	polysulfone
PSS	poly(sodium 4-styrene-sulfonate)
RO	reverse osmosis
TFC	thin film composite
TMC	trimesoyl chloride

Author details

Amira Abdelrasoul[1]*, Huu Doan[2], Ali Lohi[2] and Chil-Hung Cheng[2]

*Address all correspondence to: amira.abdelrasoul@usask.ca

1 Department of Chemical and Biological Engineering, University of Saskatchewan, Saskatoon, Saskatchewan, Canada

2 Department of Chemical Engineering, Ryerson University, Toronto, Ontario, Canada

References

[1] Shannon MA, Bohn PW, Elimelech M, Georgiadis JG, Marinas BJ, Mayes AM. Science and technology for water purification in the coming decades. Nature. 2008;**452**: 301-310

[2] E.I.A. International. World Energy Outlook 2010. The Energy Information Administration. Washington DC; 2010

[3] Elimelech M, Phillip WA. The future of seawater desalination: Energy, technology, and the environment. Science. 2011;**333**:712-717

[4] Montgomery MA, Elimelech M. Water and sanitation in developing countries: Including health in the equation. Environmental Science & Technology. 2007;**41**:17-24

[5] Elimelech M. The global challenge for adequate and safe water. Journal of Water Supply: Research and Technology—AQUA. 2006;**55**:3-10

[6] Gleick PH. Water resources. In: Schneider SH, editor. Encyclopedia of Climate and Weather. New York: Oxford University Press; 1996

[7] King CW, Webber ME. Water intensity of transportation. Environmental Science & Technology. 2008;**42**:7866-7872

[8] Geise GM, Lee H-S, Miller DJ, Freeman BD, McGrath JE, Paul DR. Water purification by membranes: The role of polymer science. Journal of Polymer Science Part B: Polymer Physics. 2010;**48**:1685-1718

[9] McCutcheon JR, McGinnis RL, Elimelech M. A novel ammonia–carbon dioxide forward (direct) osmosis desalination process. Desalination. 2005;**174**:1-11

[10] McCutcheon JR, McGinnis RL, Elimelech M. Desalination by ammonia–carbon dioxide forward osmosis: Influence of draw and feed solution concentrations on process performance. Journal of Membrane Science. 2006;**278**:114-123

[11] Cath TY, Childress AE, Elimelech M. Forward osmosis: Principles, applications, and recent developments. Journal of Membrane Science. 2006;**281**:70-87

[12] Petrotos KB, Quantick P, Petropakis H. A study of the direct osmotic concentration of tomato juice in tubular membrane-module configuration. I. The effect of certain basic process parameters on the process performance. Journal of Membrane Science. 1998;**150**: 99-110

[13] Petrotos KB, Quantick PC, Petropakis H. Direct osmotic concentration of tomato juice in tubular membrane-module configuration. II. The effect of using clarified tomato juice on the process performance. Journal of Membrane Science. 1999;**160**:171-177

[14] Petrotos KB, Lazarides HN. Osmotic concentration of liquid foods. Journal of Food Engineering. 2001;**49**:201-206

[15] Garcia-Castello EM, McCutcheon JR, Elimelech M. Performance evaluation of sucrose concentration using forward osmosis. Journal of Membrane Science. 2009;**338**:61-66

[16] Lee KL, Baker RW, Lonsdale HK. Membranes for power generation by pressure-retarded osmosis. Journal of Membrane Science. 1981;**8**:141-171

[17] Seppälä A, Lampinen MJ. Thermodynamic optimizing of pressure-retarded osmosis power generation systems. Journal of Membrane Science. 1999;**161**:115-138

[18] McGinnis RL, Elimelech M. Global challenges in energy and water supply: The promise of engineered osmosis. Environmental Science & Technology. 2008;**42**:8625-8629

[19] Achilli A, Cath TY, Childress AE. Power generation with pressure retarded osmosis: An experimental and theoretical investigation. Journal of Membrane Science. 2009;**343**:42-52

[20] Achilli A, Cath TY, Marchand EA, Childress AE. The forward osmosis membrane bioreactor: A low fouling alternative to MBR processes. Desalination. 2009;**239**:10-21

[21] Holloway RW, Childress AE, Dennett KE, Cath TY. Forward osmosis for concentration of anaerobic digester centrate. Water Research. 2007;**41**:4005-4014

[22] Liu Y, Mi B. Combined fouling of forward osmosis membranes: Synergistic foulant interaction and direct observation of fouling layer formation. Journal of Membrane Science. 2012;**407-408**:136-144

[23] Mi B, Elimelech M. Organic fouling of forward osmosis membranes: Fouling reversibility and cleaning without chemical reagents. Journal of Membrane Science. 2010;**348**:337-345

[24] McGinnis RL, Elimelech M. Energy requirements of ammonia–carbon dioxide forward osmosis desalination. Desalination. 2007;**207**:370-382

[25] Martinetti CR, Childress AE, Cath TY. High recovery of concentrated RO brines using forward osmosis and membrane distillation. Journal of Membrane Science. 2009;**331**:31-39

[26] Zhao S, Zou L. Effects of working temperature on separation performance, membrane scaling and cleaning in forward osmosis desalination. Desalination. 2011;**278**:157-164

[27] Mi B, Elimelech M. Gypsum scaling and cleaning in forward osmosis: Measurements and mechanisms. Environmental Science & Technology. 2010;**44**:2022-2028

[28] Lee S, Boo C, Elimelech M, Hong S. Comparison of fouling behavior in forward osmosis (FO) and reverse osmosis (RO). Journal of Membrane Science. 2010;**365**:34-39

[29] Cartinella JL, Cath TY, Flynn MT, Miller GC, Hunter KW, Childress AE. Removal of natural steroid hormones from wastewater using membrane contactor processes. Environmental Science & Technology. 2006;**40**:7381-7386

[30] Cath TY, Hancock NT, Lundin CD, Hoppe-Jones C, Drewes JE. A multi-barrier osmotic dilution process for simultaneous desalination and purification of impaired water. Journal of Membrane Science. 2010;**362**:417-426

[31] Yang Q, Wang KY, Chung T-S. A novel dual-layer forward osmosis membrane for protein enrichment and concentration. Separation and Purification Technology. 2009;**69**:269-274

[32] Jiao B, Cassano A, Drioli E. Recent advances on membrane processes for the concentration of fruit juices: A review. Journal of Food Engineering. 2004;**63**:303-324

[33] Wang C-Y, Ho H-O, Lin L-H, Lin Y-K, Sheu M-T. Asymmetric membrane capsules for delivery of poorly water-soluble drugs by osmotic effects. International Journal of Pharmaceutics. 2005;**297**:89-97

[34] Shokri J, Ahmadi P, Rashidi P, Shahsavari M, Rajabi-Siahboomi A, Nokhodchi A. Swellable elementary osmotic pump (SEOP): An effective device for delivery of poorly water-soluble drugs. European Journal of Pharmaceutics and Biopharmaceutics. 2008;**68**:289-297

[35] Bamaga OA, Yokochi A, Zabara B, Babaqi AS, Hybrid FO. RO desalination system: Preliminary assessment of osmotic energy recovery and designs of new FO membrane module configurations. Desalination. 2011;**268**:163-169

[36] Tang W, Ng HY. Concentration of brine by forward osmosis: Performance and influence of membrane structure. Desalination. 2008;**224**:143-153

[37] Mehta GD. Further results on the performance of present-day osmotic membranes in various osmotic regions. Journal of Membrane Science. 1982;**10**:3-19

[38] McCutcheon JR, Elimelech M. Influence of concentrative and dilutive internal concentration polarization on flux behavior in forward osmosis. Journal of Membrane Science. 2006;**284**:237-247

[39] Zydney AL. Stagnant film model for concentration polarization in membrane systems. Journal of Membrane Science. 1997;**130**:275-281

[40] Sablani SS, Goosen MFA, Al-Belushi R, Wilf M. Concentration polarization in ultrafiltration and reverse osmosis: A critical review. Desalination. 2001;**141**:269-289

[41] Thorsen T. Concentration polarisation by natural organic matter (NOM) in NF and UF. Journal of Membrane Science. 2004;**233**:79-91

[42] Kim S, Hoek EMV. Modeling concentration polarization in reverse osmosis processes. Desalination. 2005;**186**:111-128

[43] McCutcheon JR, Elimelech M. Modeling water flux in forward osmosis: Implications for improved membrane design. AICHE Journal. 2007;**53**:1736-1744

[44] Su J, Chung T-S. Sublayer structure and reflection coefficient and their effects on concentration polarization and membrane performance in FO processes. Journal of Membrane Science. 2011;**376**:214-224

[45] Mehta GD, Loeb S. Performance of permasep B-9 and B-10 membranes in various osmotic regions and at high osmotic pressures. Journal of Membrane Science. 1978;**4**:335-349

[46] Gray GT, McCutcheon JR, Elimelech M. Internal concentration polarization in forward osmosis: role of membrane orientation. Desalination. 2006;**197**:1-8

[47] Mehta GD, Loeb S. Internal polarization in the porous substructure of a semipermeable membrane under pressure-retarded osmosis. Journal of Membrane Science. 1978;**4**:261-265

[48] Zhao S, Zou L. Relating solution physicochemical properties to internal concentration polarization in forward osmosis. Journal of Membrane Science. 2011;**379**:459-467

[49] Loeb S, Titelman L, Korngold E, Freiman J. Effect of porous support fabric on osmosis through a Loeb–Sourirajan type asymmetric membrane. Journal of Membrane Science. 1997;**129**:243-249

[50] Tang CY, She Q, Lay WCL, Wang R, Fane AG. Coupled effects of internal concentration polarization and fouling on flux behavior of forward osmosis membranes during humic acid filtration. Journal of Membrane Science. 2010;**354**:123-133

[51] Phillip WA, Yong JS, Elimelech M. Reverse draw solute permeation in forward osmosis: Modeling and experiments. Environmental Science & Technology. 2010;**44**: 5170-5176

[52] Gruber MF, Johnson CJ, Tang CY, Jensen MH, Yde L, Hélix-Nielsen C. Computational fluid dynamics simulations of flow and concentration polarization in forward osmosis membrane systems. Journal of Membrane Science. 2011;**379**:488-495

[53] Jung DH, Lee J, Kim DY, Lee YG, Park M, Lee S, Yang DR, Kim JH. Simulation of forward osmosis membrane process: Effect of membrane orientation and flow direction of feed and draw solutions. Desalination. 2011;**277**:83-91

[54] Li W, Gao Y, Tang CY. Network modeling for studying the effect of support structure on internal concentration polarization during forward osmosis: Model development and theoretical analysis with FEM. Journal of Membrane Science. 2011;**379**:307-321

[55] Sagiv A, Semiat R. Finite element analysis of forward osmosis process using NaCl solutions. Journal of Membrane Science. 2011;**379**:86-96

[56] Jarusutthirak C, Amy G, Croué J-P. Fouling characteristics of wastewater effluent organic matter (EfOM) isolates on NF and UF membranes. Desalination. 2002;**145**:247-255

[57] Seidel A, Elimelech M. Coupling between chemical and physical interactions in natural organic matter (NOM) fouling of nanofiltration membranes: Implications for fouling control. Journal of Membrane Science. 2002;**203**:245-255

[58] Hoek EMV, Elimelech M. Cake-enhanced concentration polarization: A new fouling mechanism for salt-rejecting membranes. Environmental Science & Technology. 2003; **37**:5581-5588

[59] Le-Clech P, Chen V, Fane TAG. Fouling in membrane bioreactors used in wastewater treatment. Journal of Membrane Science. 2006;**284**:17-53

[60] Ang WS, Elimelech M. Protein (BSA) fouling of reverse osmosis membranes: Implications for wastewater reclamation. Journal of Membrane Science. 2007;**296**:83-92

[61] Tang CY, Chong TH, Fane AG. Colloidal interactions and fouling of NF and RO membranes: A review. Advances in Colloid and Interface Science. 2011;**164**:126-143

[62] Mi B, Elimelech M. Chemical and physical aspects of organic fouling of forward osmosis membranes. Journal of Membrane Science. 2008;**320**:292-302

[63] Wang Y, Wicaksana F, Tang CY, Fane AG. Direct microscopic observation of forward osmosis membrane fouling. Environmental Science & Technology. 2010;**44**:7102-7109

[64] Cath TY, Gormly S, Beaudry EG, Flynn MT, Adams VD, Childress AE. Membrane contactor processes for wastewater reclamation in space: Part I. Direct osmotic concentration as pretreatment for reverse osmosis. Journal of Membrane Science. 2005;**257**:85-98

[65] Cath TY, Adams D, Childress AE. Membrane contactor processes for wastewater reclamation in space: II. Combined direct osmosis, osmotic distillation, and membrane distillation for treatment of metabolic wastewater. Journal of Membrane Science. 2005;**257**:111-119

[66] Meng F, Chae S-R, Drews A, Kraume M, Shin H-S, Yang F. Recent advances in membrane bioreactors (MBRs): Membrane fouling and membrane material. Water Research. 2009;**43**:1489-1512

[67] Lay WCL, Chong TH, Tang C, Fane AG, Zhang J, Liu Y. Fouling propensity of forward osmosis: Investigation of the slower flux decline phenomenon. Water Science and Technology. 2010;**61**:927-936

[68] Kang S-T, Subramani A, Hoek EMV, Deshusses MA, Matsumoto MR. Direct observation of biofouling in cross-flow microfiltration: Mechanisms of deposition and release. Journal of Membrane Science. 2004;**244**:151-165

[69] Wang S, Guillen G, Hoek EMV. Direct observation of microbial adhesion to membranes. Environmental Science & Technology. 2005;**39**:6461-6469

[70] Li H, Fane AG, Coster HGL, Vigneswaran S. Direct observation of particle deposition on the membrane surface during crossflow microfiltration. Journal of Membrane Science. 1998;**149**:83-97

[71] Li H, Fane AG, Coster HGL, Vigneswaran S. Observation of deposition and removal behaviour of submicron bacteria on the membrane surface during crossflow microfiltration. Journal of Membrane Science. 2003;**217**:29-41

[72] Bacchin P, Aimar P, Field RW. Critical and sustainable fluxes: Theory, experiments and applications. Journal of Membrane Science. 2006;**281**:42-69

[73] Zhang YP, Fane AG, Law AWK. Critical flux and particle deposition of bidisperse suspensions during crossflow microfiltration. Journal of Membrane Science. 2006;**282**:189-197

[74] Zhang YP, Fane AG, Law AWK. Critical flux and particle deposition of fractal flocs during crossflow microfiltration. Journal of Membrane Science. 2010;**353**:28-35

[75] Field RW, Wu D, Howell JA, Gupta BB. Critical flux concept for microfiltration fouling. Journal of Membrane Science. 1995;**100**:259-272

[76] Zhao S, Zou L, Mulcahy D. Effects of membrane orientation on process performance in forward osmosis applications. Journal of Membrane Science. 2011;**382**:308-315

[77] Li Z-Y, Yangali-Quintanilla V, Valladares-Linares R, Li Q, Zhan T, Amy G. Flux patterns and membrane fouling propensity during desalination of seawater by forward osmosis. Water Research. 2012;**46**:195-204

[78] Valladares Linares R, Yangali-Quintanilla V, Li Z, Amy G. Rejection of micropollutants by clean and fouled forward osmosis membrane. Water Research. 2014;**45**:6737-6744

[79] Hancock NT, Xu P, Heil DM, Bellona C, Cath TY. Comprehensive benchand pilot-scale investigation of trace organic compounds rejection by forward osmosis. Environmental Science & Technology. 2011;**45**:8483-8490

[80] Jin X, She Q, Ang X, Tang CY. Removal of boron and arsenic by forward osmosis membrane: Influence of membrane orientation and organic fouling. Journal of Membrane Science. 2012;**389**:182-187

[81] Hancock NT, Cath TY. Solute coupled diffusion in osmotically driven membrane processes. Environmental Science & Technology. 2009;**43**:6769-6775

[82] Zou S, Gu Y, Xiao D, Tang CY. The role of physical and chemical parameters on forward osmosis membrane fouling during algae separation. Journal of Membrane Science. 2011;**366**:356-362

[83] Wei J, Liu X, Qiu C, Wang R, Tang CY. Influence of monomer concentrations on the performance of polyamide-based thin film composite forward osmosis membranes. Journal of Membrane Science. 2011;**381**:110-117

[84] Lin Y-K, Ho H-O. Investigations on the drug releasing mechanism from an asymmetric membrane-coated capsule with an in situ formed delivery orifice. Journal of Controlled Release. 2003;**89**:57-69

[85] Herbig SM, Cardinal JR, Korsmeyer RW, Smith KL. Asymmetric-membrane tablet coatings for osmotic drug delivery. Journal of Controlled Release. 1995;**35**:127-136

[86] Baker RW. Membrane Technology and Applications. 2nd ed. Etobicoke, Canada: John Wiley & Sons, Ltd.; 2004

[87] Zhang S, Wang KY, Chung T-S, Chen H, Jean YC, Amy G. Well-constructed cellulose acetate membranes for forward osmosis: Minimized internal concentration polarization with an ultra-thin selective layer. Journal of Membrane Science. 2010;**360**:522-535

[88] Gerstandt K, Peinemann KV, Skilhagen SE, Thorsen T, Holt T. Membrane processes in energy supply for an osmotic power plant. Desalination. 2008;**224**:64-70

[89] Su J, Yang Q, Teo JF, Chung T-S. Cellulose acetate nanofiltration hollow fiber membranes for forward osmosis processes. Journal of Membrane Science. 2010;**355**:36-44

[90] Wang KY, Ong RC, Chung T-S. Double-skinned forward osmosis membranes for reducing internal concentration polarization within the porous sublayer. Industrial & Engineering Chemistry Research. 2010;**49**:4824-4831

[91] Zhang S, Wang KY, Chung T-S, Jean YC, Chen H. Molecular design of the cellulose ester-based forward osmosis membranes for desalination. Chemical Engineering Science. 2011;**66**:2008-2018

[92] Tang CY, She Q, Lay WCL, Wang R, Field R, Fane AG. Modeling double skinned FO membranes. Desalination. 2014;**283**:178-186

[93] Sairam M, Sereewatthanawut E, Li K, Bismarck A, Livingston AG. Method for the preparation of cellulose acetate flat sheet composite membranes for forward osmosis–desalination using $MgSO_4$ draw solution. Desalination. 2011;**273**:299-307

[94] Vos KD, Burris FO, Riley RL. Kinetic study of the hydrolysis of cellulose acetate in the pH range of 2–10. Journal of Applied Polymer Science. 1966;**10**:825-832

[95] Merten U. Flow relationships in reverse osmosis. Industrial & Engineering Chemistry Fundamentals. 1963;**2**:229-232

[96] Widjojo N, Chung T-S, Weber M, Maletzko C, Warzelhan V. The role of sulphonated polymer and macrovoid-free structure in the support layer for thin-film composite (TFC) forward osmosis (FO) membranes. Journal of Membrane Science. 2011;**383**:214-223

[97] McCutcheon JR, Elimelech M. Influence of membrane support layer hydrophobicity on water flux in osmotically driven membrane processes. Journal of Membrane Science. 2008;**318**:458-466

[98] Yu Y, Seo S, Kim I-C, Lee S. Nanoporous polyethersulfone (PES) membrane with enhanced flux applied in forward osmosis process. Journal of Membrane Science. 2011;**375**:63-68

[99] Song X, Liu Z, Sun DD. Nano gives the answer: Breaking the bottleneck of internal concentration polarization with a nanofiber composite forward osmosis membrane for a high water production rate. Advanced Materials. 2015;**23**:3256-3260

[100] Bui N, Lind ML, Hoek EMV, McCutcheon JR. Electrospun nanofiber supported thin film composite membranes for engineered osmosis. Journal of Membrane Science. 2011:385, 10-386, 19

[101] Fayyazi F, Feijani E, Mahdavi H. Chemically modified polysulfone membrane containing palladium nanoparticles: Preparation, characterization and application as an efficient catalytic membrane for Suzuki reaction. Chemical Engineering Science. 2015;**134**: 549-554

[102] Setiawan L, Wang R, Li K, Fane AG. Fabrication of novel poly(amide–imide) forward osmosis hollow fiber membranes with a positively charged nanofiltration-like selective layer. Journal of Membrane Science. 2011;**369**:196-205

[103] Saren Q, Qiu CQ, Tang CY. Synthesis and characterization of novel forward osmosis membranes based on layer-by-layer assembly. Environmental Science & Technology. 2011;**45**:5201-5208

[104] Qiu C, Qi S, Tang CY. Synthesis of high flux forward osmosis membranes by chemically crosslinked layer-by-layer polyelectrolytes. Journal of Membrane Science. 2011; **381**:74-80

[105] Hong SU, Bruening ML. Separation of amino acid mixtures using multilayer polyelectrolyte nanofiltration membranes. Journal of Membrane Science. 2006;**280**:1-5

[106] Hong SU, Ouyang L, Bruening ML. Recovery of phosphate using multilayer polyelectrolyte nanofiltration membranes. Journal of Membrane Science. 2009;**327**:2-5

[107] Bruening ML, Dotzauer DM, Jain P, Ouyang L, Baker GL. Creation of functional membranes using polyelectrolyte multilayers and polymer brushes. Langmuir. 2008;**24**:7663-7673

[108] Stanton BW, Harris JJ, Miller MD, Bruening ML. Ultrathin, multilayered polyelectrolyte films as nanofiltration membranes. Langmuir. 2013;**19**:7038-7042

[109] Malaisamy R, Bruening ML. High-flux nanofiltration membranes prepared by adsorption of multilayer polyelectrolyte membranes on polymeric supports. Langmuir. 2005;**21**: 10587-10592

[110] Zhang G, Yan H, Ji S, Liu Z. Self-assembly of polyelectrolyte multilayer pervaporation membranes by a dynamic layer-by-layer technique on a hydrolyzed polyacrylonitrile ultrafiltration membrane. Journal of Membrane Science. 2007;**292**:1-8

[111] Jin W, Toutianoush A, Tieke B. Use of polyelectrolyte layer-by-layer assemblies as nanofiltration and reverse osmosis membranes. Langmuir. 2003;**19**:2550-2553

[112] Lee H, Lee Y, Statz AR, Rho J, Park TG, Messersmith PB. Substrateindependent layer-by-layer assembly by using mussel-adhesive-inspired polymers. Advanced Materials. 2008;**20**:1619-1623

[113] Akbari A, Desclaux S, Rouch JC, Aptel P, Remigy JC. New UV-photografted nanofiltration membranes for the treatment of colored textile dye effluents. Journal of Membrane Science. 2006;**286**:342-350

[114] Akbari A, Desclaux S, Rouch JC, Remigy JC. Application of nanofiltration hollow fibre membranes, developed by photografting, to treatment of anionic dye solutions. Journal of Membrane Science. 2007;**297**:243-252

[115] Li X-L, Zhu L-P, Xu Y-Y, Yi Z, Zhu B-K. A novel positively charged nanofiltration membrane prepared from N,N-dimethylaminoethyl methacrylate by quaternization cross-linking. Journal of Membrane Science. 2011;**374**:33-42

[116] Deng H, Xu Y, Chen Q, Wei X, Zhu B. High flux positively charged nanofiltration membranes prepared by UV-initiated graft polymerization of methacrylatoethyl trimethyl ammonium chloride (DMC) onto polysulfone membranes. Journal of Membrane Science. 2011;**366**:363-372

[117] Miao J, Chen G-H, Gao C-J. A novel kind of amphoteric composite nanofiltration membrane prepared from sulfated chitosan (SCS). Desalination. 2005;**181**:173-183

[118] He T, Frank M, Mulder MHV, Wessling M. Preparation and characterization of nanofiltration membranes by coating polyethersulfone hollow fibers with sulfonated poly (ether ether ketone) (SPEEK). Journal of Membrane Science. 2008;**307**:62-72

[119] Achilli A, Cath TY, Childress AE. Selection of inorganic-based draw solutions for forward osmosis applications. Journal of Membrane Science. 2010;**364**:233-241

[120] Kim T-W, Kim Y, Yun C, Jang H, Kim W, Park S. Systematic approach for draw solute selection and optimal system design for forward osmosis desalination. Desalination. 2012;**284**:253-260

[121] Yen SK, Mehnas Haja F, Su NM, Wang KY, Chung T-S. Study of draw solutes using 2-methylimidazole-based compounds in forward osmosis. Journal of Membrane Science. 2010;**364**:242-252

[122] Ling MM, Chung T-S. Desalination process using super hydrophilic nanoparticles via forward osmosis integrated with ultrafiltration regeneration. Desalination. 2011;**278**:194-202

[123] Ling MM, Wang KY, Chung T-S. Highly water-soluble magnetic nanoparticles as novel draw solutes in forward osmosis for water reuse. Industrial & Engineering Chemistry Research. 2010;**49**:5869-5876

[124] Ge Q, Su J, Chung T-S, Amy G. Hydrophilic superparamagnetic nanoparticles: Synthesis, characterization, and performance in forward osmosis processes. Industrial & Engineering Chemistry Research. 2011;**50**:382-388

[125] Ling MM, Chung T-S, Lu X. Facile synthesis of thermosensitive magnetic nanoparticles as smart draw solutes in forward osmosis. Chemical Communications. 2011;**47**:10788-10790

[126] Li D, Zhang X, Yao J, Simon GP, Wang H. Stimuli-responsive polymer hydrogels as a new class of draw agent for forward osmosis desalination. Chemical Communications. 2011;**47**:1710-1712

[127] Li D, Zhang X, Yao J, Zeng Y, Simon GP, Wang H. Composite polymer hydrogels as draw agents in forward osmosis and solar dewatering. Soft Matter. 2011;**7**:10048-10056

[128] Liu Z, Bai H, Lee J, Sun DD. A low-energy forward osmosis process to produce drinking water. Energy & Environmental Science. 2011;**4**:2582-2585